

1967

Soil bearing tests using a spherical penetration device

Ghulam Safdar Butt
Iowa State University

Follow this and additional works at: <https://lib.dr.iastate.edu/rtd>



Part of the [Civil Engineering Commons](#)

Recommended Citation

Butt, Ghulam Safdar, "Soil bearing tests using a spherical penetration device " (1967). *Retrospective Theses and Dissertations*. 3148.
<https://lib.dr.iastate.edu/rtd/3148>

This Dissertation is brought to you for free and open access by the Iowa State University Capstones, Theses and Dissertations at Iowa State University Digital Repository. It has been accepted for inclusion in Retrospective Theses and Dissertations by an authorized administrator of Iowa State University Digital Repository. For more information, please contact digirep@iastate.edu.

**This dissertation has been
microfilmed exactly as received**

67-8903

**BUTT, Ghulam Safdar, 1928-
SOIL BEARING TESTS USING A SPHERICAL
PENETRATION DEVICE.**

**Iowa State University of Science and Technology,
Ph.D., 1967
Engineering, civil**

University Microfilms, Inc., Ann Arbor, Michigan

SOIL BEARING TESTS USING A SPHERICAL PENETRATION DEVICE

by

Ghulam Safdar Butt

A Dissertation Submitted to the
Graduate Faculty in Partial Fulfillment of
The Requirements for the Degree of
DOCTOR OF PHILOSOPHY

Major Subject: Soil Engineering

Approved:

Signature was redacted for privacy.

In Charge of Major Work

Signature was redacted for privacy.

Head of Major Department

Signature was redacted for privacy.

Dean of Graduate College

Iowa State University
Of Science and Technology
Ames, Iowa

1967

TABLE OF CONTENTS

	Page
I. INTRODUCTION -----	1
A. Objectives -----	4
II. REVIEW OF LITERATURE -----	6
A. Penetration Tests to Determine Soil Strength -----	6
1. California Bearing Ratio test -----	7
2. North Dakota cone penetrometer -----	9
3. Spherical penetrometers -----	10
III. THEORETICAL ANALYSIS -----	17
A. Application of Similitude Theory and Dimensional Analysis -	21
1. Size effect in plate bearing tests -----	28
B. Development of Classical Bearing Capacity Theory -----	30
1. Deformation of a flat punch -----	30
2. Deformation by a spherical indenter -----	33
IV. MODEL INVESTIGATION OF THE DEFORMED ZONE UNDER A SPHERICAL PENETROMETER -----	38
A. Experimental Methods -----	38
B. Deformation Analysis -----	40
1. Deformation mechanism in silt -----	40
2. Deformation mechanism in clay -----	45
3. Deformation mechanism in sand -----	46
4. Discussion -----	52
V. PROCEDURE -----	56
A. Preliminary Investigation -----	56
1. Loading device -----	56
2. Specimen size -----	56
3. Measurement of indentation -----	58
4. Period of loading -----	59
5. Establishing zero point -----	62
6. Load-area relation -----	64
7. Surface variation in specimens -----	64
8. Limit of penetration -----	67
B. Laboratory Investigations -----	67
1. Description of soils -----	67
2. Mixing -----	68
3. Molding -----	71
4. Storage -----	72
5. Spherical penetration test -----	73
6. CBR test -----	76
7. Unconfined compressive strength-test -----	76
8. Direct shear test -----	77
9. Triaxial compression test -----	77
10. Laboratory tests on sand specimens -----	77

TABLE OF CONTENTS
(Continued)

	Page
C. Field Investigations -----	79
1. Description of soils -----	79
2. Field spherical penetrometer -----	80
3. Spherical penetrometer test procedure -----	84
4. Plate bearing test -----	86
5. Steel wedge test -----	86
6. Layout of test site -----	86
VI. PRESENTATION AND DISCUSSION OF RESULTS -----	89
A. Presentation of Data -----	89
B. Statistical Analysis -----	99
1. General -----	99
2. Comparison of variability of SBV and CBR -----	99
3. Estimation of CBR from SBV -----	102
4. Estimation of plate bearing from the SBV -----	107
5. Estimation of unconfined compressive strength from the SBV -----	108
C. Discussion of Results -----	111
1. Sphere Bearing Value versus California Bearing Ratio -----	111
2. Sphere Bearing test versus plate bearing test -----	119
3. Sphere Bearing test versus steel wedge test -----	123
4. Sphere Bearing test versus unconfined compressive strength -----	125
5. Sphere Bearing Value and ultimate bearing capacity of soil -----	130
D. Pavement Design Method from the Sphere Bearing Value -----	134
VII. SUMMARY AND CONCLUSIONS -----	141
VIII. SUGGESTIONS FOR FURTHER RESEARCH -----	147
IX. LITERATURE CITED -----	148
X. ACKNOWLEDGEMENT -----	152

I. INTRODUCTION

The behavior of soil under stress is generally more complex than, for example, metals; the latter are homogeneous and have a better defined elastic-plastic boundary, whereas soil beneath a foundation is seldom homogeneous, large variations in strength often occurring in both the vertical and horizontal directions. Soil properties also vary due to differences in moisture content, bulk density, internal structure, and the way in which stress is applied.

In any soil engineering problem the most important task is the determination of strength properties of soil. Three widely used methods are shear tests, bearing tests and penetration tests. Usually these tests are for specific design purposes.

Shear tests include the unconfined compression test, shear box tests and triaxial tests. These tests are made on comparatively small samples in the laboratory to determine the ultimate bearing capacity of the soil mass, stability of embankments and cuts, earth pressures on retaining walls and sometimes thickness of pavements.

The usual objective of shear tests is to determine cohesion and angle of internal friction under loading and drainage conditions similar to those that will occur in the soil mass. These constants are then used in conjunction with theories of stress distribution or theory of plastic failure in the soil mass.

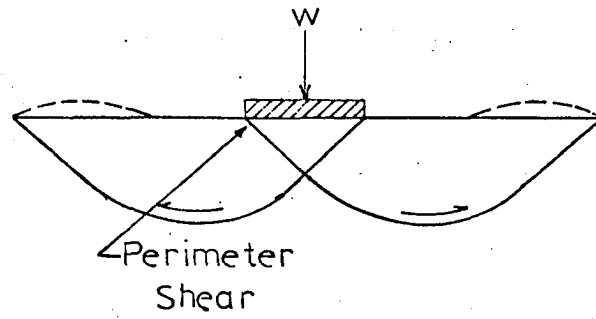
Because of the small sample size, these tests in effect determine the strength properties only at a point in the soil mass. A number of tests on

samples from different points must be made in order to obtain an overall evaluation of the strength of the soil mass. An alternative short-cut method is to utilize rapid field tests for design and quality control, even though basic soil parameters are not directly indicated.

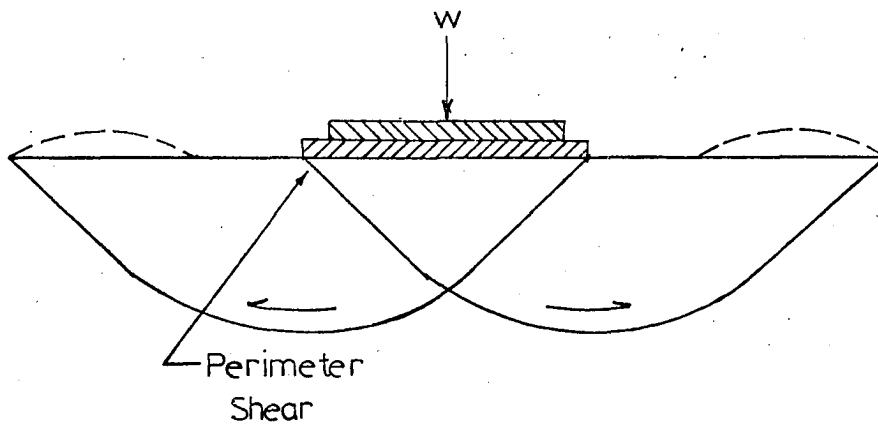
Plate bearing is a commonly used field test made by loading on the surface of the soil mass. Circular plates of various sizes, of the order of several square feet, are loaded in increments, much as occurs during construction. Each applied load causes deflection which is partly elastic and partly due to the compression of the soil. A perimeter shear factor is taken into account by using several different sizes of plates with varying perimeter/area ratios (50). Failure surfaces are shown in Figure 1. The principal uses of bearing tests are to determine stresses within concrete pavements by means of Westergaard's analysis (48), to design pavements taking into account subgrade and subbase strength, to test the stability of existing road and airfield pavements, to predict settlement and bearing capacity under foundations, and to determine the elastic or deformation properties of soils in situ.

Disadvantages of plate bearing tests were discussed at length in an ASTM Symposium (4). Some of the principal disadvantages are:

- a. The test is exceedingly time-consuming and expensive.
- b. The results may be evaluated only for the specific conditions under which the tests are performed. No set procedure for testing can be laid down.
- c. There is difficulty in selecting a proper critical deflection value.



(a) Small plate



(b) Large plate

Figure 1. Failure surfaces in plate bearing tests

In order to overcome some of these disadvantages many new devices have been developed. These devices are either for use in bore holes, like the vane shear test, the standard penetration test, the Menard pressure meter and the bore hole shear device (14), or are surface penetrometers used to evaluate strength properties of soil surface. Determination of strength properties of soil surface is essential in all pavement designs. Many of the methods in use are empirical and give only an index value. Highway engineers have often felt the need for a device which is simple to use and yet gives a basis for rational design of pavements.

A. Objectives

Dr. T. Demirel performed preliminary investigations with a spherical penetration device in 1955 (10). The device was simple to assemble and operate and did not require any elaborate equipment. Such a device could be used to measure bearing strength of subgrade both in the field and laboratory.

In 1965 Iowa State Highway Commission sanctioned a research project to devise bearing test for field or laboratory use, which would avoid some of the limitations and empiricism of the present bearing tests.

The aims of this investigation were:

1. To investigate mechanics of deformation and failure of surface soils.
2. To investigate load-area relationship of different sized spheres and determine size effect.

3. To conduct laboratory tests under controlled conditions on a variety of compacted soils and determine effect of moisture, density and compactive effort on the bearing value. Tests were to be conducted in three types of soils -- silt (loess), clay and sand.
4. Correlate bearing value of spherical penetration device with the CBR (California Bearing Ratio) values.
5. To evaluate bearing values of spherical device in terms of basic strength parameters, i.e., cohesion, angle of internal friction and unconfined compressive strength.
6. To correlate bearing values of spherical device with modulus of subgrade reaction, obtained from plate bearing tests.
7. To investigate the use of spherical penetration bearing values in pavement and foundation design.
8. To recommend an apparatus and test procedure for use in the laboratory and the field.

II. REVIEW OF LITERATURE

A. Penetration Tests to Determine Soil Strength

The use of penetrometers in soils has its origin in hardness tests for metals. The methods most widely used in determining the hardness of metals are static indentation methods, described in detail by Bowden and Tabor (7). These involve the formation of a permanent indentation in the surface of the metal, the hardness being determined by the load and the size of the indentation formed. In the Brinell and Meyer tests the indenter consists of a hard steel ball, in the Vickers test it is a square-based pyramid made of diamond and in the Rockwell test it is a conical shaped indenter. Wedge shaped indenters (16) have also been tried to determine deformation properties of metals. Our interest in these methods is purely historical, as they precede methods used in soil mechanics for similar purposes.

The first static soil penetrometer that appears in the literature was described in 1917 and was developed by the Swedish State Railways. It consists of an auger-shaped point attached to the lower end of a solid stem. This and many other penetrometers for subsurface exploration are described by Terzaghi and Peck (43). Although the shapes of the tips and the test procedures of these penetrometers vary considerably, all are used for determining consistency and resistance to deformation of soils. The scope of our investigation is determination of strength properties of soil surfaces, so subsurface exploration penetrometers will not be discussed here.

To determine the strength properties of soil surfaces three shapes

of penetrometers are in use. California Bearing Ratio (CBR) test and Proctor plasticity needle both involve flat circular punches. Cone-shaped punches include the Housel penetrometer (18), North Dakota Cone penetrometer (8) and U. S. Army Corps of Engineers penetrometer (46). Spherical penetrometers are somewhat new in soils; the first appeared in 1954 and was used by Demirel and Enustun for pavement design. Some of the penetrometer devices will be discussed here.

1. California Bearing Ratio test

Abbreviated to CBR Test, this is an ad hoc penetration test developed by the California State Highway Department (30) for the evaluation of subgrade strengths. The load required to cause a plunger of standard size to penetrate a specimen of soil at a standard rate is measured either before or after the soil has been soaked for four days. The test has been adopted and modified by the U. S. Corps of Engineers for the design of flexible pavements(47). The latter test procedure is most widely used, although it differs slightly from the original California procedure. The test is arbitrary in that the results cannot be accurately related to any of the fundamental properties governing soil strength. Bearing strength is determined as the ratio of the penetration value of a soil to that of a standard rolled stone (13).

The CBR is essentially a punching shear test. At least two sources of error are recognized. First, the perimeter shear effect (Figure 2) is undoubtedly large because of the large perimeter of the plunger compared to its face area. Second, although the shearing strength of granular soils

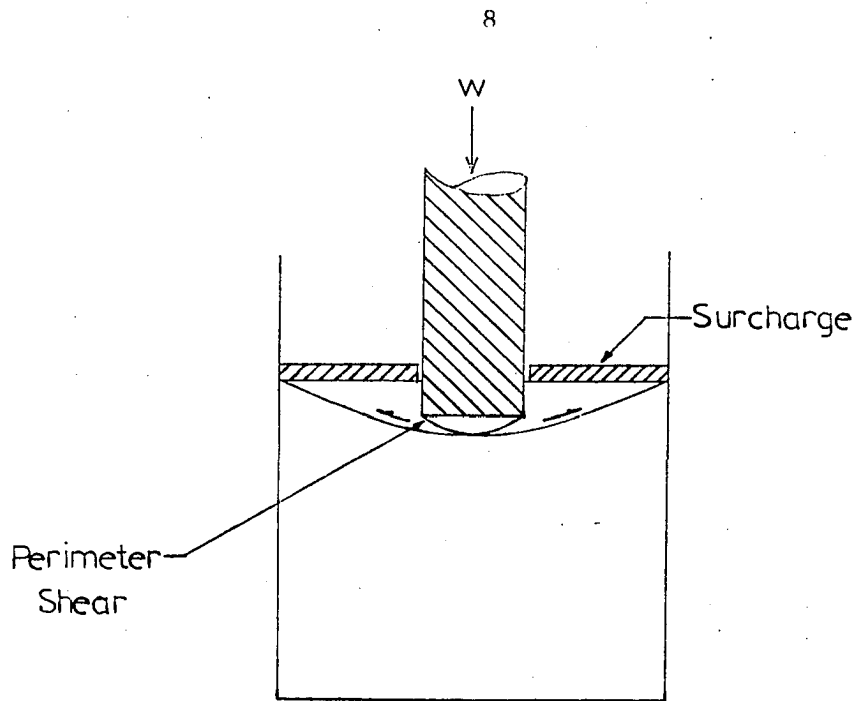


Figure 2. Failure surfaces in GBR test

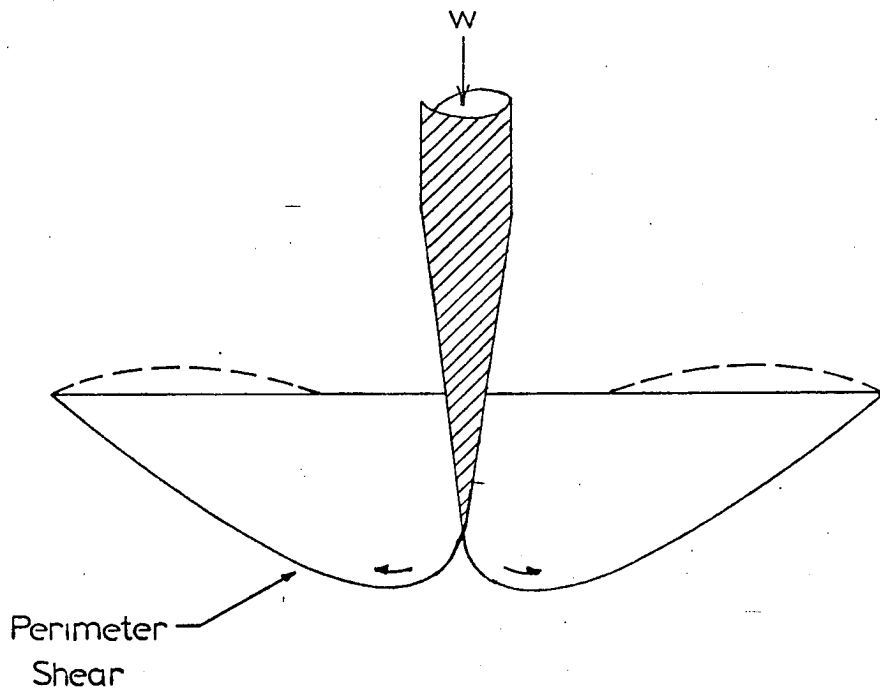


Figure 3. Failure surfaces in North Dakota cone test

is largely a function of confinement from the weight of the pavement, the large confining pressures from the walls and floor of the CBR mold have no counterpart in the field, and unquestionably influence the results. On the other hand the CBR test is more flexible than many other such tests and can be made on nearly all soils ranging from clay to fine gravel both in the field and laboratory. Since the deformation of the soil specimen is predominately a shear deformation, the CBR value can be regarded as an indirect measure of shear strength.

The limitations of the CBR test are those of any ad hoc test, viz--

- a. The test procedure must be strictly adhered to, if results are to be comparable with those previously obtained.
- b. The results only have a direct application to the method of design for which the test was designed.

2. North Dakota cone penetrometer

The North Dakota State Highway Department (8) developed a cone test for use in a pavement design method similar to that associated with the CBR. The test employs a simple apparatus which can easily be used for in-situ field tests. The test is simpler and more rapid than the CBR test, it may be made on the subgrade either in its natural state or after it has been prepared by compaction or stabilization, and it can be applied directly in an empirical method of pavement design. Although originally designed for in situ tests, the test can also be made on soils remolded in large molds such as the CBR mold.

The cone penetration test may be considered as a small scale bearing test in which the ratio of penetration to size of the loaded area is much greater than in bearing tests. The results of penetration tests are correlated with past experience of the behavior of structures on soils of similar strength, as in all empirical methods of designing the thickness of road or airfield pavements. This device in effect substitutes the cone for the shearing wedge of soil underneath a blunt-ended penetrometer. Probable shearing planes are indicated in Figure 3.

The main disadvantage of the test is that its use is restricted to fine-grained soils and reliable only for clayey soils. The presence of small pebbles within the volume of soil affected by the cone penetration has caused erratic results (33), and the tests did not appear to be reliable for use in coarser granular materials or pebbly glacial tills.

3. Spherical penetrometers

The use of a spherical penetrometer on soft engineering materials was demonstrated by Kelly (2, 21) in 1950 to evaluate the consistency of concrete. The "Kelly Ball" apparatus consists of a cylinder with a hemispherically shaped bottom and a handle, the total weighing 30 lbs. The apparatus is placed on plastic concrete and allowed to penetrate. Penetration is read when the ball comes to rest.

In 1955 Demirel and Enustun (10) used a spherical penetration device (Figure 4) for evaluation of subgrade materials in Turkey. To perform this test the subgrade was levelled and bearing apparatus placed on smooth surface. Two sizes of hard metallic spheres, namely 4.28 cm and 2.38 cm diameter were

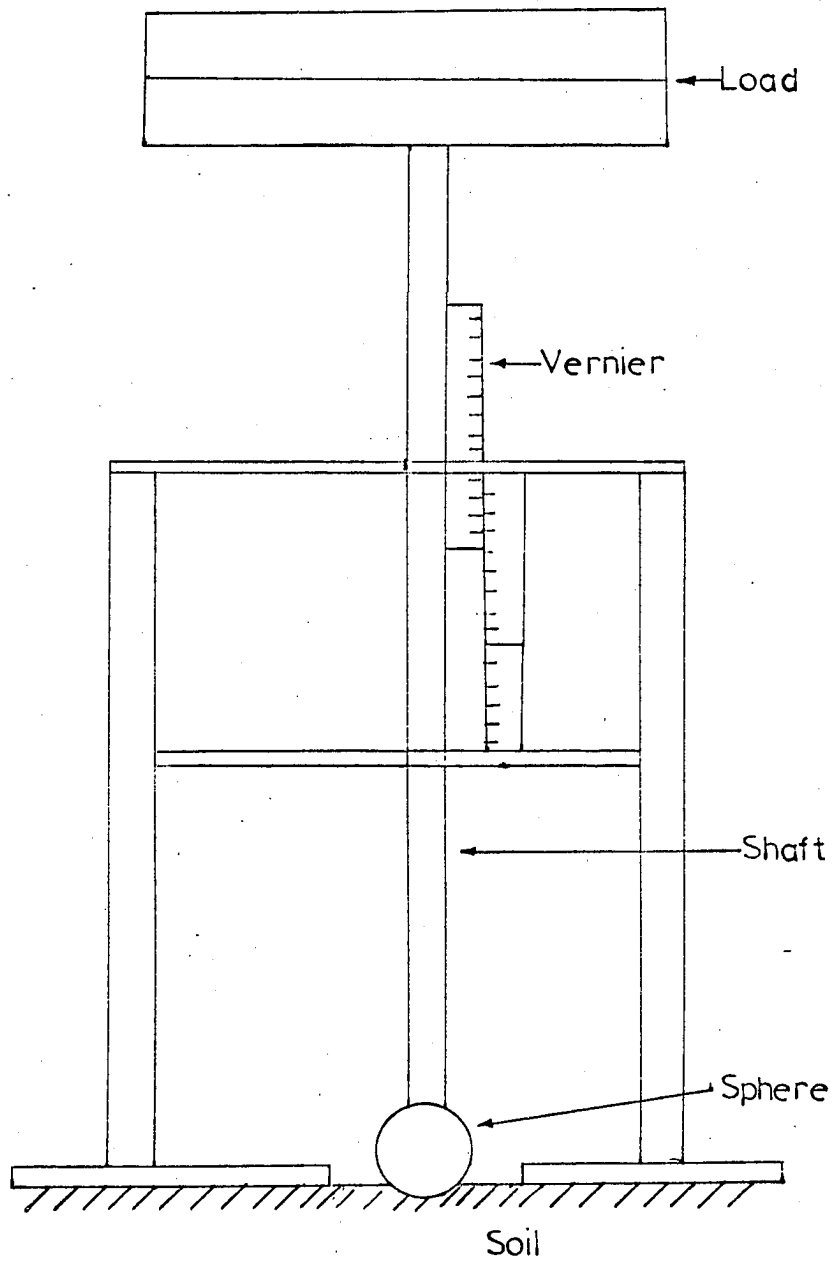


Fig. 4. Demirel's spherical penetrometer

used with a constant static load of 36 kg. Either of the spheres was placed on the subgrade and shaft head was lowered to provide a perfect contact but without developing any pressure. The apparatus was then loaded and the shaft slowly released to prevent impact. When penetration reached a constant value the reading was taken to the nearest 0.1 mm by means of a vernier scale on the apparatus. Bearing value of subgrade were determined by the formula:

$$B = \frac{W}{\pi dh}$$

where B is the bearing value, W the static load including weight of shaft, d the diameter of sphere and h the depth of penetration of sphere into subgrade. It was observed that regardless of diameter of sphere used, the ratio $\frac{W}{\pi dh}$ was constant for a location.

Tsysovitch (44) used a similar device to determine the value of cohesive forces in frozen soils. In his ball test Figure 5, a steel ball of known diameter is pressed on the soil surface by a known load. When penetration ceases the maximum depth of ball in soil is measured and value of cohesion determined by the formula

$$C = 0.18 \frac{P}{\pi DS}$$

in which P is the pressure on the ball, D is the diameter of the ball, and S is the final depth of penetration of the ball. This formula is reported to have been derived by a rigorous solution of the theory of plasticity for ideal plastic soils with an angle of internal friction less than 7° . For soils with a larger angle of internal friction a correction, M, is introduced

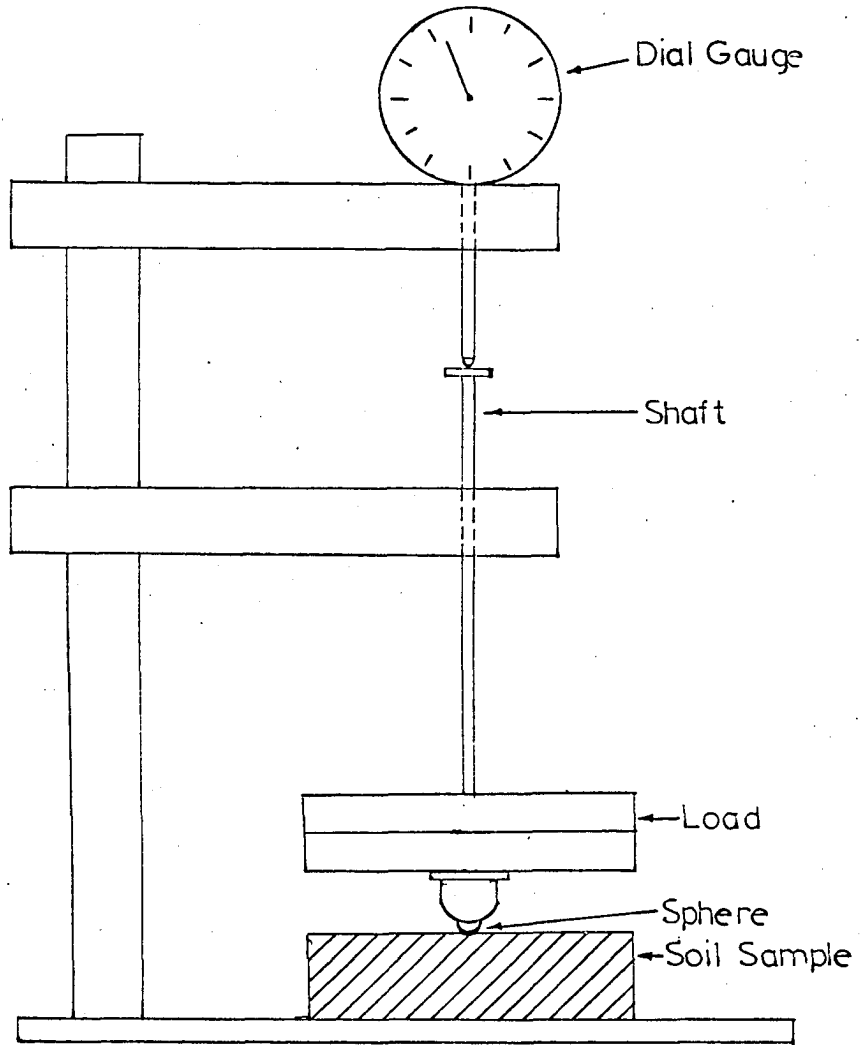


Figure 5. Tsyrovitch's spherical penetrometer

as a multiplier. The value of M is

<u>Friction angle</u>	<u>Multiplier M</u>
10°	0.61
20°	0.28
30°	0.12

Impact or drop type tests with spheres have been conducted by some soil engineers to determine bearing capacity of soils. Some testing was done at Kyoto University, Japan (26) with a view to measure the CBR-value of subgrade soil with impact type sphere test. In this test a sphere of 4.52 cm in radius and 4.07 kg in weight is dropped from a fixed height of 60 cm on a compacted and levelled surface, Figure 6. By measuring the diameter of the depression produced the CBR-value can be determined by an empirical formula. The correlation is based on the assumption that the work done by the vertical pressure of the dropped ball upon the soil is equal to the work done by the penetration of the plunger in a CBR test. The authors do not claim to have found the bearing capacity of soils in classical terms but advocate use of CBR pavement design curves with their rapid method. The laboratory tests were performed on sandy and loamy soil, but for the field tests the soil type was not given. It is assumed that the field tests were also on sandy and silty soils. It has been found (17) that whereas in cohesionless soils the rate of loading has no effect on shear strength of soils, in cohesive soils the permanent resistance is only 25 percent of the instantaneous or temporary resistance. Schimming (34) observed that apparent cohesion was approximately twice as large as that for the "rapid static test" (failure time from 30 sec to 50 sec) as in the dynamic tests

(maximum shear force attained in 1 to 5 millisecond). It would appear that for cohesive soils the empirical correlation will not be accurate in predicting the GBR values from impact penetration tests.

In 1964 tests were carried out at the Jet Propulsion Laboratory (6) in vacuum, simulating lunar surface. These tests were miniature plate bearing tests under static load. The load per unit area of plate was termed the bearing capacity, from the following formula:

$$p = \frac{P}{\pi R^2}$$

where p is the average pressure or bearing capacity at failure, P the total load and R the radius of miniature plate. Bearing capacity was found to be 5.33 times the cohesion of soils.

This analysis was applied to determine the bearing capacity of lunar surface. The Luna 9 landing capsule has spherical landing pads (20) and the first photographs transmitted were of its own pad. From this photo the depth of penetration into lunar soil was estimated, and the cross-section of the indentation determined. Static bearing capacity was then determined as simply the total mass divided by the cross-sectional area of the pads. A dynamic solution of this problem is based on energy balance and assumes that the surface is deformed by compression under a local bearing load. The dynamic bearing capacity is estimated to be 20 to 40 times the static bearing capacity. This may appear to be somewhat conservative, but if we keep in view the uncertainties regarding the shock-absorbing system used and the uncertain direction of the velocity vector at impact, this system may not be conservative.

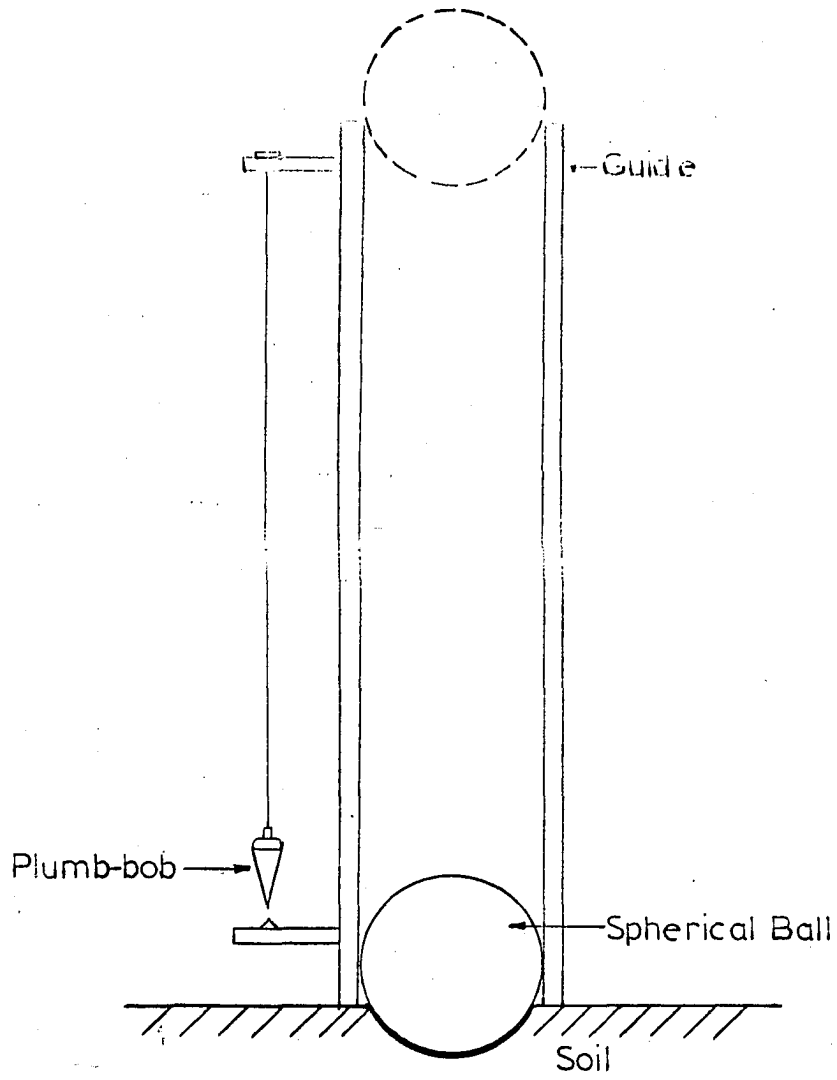


Figure 6. "Ball-drop type test" device

III. THEORETICAL ANALYSIS

In the Brinell test (40) a hard steel ball is pressed under a fixed normal load onto the smooth surface of a metal. When equilibrium has been reached the load and ball are removed and the diameter of the permanent impression is measured. The Brinell Hardness Number (B.H.N.) is then expressed as the ratio of the load W to the curved area of the indentation:

$$\text{B.H.N.} = \frac{2W}{\pi D^2 \left[1 - \sqrt{1 - \left(\frac{d}{D}\right)^2} \right]} \quad (1)$$

where D is the diameter of the ball and d the chordal diameter of the indentation.

In most cases the B.H.N. is not a constant for a given metal but depends on the load and size of the ball. In making Brinell measurements of hard materials it is customary to use a 10 mm ball and a load of 3000 kg. Intuitively it would be expected that for geometrically similar indentations, whatever their actual size, the hardness number should be constant.

If a ball of diameter D_1 produces an indentation of diameter d_1 , the hardness number will be the same as that obtained with a ball of diameter D_2 producing an indentation of diameter d_2 , provided the indentations are geometrically similar, i.e., provided the angle of indentation ϕ is the same in both cases (Figure 7). This occurs when

$$\frac{d_1}{D_1} = \frac{d_2}{D_2}$$

According to Tabor (40) the B.H.N. is not a satisfactory physical concept, for the ratio of the load to the curved area of the indentation does not give the mean pressure over the surface of the indentation. If we

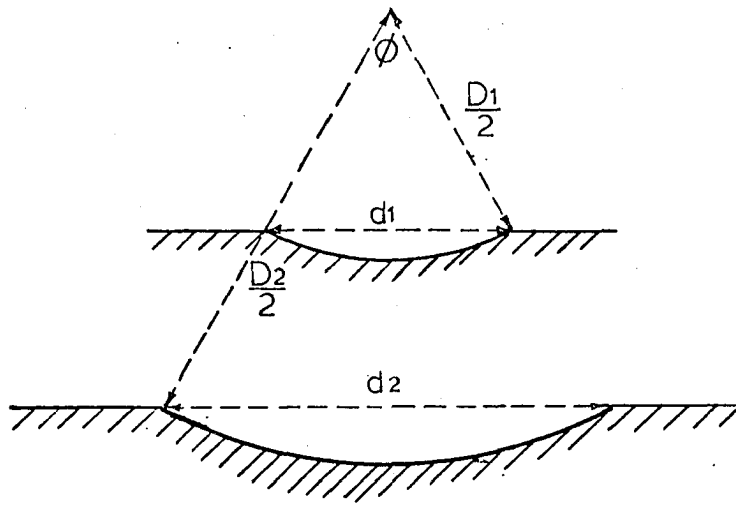


Figure 7. Geometrically similar indentations produced by spherical indenters of different diameters .

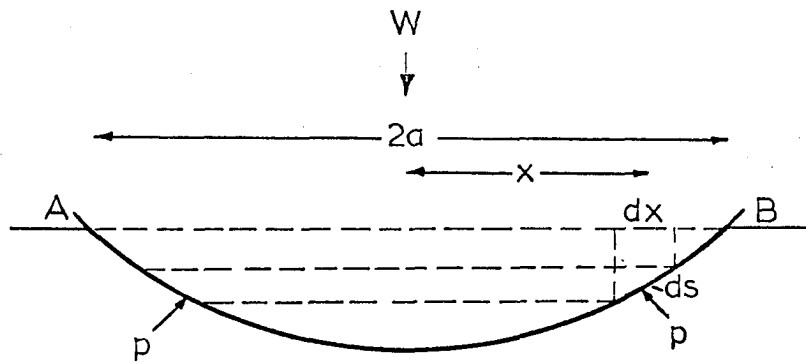


Figure 8. Calculation of mean pressure between a spherical indenter and the indentation

assume that the mean pressure is p and there is no friction between the surface of the ball and the indentation, the pressure p is normal to the surface of the indentation (Figure 8). The horizontal component of this force, by symmetry considerations, is zero, whereas the vertical component is $p \cdot 2\pi x \cdot dx$. The resultant vertical force is equal to the normal load, W , i.e.

$$W = \int_a^a p \cdot 2\pi x \cdot dx = p \pi a^2$$

where $2a$ is the chordal diameter of the indentation. Thus the mean pressure is given by

$$p = \frac{W}{\pi a^2}$$

and is equal to the ratio of the load to the projected area of indentation. This quantity is called Meyer hardness number and is expressed as

$$\text{M.H.N.} = \frac{4W}{\pi d^2} \quad (2)$$

Meyer in Tabor (40) also expressed that for a ball of fixed diameter, if W is the load and d the chordal diameter of indentation then

$$W = k d^n \quad (3)$$

where k and n are constants for the material under examination. The value of n is generally greater than 2 and usually is between 2 and 2.5. When the balls of different diameters are used, the values of k and n change. For balls of diameters $D_1, D_2, D_3 \dots$, giving impressions of chordal diameters $d_1, d_2, d_3 \dots$, a series of relations is obtained of the type

$$W = k_1 d_1^{n_1} = k_2 d_2^{n_2} = k_3 d_3^{n_3} \dots \quad (4)$$

In experimental investigations Meyer found that the index n was independent

of D but that k decreased with increasing D in such a way that

$$A = k_1 D_1^{n-2} = k_2 D_2^{n-2} = k_3 D_3^{n-2} \quad (5)$$

where A is a constant. Thus a general relation involving both d and D is

$$W = \frac{A d_1^n}{D_1^{n-2}} = \frac{A d_2^n}{D_2^{n-2}} = \frac{A d_3^n}{D_3^{n-2}} \quad (6)$$

Equation (6) can be rewritten as

$$\frac{W}{d^2} = A \left(\frac{d}{D}\right)^{n-2} \quad (6a)$$

i.e. for geometrically similar impressions the ratio $\frac{d}{D}$ must be constant and hence $\frac{W}{d^2}$ is constant. This means that both hardness numbers must be the same.

We may also write equation (6) in the form

$$\frac{W}{D^2} = A \left(\frac{d}{D}\right)^n \quad (6b)$$

which states that for geometrically similar indentations the ratio $\frac{W}{D^2}$ must be constant.

It was also stated earlier that according to Tabor (40), in most cases the B.H.N. is not a constant but depends on the load and size of the ball. This gives rise to a suspicion that the test is subject to size effect of sphere. This aspect may be analyzed here by principles of similitude and dimensional analysis as outlined by Murphy (27).

A. Application of Similitude Theory and Dimensional Analysis

Similitude involves (a) identification of variables pertinent to the studied phenomenon, (b) formation of a set of dimensionless and independent

pi terms composed of these variables, and (c) the determination of the design equations and prediction equation.

Identification of pertinent variables, which significantly affect the behavior of the system, is the most important step in model theory. The variables are generally categorized as variables of dimensions and geometry, variables of material properties, and variables of force.

In this analysis the quantity to be predicted is the ultimate mean pressure exerted by soil in contact with a sphere, and is called the dependent variable. The independent variables associated with geometry are D , diameter of the sphere; and h , maximum penetration of the sphere.

The variables pertaining to properties of soils considered pertinent to the problem include cohesion, C , and the angle of internal friction, ϕ ; these are the soil shear strength parameters which define the Coulomb failure envelope. Bulk density of the soil is designated γ and is defined as the weight of the soil plus soil water per unit volume. Other variables included are the coefficient of permeability or coefficient of hydraulic conductivity k (36), whose value depends on the size of the void spaces, which in turn depends on the size, shape and state of packing of the soil grain; and a coefficient of compressibility S , which is the slope of the void ratio-pressure curve. The variable pertaining to force considered is the applied load, W , on the sphere, which also includes the weight of the sphere.

Additional variables considered but not included in the dimensional analysis are (a) moisture content because it will be reflected in C and ϕ parameters which have already been included, (b) the coefficient of friction

between sphere and soil because it is assumed to be frictionless, and (c) thickness of soil layer because it is assumed to be homogeneous and semi-infinite.

<u>Symbol</u>	<u>Variable</u>	<u>Dimension</u>
B	Ultimate mean pressure of soil on curved surface of sphere in contact with soil	FL^{-2}
D	diameter of sphere	L
h	depth of penetration of sphere in soil	L
γ	bulk density of the soil	FL^{-3}
C	cohesive shear strength of the soil	FL^{-2}
ϕ	angle of internal friction of the soil	dimensionless
S	coefficient of compressibility of the soil	$F^{-1}L^2$
W	applied load on the sphere	F

There are 8 variables. From Buckingham Pi Theorem 6 dimensionless and independent pi terms are necessary to describe the phenomenon. The pi terms selected are:

$$\frac{BhD}{W}, \frac{h}{D}, \frac{W}{CD^2}, \frac{WS}{D^2}, \frac{W}{\gamma D^3}, \phi$$

The dependent pi term is $\frac{BhD}{W}$ and is a function of the remaining independent pi terms. The equation for prototype can be written as:

$$\frac{BhD}{W} = f\left(\frac{h}{D}, \frac{W}{CD^2}, \frac{WS}{D^2}, \frac{W}{\gamma D^3}, \phi\right).$$

A similar equation may be written for the model system, using the subscript m to designate model system variables:

$$\frac{B_m h_m D_m}{W_m} = f\left(\frac{h_m}{D_m}, \frac{W_m}{C_m D_m^2}, \frac{W_m S_m}{D_m^2}, \frac{W_m}{\gamma_m D_m^3}, \phi_m\right).$$

Since each equation refers to the same type of system, the functions are identical in form. For a true model all the design conditions as given by pi terms must be satisfied:

$$a) \quad \frac{h_m}{D_m} = \frac{h}{D}$$

$$b) \quad \frac{W_m}{C_m D_m^2} = \frac{W}{C D^2}$$

$$c) \quad \frac{W_m S_m}{D_m^2} = \frac{W S}{D^2}$$

$$d) \quad \frac{W_m}{\gamma_m D_m^3} = \frac{W}{\gamma D^3}$$

$$e) \quad \phi_m = \phi.$$

From design condition a) we get

$$h_m = \frac{h}{D/D_m} \quad (\text{Eq. 1})$$

Since model and prototype are geometrically similar, the ratio of diameters $\frac{D}{D_m}$ is the linear scale ratio, designated n . Thus h_m must = $\frac{h}{n}$ for this equation to be satisfied.

In design condition (b) since $C_m = C$, because it is the same soil then

$$\frac{W_m}{D_m^2} = \frac{W}{D^2} \quad \text{or}$$

$$W_m = \frac{W}{n^2} \quad (\text{Eq. 2})$$

In design condition (c) $S_m = S$, since it is the same soil then

$$\frac{W_m}{D_m^2} = \frac{W}{D^2} \quad \text{or}$$

$$W_m = \frac{W}{n^2} \quad (\text{Eq. 3})$$

In design condition (d) $\gamma_m = \gamma$, since it is the same soil then

$$\frac{W_m}{D_m^3} = \frac{W}{D^3} \quad \text{or}$$

$$W_m = \frac{W}{n^3} \quad (\text{Eq. 4})$$

Equations 2 and 3 suggest that load applied on the model must be $\frac{1}{n^2}$ of load on the prototype, whereas equation 4 suggests that load on model be $\frac{1}{n^3}$ of load on the prototype. Both these conditions cannot be satisfied unless $n = 1$. When $n = 1$ model and prototype are the same size, which is impractical. Therefore a distortion exists.

Design condition (e) indicates that angle of internal friction of model soil must equal that in prototype soil. This condition will be satisfied if tests are conducted in the same soil.

It will be seen that apart from conflict in equations pertaining to the loading condition, all other equations are without distortion and are satisfied. In order to ascertain a loading condition we let equations 2 and 3 govern, and

$$W_m = \frac{W}{n^2} .$$

Now these two design equations are satisfied but design equation 4 is not, since $W_m \neq \frac{W}{n^3}$.

We can satisfy this design condition by applying distorted model

theory (21) whereby a coefficient called a "distortion factor" is assigned to the unsatisfied design condition. Thus design condition (d) becomes

$$\frac{W_m}{\gamma_m D_m^3} = \alpha \frac{W}{\gamma D^3}, \text{ where } \alpha \text{ is the distortion factor. Since } \gamma_m = \gamma \text{ of}$$

the same soil and further according to equations (2) and (3) $\frac{W_m}{D_m^2} = \frac{W}{D^2}$,

then $\frac{1}{D_m} = \alpha \frac{1}{D}$, or $\alpha = \frac{D}{D_m}$, and $\alpha = n$. Thus if the diameter of the model is $\frac{1}{2}$ the diameter of prototype, the distortion factor is 2.

The prediction equation for true models in this phenomena is

$$\frac{BhD}{W} = \frac{B_m h_m D_m}{W_m} \quad (\text{Eq. 6})$$

Since distortion is assumed to exist in loading conditions, the prediction equation is modified to:

$$\frac{BhD}{W} = \int \frac{B_m h_m D_m}{W_m}$$

where \int is the prediction factor. Since $W_m = \frac{W}{n^2}$ (loading condition), then $B = \int B_m$ or $\int = \frac{B}{B_m}$. If $\int = 1$ no distortion exists.

To confirm this experimentally, three specimens of loess were compacted at different moisture contents and with different compactive efforts in CBR molds. Three sizes of sphere diameters were selected; a sphere 0.75 in. in diameter was considered the prototype, and spheres 0.562 in. and 0.50 in. in diameter were considered the models. On each specimen three tests were run, one with each sphere, under similar conditions. Results of these tests are plotted in Figure 9 as load vs. area of sphere in contact with soil. It will be seen that apart from some scatter the size of the sphere does not seem to influence the result.

According to the loading condition of equations 2 and 3,

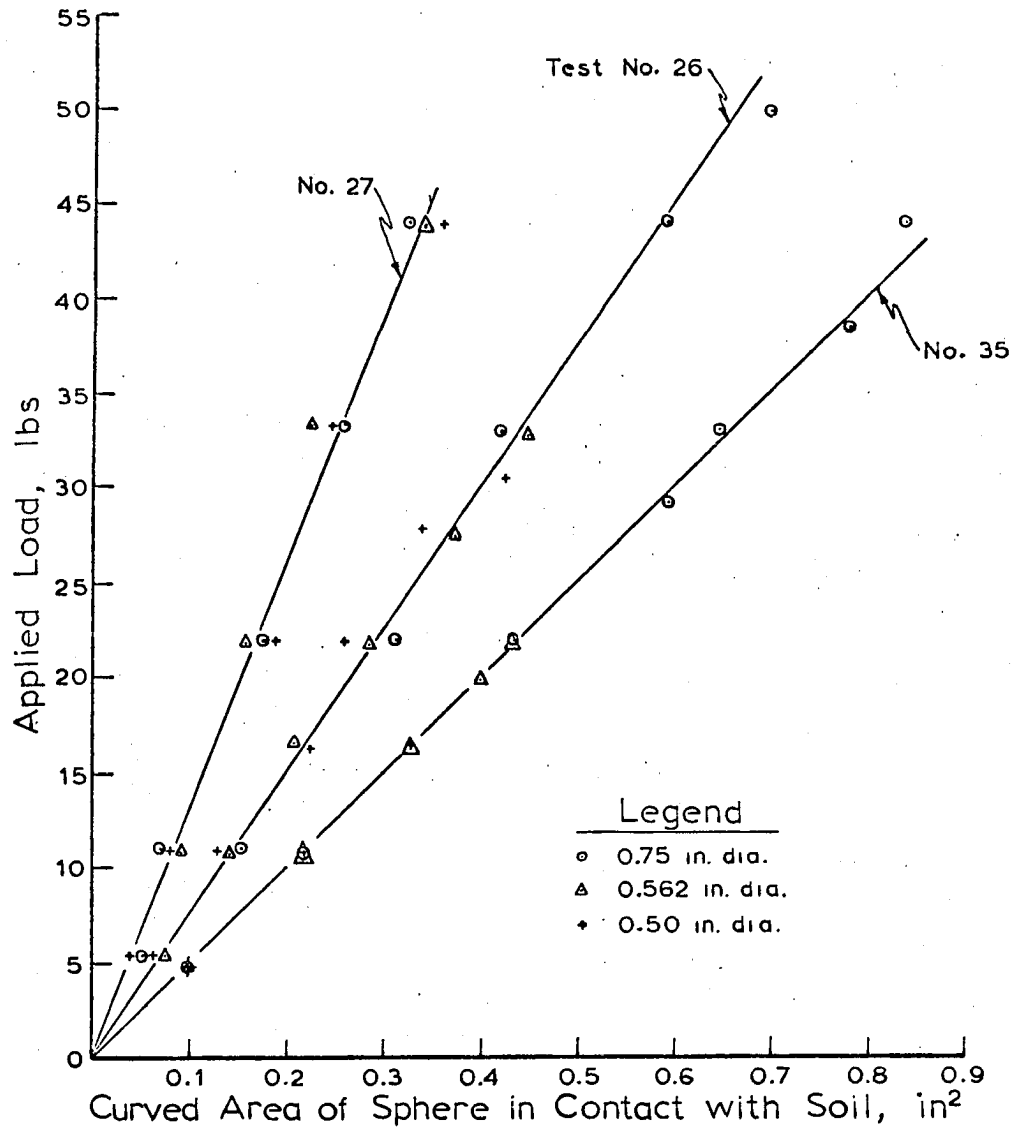


Figure 9. Relationship between load and curved area of sphere in contact with soil for three soil specimens. On each specimen tests were performed with three different sizes of spheres

$$\frac{W_m}{D_m^2} = \frac{W}{D^2}$$

From the experimental results

$$\frac{BhD}{W} = \frac{B_m h_m D_m}{W_m}$$

and

$$\frac{B_m}{B} = \frac{hD/W}{h_m D_m / W_m}$$

$$\text{Let } B = \frac{W}{hD} \text{ and } B_m = \frac{W_m}{h_m D_m};$$

then prediction equation 6 becomes $1 = 1$, which is satisfied. Therefore the choice of loading assumed is reasonable. Now, experimental results show that

$$\frac{W}{AhD} = \frac{W_m}{Ah_m D_m} \quad (\text{Eq. 7})$$

By definition $B = B_m$ and the imposed loading condition is reasonable.

This analysis confirms that there is no effect of size of sphere in testing of cohesive soils.

1. Size effect in plate bearing tests

Whereas it has been shown that there is no size effect in spherical testing device, the same is not true in plate bearing tests. In determining the modulus of subgrade reaction with various sizes of plates, Stranton (38) has drawn a curve showing effect of diameter of bearing plate on the modulus of subgrade reaction (Figure 10). This curve is in part a straight line and in part an exponential function which shows that the length scale is not the only cause of distortion; distortion may also be a function of perimeter/area ratio, variable soil pressure, and warping of the plates

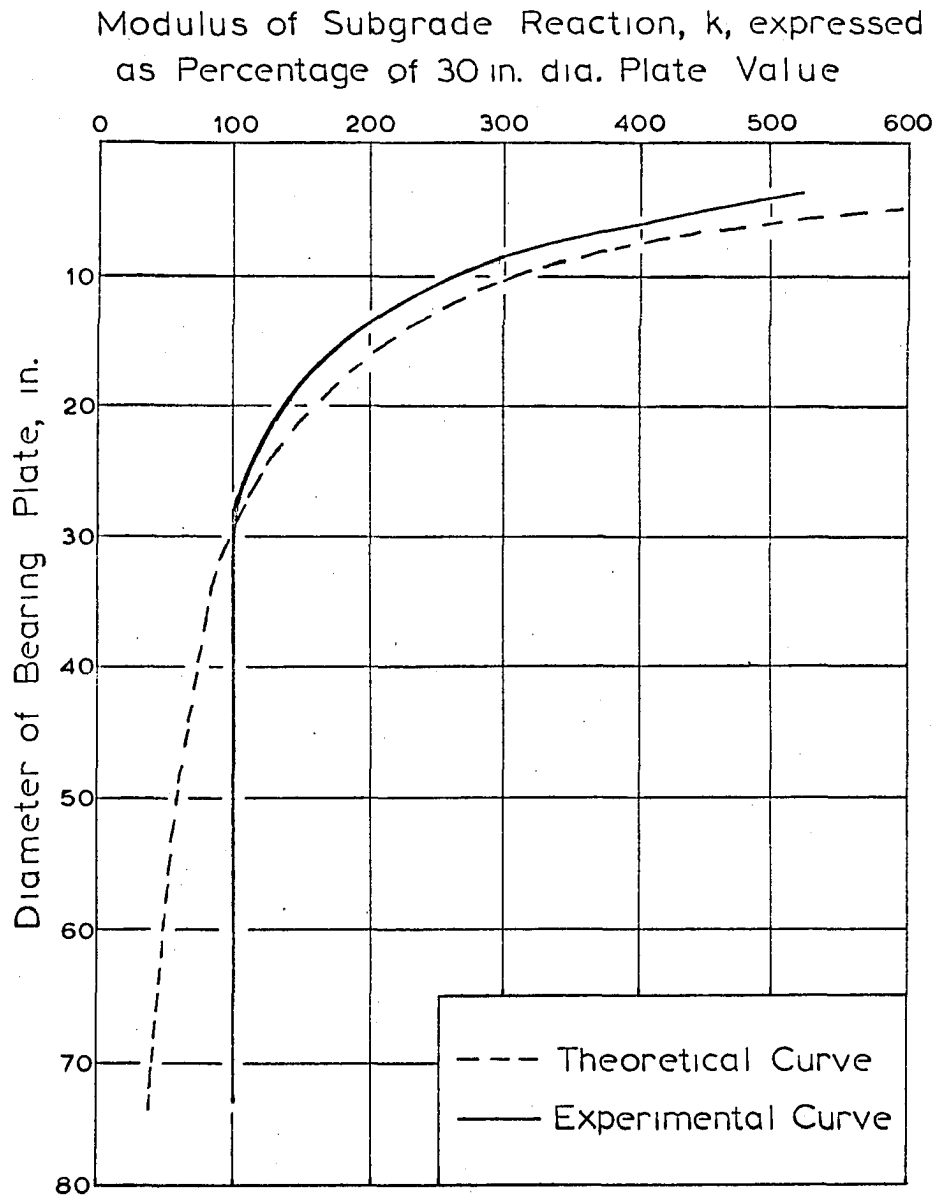


Figure 10. Relationship between modulus of subgrade reaction and diameter of bearing plate

under loads.

Taylor (41) in his discussion of size effect of such tests states that both the settlement and load intensities which cause settlement are somewhat proportional to size but vary considerably due to many other influencing factors.

Distortion in plate bearing tests has also been demonstrated by use of similitude by Kondler (22) and Goodman (12). Goodman concluded that to perform a dimensional analysis an experimental relationship would have to be developed for each soil of interest, and that the relationship for various sizes of plates cannot be reduced to a single curve for a given plate geometry.

B. Development of Classical Bearing Capacity Theory

Classical bearing capacity theories in soil mechanics are modifications of theories of plastic deformation of metals. The shape of the deformation zone or plastic flow zone plays an important role in interpretation of these theories for our purpose. It is therefore essential to investigate shape of the failure surfaces and determine their influence on bearing capacity of soil surface.

The problems of deformations of metals were studied by Prandtl (1920), Hencky (1923), Ishlinsky (1944) and some others. Their analysis is too involved to give here, but we may summarize descriptively their conclusions without attempting a rigorous proof.

1. Deformation of a flat punch

This analysis is the basis for determining ultimate bearing capacity

of a strip footing with infinite length.

According to Prandtl and Hencky, when a load is first applied to a flat rectangular punch, the shear stresses at the edge of the punch will be very high; consequently even for a small applied load these regions will be in a state of incipient plasticity. As the load on the punch is increased the whole of the material around the punch is in a state of plasticity and the indenter begins to penetrate. Figure 11 shows the slip line pattern which satisfies the plastic equation. Because friction between the punch and the surface of the material is assumed to be negligible, the slip lines are at 45° with the face of the punch. The region in which material is flowing plastically is defined by the boundary ABC. When the load is increased a conical wedge with an apex angle of 90° is assumed to be formed directly below the punch and is forced into the material. At this stage full-scale plastic flow and consequently indentation occurs. The normal pressure is assumed to be uniform over the face of the punch and is given by:

$$p = 5.14 k$$

where k is a constant for a metal.

It will be observed that the assumed slip lines of this conceptual model and analytical solution have been adopted by Terzaghi (42) for determining the ultimate bearing capacity of continuous footings with a smooth base for conditions of local shear failure. The equation for ultimate bearing capacity per unit of area is:

$$q_D = 5.14 C,$$

where C is the cohesion of the soil. This example also demonstrates that ultimate bearing capacity of soil is analogous to mean pressure at the instant of full-scale plastic flow in metals.

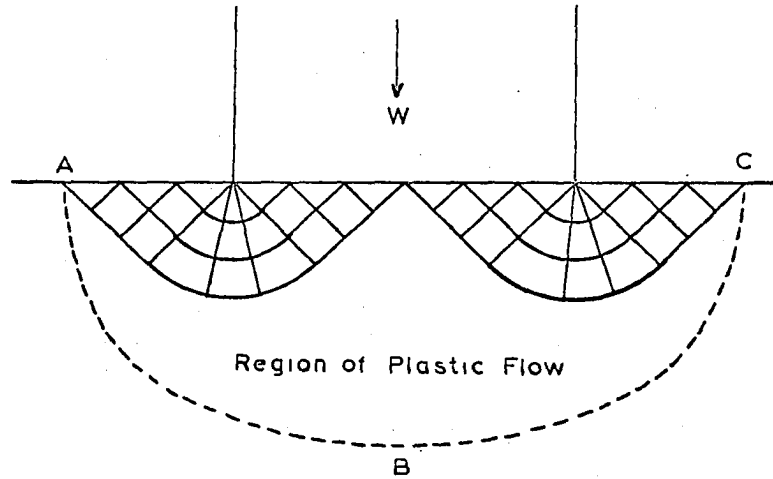


Figure 11. The slip-line pattern in an ideally plastic metal deformed by a flat punch when large scale deformation occurs. Plain strain (Hill, 1950)

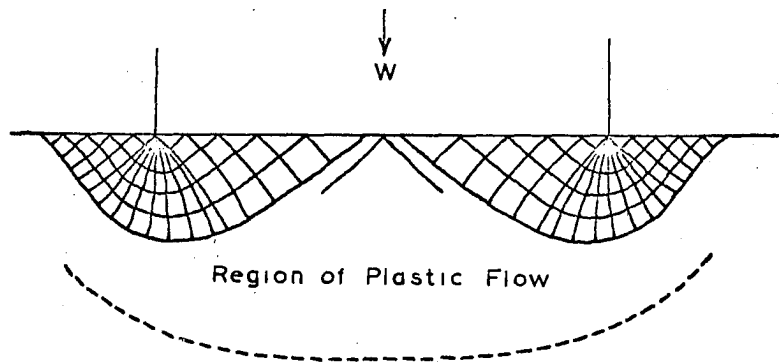


Figure 12. The slip-line pattern for a flat circular punch penetrating an ideally plastic material. The broken line is an approximate representation of the elastic plastic boundary, corresponding to the line ABC in Figure 11.

In a manner similar to the one outlined above, Hencky (1923) and more recently Ishlinsky (1944) have shown that the pressure of a circular punch to penetrate the surface of a metal is of the order of

$$p = 5.2 k \text{ to } 6 k.$$

The slip line pattern obtained by Ishlinsky (19) is shown in Figure 12. This technique of limiting equilibrium has been made use of by Sokolovsky (35) and Harr (15) in determining the ultimate bearing capacity of soil. Terzaghi, however, uses the following empirical relation to determine the ultimate bearing capacity of a smooth circular footing on a purely cohesive soil:

$$q_D = 1.3 (5.14C) .$$

We will now examine state of stress and strain and pattern of slip lines under a spherical indenter in metals to determine its application to soils.

2. Deformation by a spherical indenter

When load is applied to a spherical indenter the region of contact with the metal is a spherical zone. As the load on the indenter is increased the amount of plastic deformation around the indentation increases and the mean pressure steadily rises until the whole of the material around the indentation is in a state of plasticity. It is not easy to define the stage at which this occurs, and the simplest approach is to assume that the stage of full plasticity is reached when the plastic slip-line field covers the whole of the region around the indenter. The slip line pattern obtained by Ishlinsky is shown in Figure 13 and the pressure distribution is in Figure 14.

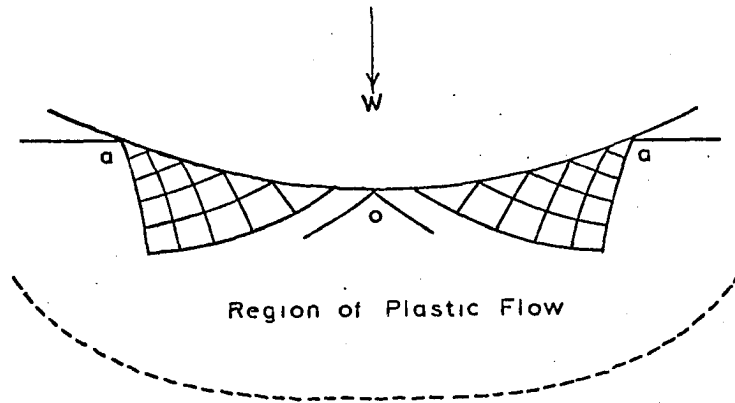


Figure 13. Part of the slip-line pattern obtained by Ishlinsky for a spherical indenter deforming an ideally plastic metal. The broken line is an approximate representation of the elastic plastic boundary, corresponding to the line ABC in Figure 11

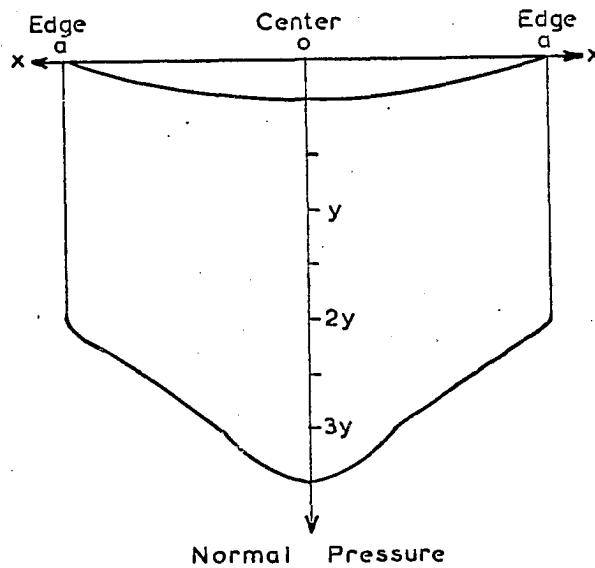


Figure 14. Pressure distribution over the indentation formed by a spherical indenter in an ideally plastic material of constant yield stress Y

The pressure over the surface of the indenter is not uniform over the region of contact but is somewhat higher in the center than at the edges. However the mean pressure, that is the load divided by the projected area, has a value of about $2.66 Y$, where Y is the constant yield stress of the material (analagous to unconfined compressive strength of soils). Tabor states that based on experimental data the condition of full plasticity is reached at mean pressure of the order of $3Y$, which he calls the yield pressure.

In here it is seen that the classical bearing capacity theories are adaptations of theories on deformation of metals, based on similarities of deformation zones. It is also apparent that a functional relationship exists between mean pressure and strength characteristics of materials. Let us, therefore, examine the shape of deformation zone under a spherical indenter in soils.

IV. MODEL INVESTIGATION OF THE DEFORMED ZONE UNDER A SPHERICAL PENETROMETER

The preceding theoretical treatments of bearing capacity necessarily assume idealized conditions: the soil is rigid-plastic, i.e., no significant strains occur until rupture occurs, and a boundary exists which has plastically deformed. Equations and calculations are therefore valid and reliably accurate only to the extent that these two assumptions are approximately satisfied. Therefore regardless of the rigor of mathematical solutions, the calculated form of the rupture surface curve may not be a true one. It is, therefore, not surprising to find that when plastic theory is applied to soils it does not provide a completely satisfactory explanation of the deformation pattern. It is also important to realize the general limitation of approximate calculation methods developed by Terzaghi and others, who empirically modified the mathematical methods to fit more closely to observed values.

The basic requirement for an understanding of the deformation mechanism is a knowledge of the pattern and extent of the deformed zone. We therefore attempted a non-quantitative verification of assumptions through a study of the modes of deformation and patterns of behavior of various soils, the existing rupture zones and other effects not predicted by the theory or mathematical models.

A. Experimental Methods

It was recognized that penetration of a sphere is a three-dimensional problem where symmetry exists on any plane which includes the central axis.

Model tests could be performed photo-elastically if the planes were easy to isolate. An easier alternative was to view the deformation zone in a vertical section along a diameter cut through the center of indentation and normal to the indented surface.

Two techniques were used to determine the pattern of the deformed zone. In the first, specimens were molded in Proctor molds at standard Proctor compaction. Various moisture contents were used for loess and clay soils, but for sand only dry specimens were molded. A line was inscribed on the top of each Proctor-size specimen, at intervals of 1 cm, and the specimen height measured at those points. A steel ball of 0.75 in. diameter was placed at the center and loaded with increments of 10 lbs. Penetration of sphere, after each increment, was recorded when it reached a state of equilibrium. After the test, the load and ball were removed from the specimen and height of the specimen at each point along the line was again measured and recorded. From the two measurements the change of elevation of the surface of the specimen was obtained. Elastic rebound at the point of indentation was obtained by measuring depth of indentation after removal of load and sphere. Any hair cracks that appeared on the surface of the specimen were examined under a magnifying glass and their length measured with vernier calipers.

In the second technique, specimens were molded by static compaction in a heavy steel mold used for ASTM Flexure Beam test (3). The specimen 3 by 3 by $11\frac{1}{4}$ in. long was transferred to a steel box the same size but having a detachable, $\frac{3}{4}$ in. thick, long Plexiglass front. Before attachment of the front, a grid was scratched on the face of the specimen and small ball-

bearings were embedded at the intersections. Since ball bearings could be located with considerable accuracy before and after deformation, it was possible to estimate the amount and direction of the displacement of each intersection. The Plexiglass wall was then bolted in position to contact the specimen. A lubricated hemisphere was placed with its flat surface against the Plexiglass, in contact with the top of specimen. The sphere was then loaded, and 1 sec. time exposure photographs were taken at no load (for reference) and at various stages during the process of deformation under each applied load. This technique does not have a very high sensitivity for detecting deformation quantitatively and a zone of lesser deformation could exist undetected on the photographs.

B. Deformation Analysis

1. Deformation mechanism in silt

The optimum moisture content at standard Proctor density for the loessal silt used in these specimens was 18%. Diagram 1 shows how the deformation characteristics change with moisture content; at a moisture content well below optimum no change of height of the specimen surface was observed, except at the point of indentation. Radial hair cracks appeared on the surface of specimen, their length increasing with increasing applied loads. The diameter of a hypothetical circle joining the extremities of these cracks was measured with vernier calipers and found to be $2.56 d$ to $2.80 d$, where d is the diameter of the indentation. Elastic compression varied between 8 to 11% of the total depth of indentation of sphere in the specimen. In this range it was observed that load vs. penetration initially showed a straight line relation, but as the load increased the line curved upwards

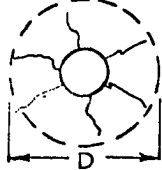
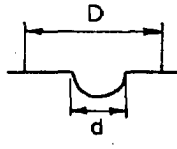
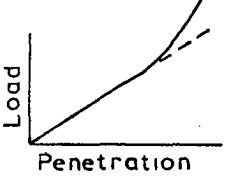
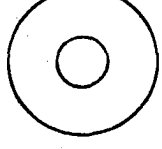
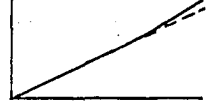
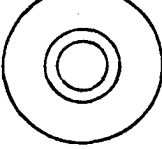
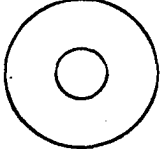
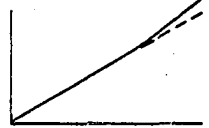
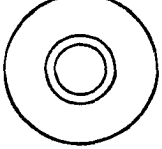
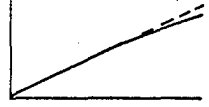
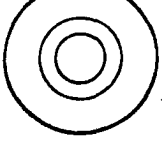
Moisture Content %	Deformation		$\frac{D}{d}$	Elastic Compression % of total	Load Penetration Curve
	Plan View	Section			
<u>Silt (Loess 20-2): Optimum Moisture Content-18%</u>					
11-14			2.5 to 2.8	8-11	
15-19			3.0 to 3.5	10-15	
20-24			3.0 to 3.5	10-14	
<u>Clay: Optimum Moisture Content-30%</u>					
26-30			2.5 to 3.0	8	
30-34			2.5 to 3.0	11	
36-40			3.2 to 3.3	12	

Diagram 1. Deformation characteristics of silt and clay

showing increased resistance of soil to penetration.

At moisture contents between 15 to 19%, no radial cracks appeared, and the surface of the specimen around the indentation showed a decrease in height. The area thus affected could be enclosed with a circle of diameter $3d$ to $3.5d$. Close to the optimum moisture content, concentric rings of cracks appeared around the indentation, new rings forming progressively outwards as the load increased. The slope of the load vs. penetration curve was similar to that observed at lower moisture contents, and the elastic recovery ranged between 10 to 16 percent of total settlement of sphere.

At moisture contents well above optimum there was another change in deformation characteristics. First, the load vs. penetration curves sloped downward and second, a raised lip of soil was formed around the sphere. The diameter of the raised surface was 2 to 3 times d , the diameter of the indentation.

Two specimens molded at optimum moisture content were subjected to very high loads. Initial load increments showed a straight-line relation which corresponds to 0-a in Figure 15; then during the next increments the line curved upwards (a-b) showing an increased resistance of the soil to penetration. At still higher loads the curve was erratic (b-c) until finally the sphere suddenly disappeared below the surface. These stages can roughly be termed state of equilibrium, compaction of soil, incipient failure, and final rupture when shear strength of soil is completely exhausted.

Figures 16 and 17 show the deformations in a vertical plane in loess molded at 16% M.C. In Figure 16, a, b, and c it will be observed that the deformed area of the grid is approximately semicircular with a center on

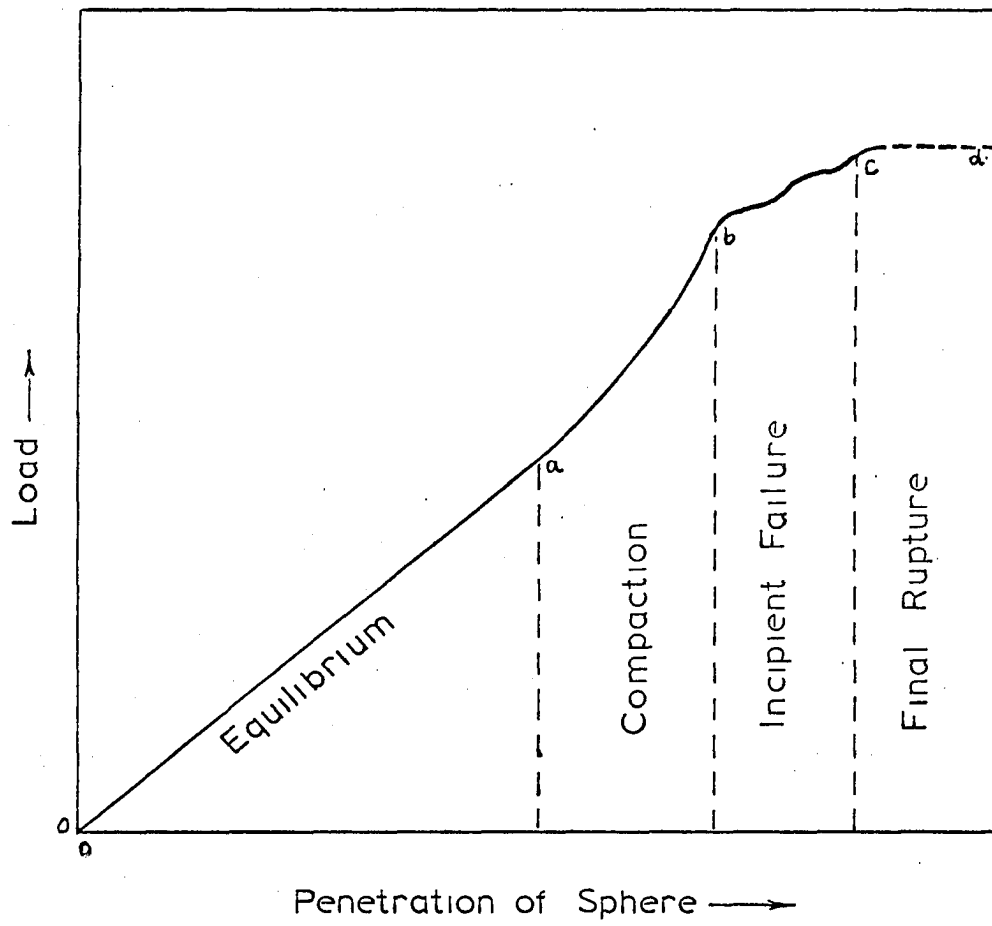
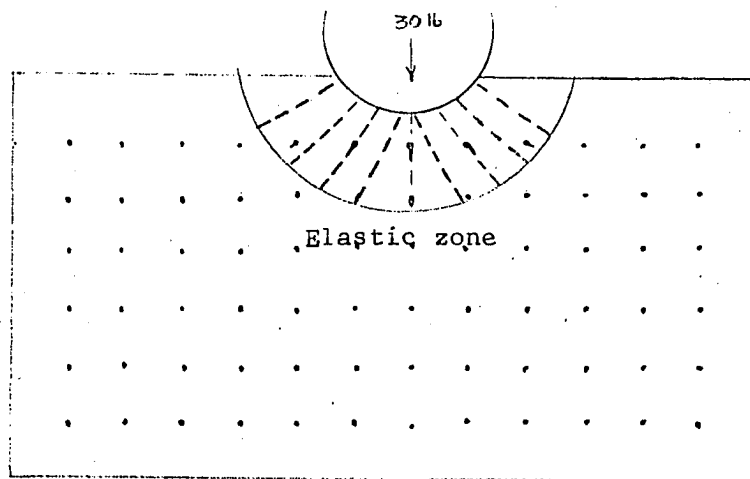
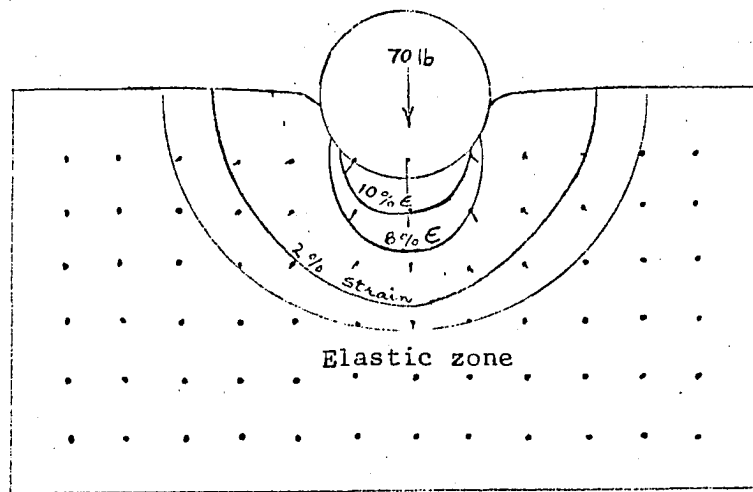


Figure 15. Stages of deformation process of soil

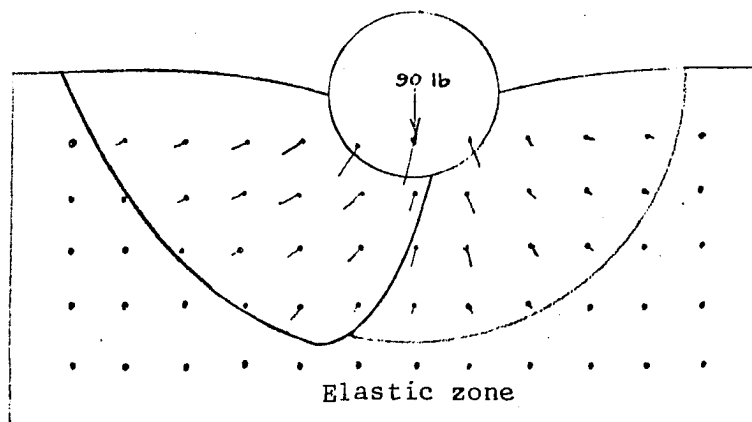
Figure 16. Stages of deformation in silt (a) the dotted lines are the flow lines (b) semicircular deformed area and strain contours (c) incipient failure conforming to one wing of a Prandtl deformation boundary



(a)



(b)



(c)

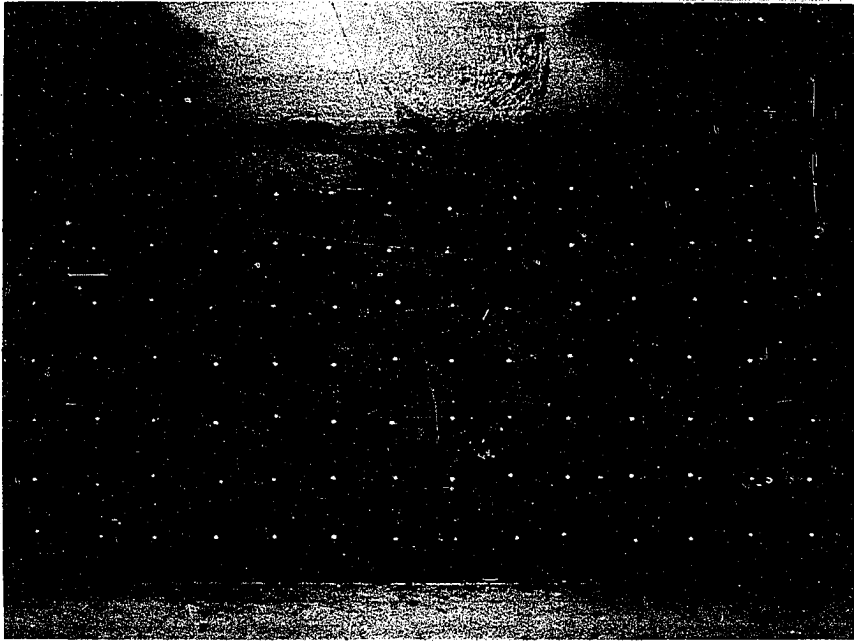


Figure 17 (a). Radial compression in silt at 35 lb applied load

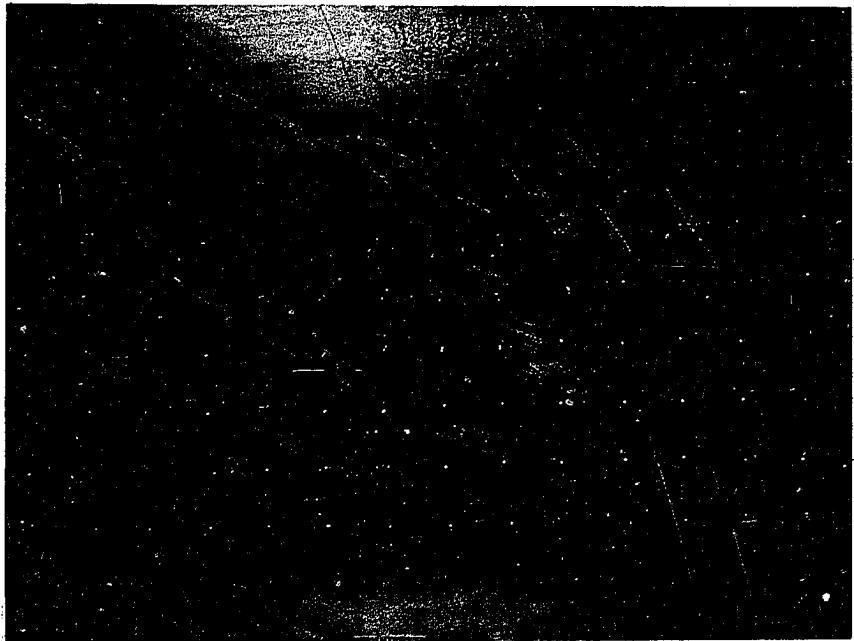


Figure 17 (b). Incipient failure in silt at 70 lb applied load

the axis of the indenter. The dotted lines in Figure 16a are the flow lines, indicated by movements of the spheres during the time exposure photographs. In Figure 16b percent strain boundaries are sketched in. The percent strain was measured and contoured; high-strain contours are nearly elliptical near the ball, merging gradually into an approximately circular plan at greater depths. The elastic-plastic boundary was sketched to enclose all detected movement.

Figure 16c, an eccentric zone of compression has emerged, conforming to one wing of a Prandtl deformation boundary. We may assume that shear failure is incipient, but it is compounded with eccentric compression. In both figures, 16b and c, the free surface of soil is depressed. If D is the diameter of the no-strain (or elastic-plastic) boundary, then the ratio $\frac{D}{d}$ varies from 2.5 at 30 lb load (Figure 16a) to 2.8 at 70 and 90 lb. Similarly the ratio of curved area formed by elastic plastic boundary and sphere in contact with soil ranges between 6.7 to 7.4. These values are in close agreement with observation in the first series of tests.

2. Deformation mechanism in clay

The optimum moisture content of the clay at standard Proctor density is 30%, and specimens were molded with moisture content ranging from 26% to 40%. Specimens molded below 26% had to be discarded because of honeycombed texture.

The surface geometry was almost identical to that observed in silt at ranges of moisture content around the optimum as shown in Diagram 1. At very high moisture contents (i.e. 36 to 40%) the lip of soil around the sphere is more rounded and plastic compared to that in silt. The ratio $\frac{D}{d}$

is approximately 3. However, the difference appears in load vs. penetration curves at moisture contents below and close to optimum, in that the curve deviates very little from straight line even at higher loads. A hypothesis to explain this difference is that since the silt is highly permeable, initial increments of load consolidate the soil and make it resistant to penetration; since the clay is relatively impermeable, higher loads do not cause compaction to the same extent.

Figures 18 and 19 show deformations in a vertical plane in the clay sample molded at 30 percent moisture content. The pattern of deformation in Figure 18a is again radial, with a hemispherical elastic-plastic boundary; the curved area ratios is 6.6.

Figures 18b and 19b show a failure pattern which can be approximated to Prandtl type failure zones. However, below the failure zone, a zone of radial compression extends up to the elastic plastic boundary. There is also bulging of the free surface adjacent to the sphere.

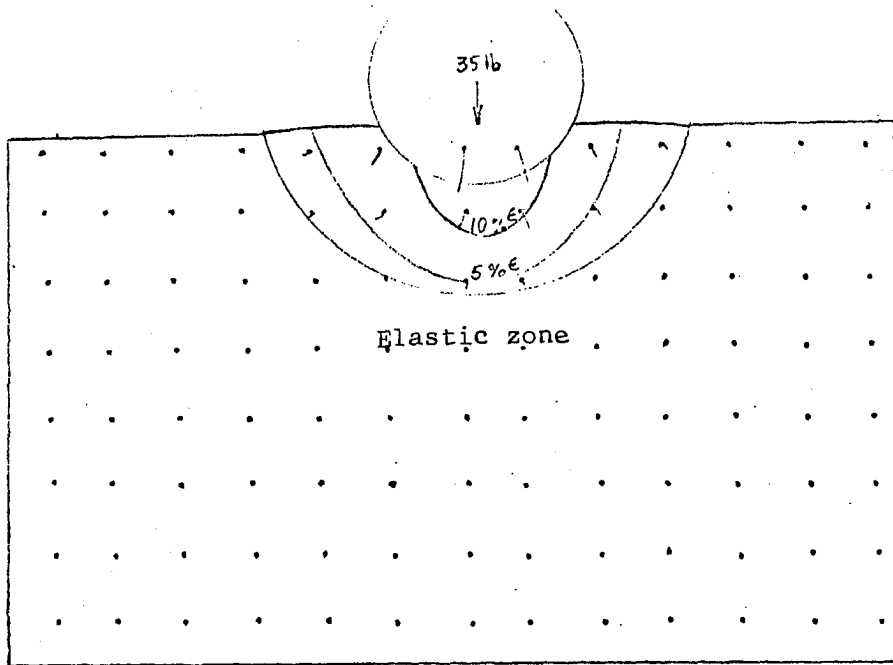
3. Deformation mechanism in sand

Dry compacted sand was used in both type of tests. Because of weakness of the sand it was not possible to take an initial zero reading, and therefore observations were entirely qualitative.

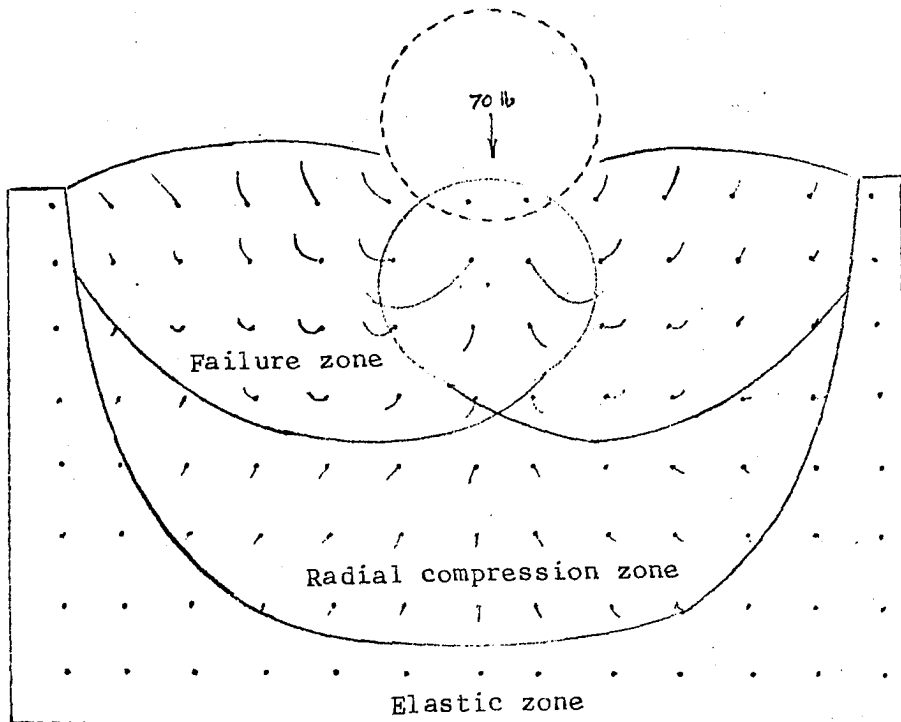
As seen in cross-section, the sand particle movement initially was vertically downward; then as settlement of the sphere increased, the soil was displaced laterally along slip surfaces. These slip surfaces curved upward to reach the free surface of soil around the sphere and form a mound, as seen in Figures 20 and 21. The rupture surfaces are curved, and sliding

Figure 18. Stages of deformation in clay (a) radial compression (b) Prandtl type failure zones and zone of radial compression which extends up to the elastic plastic boundary

47b



(a)



(b)

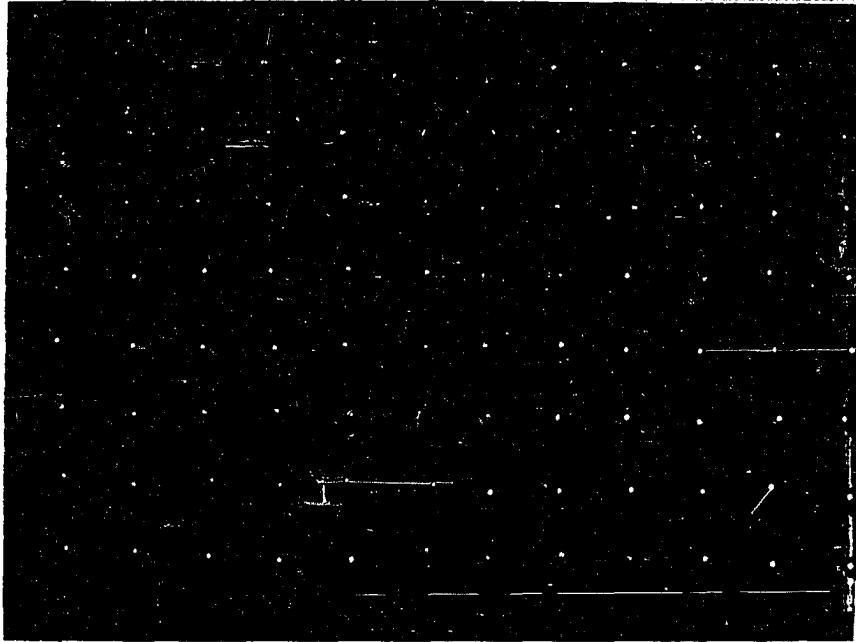


Figure 19 (a). Radial compression in clay at 15 lb applied load

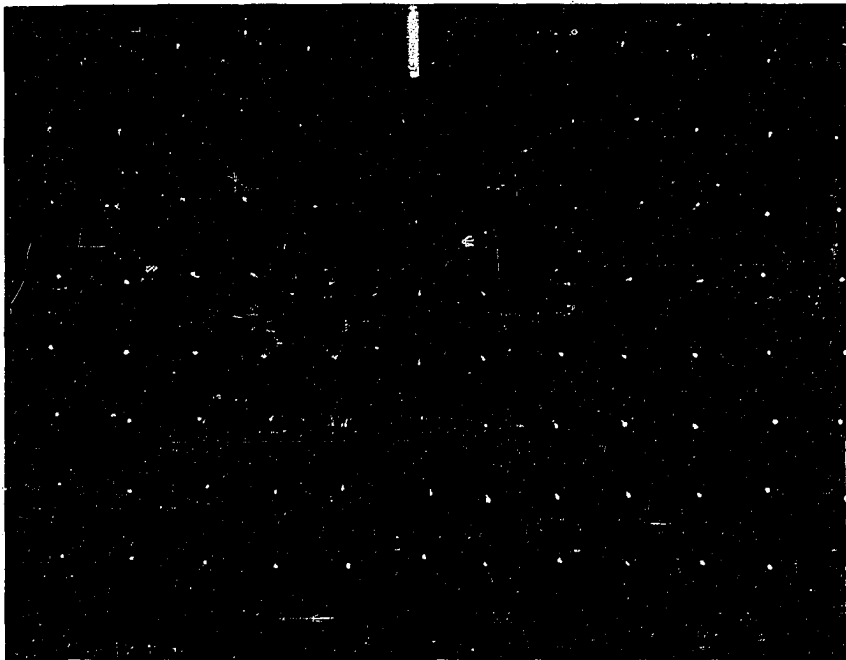
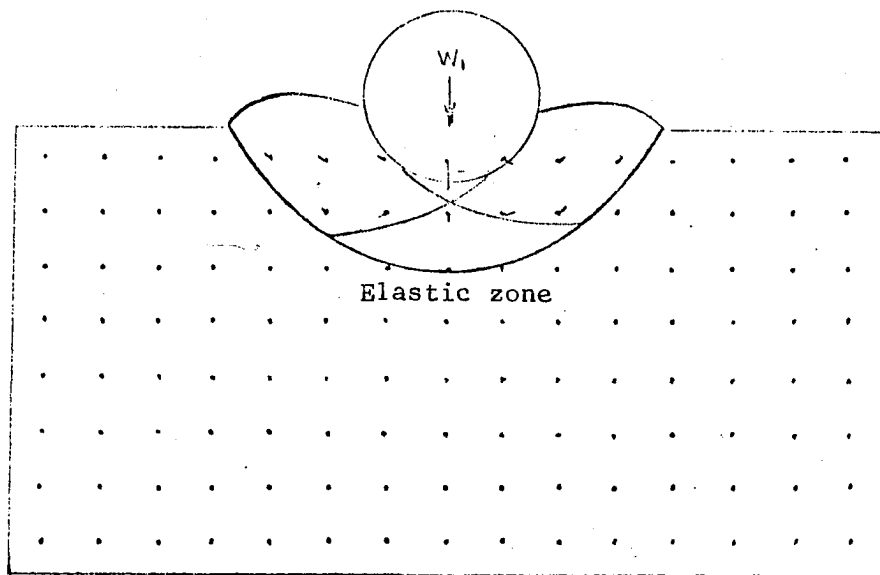
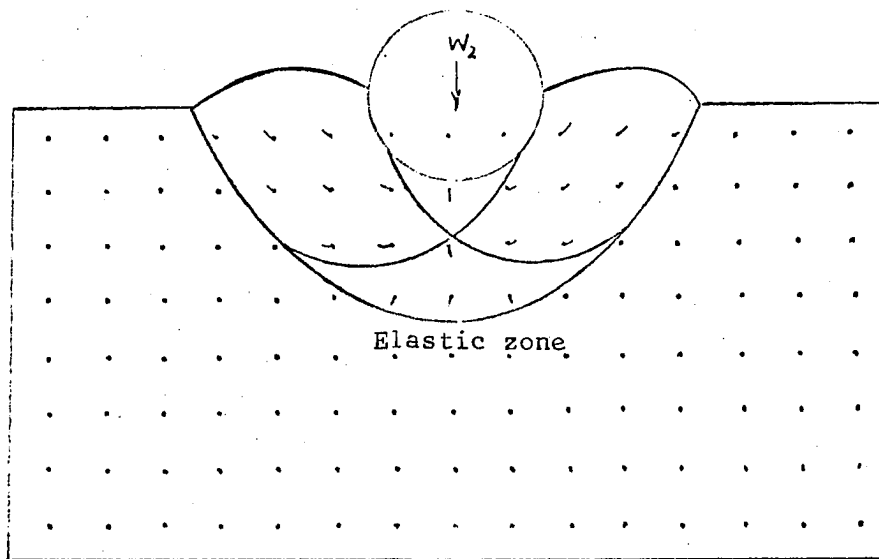


Figure 19 (b). Prandtl type failure in clay at 70 lb applied load



(a)



(b)

Figure 20. Deformation boundaries in sand with increasing applied loads. Rupture surfaces are curved and sliding takes place in a rotary motion

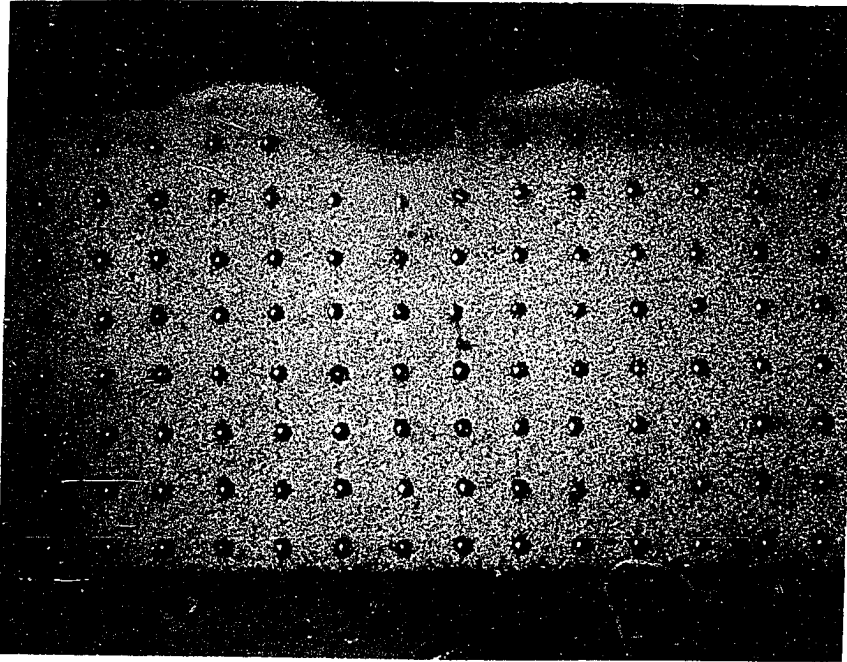


Figure 21 (a). Curved ruptured surfaces in sand

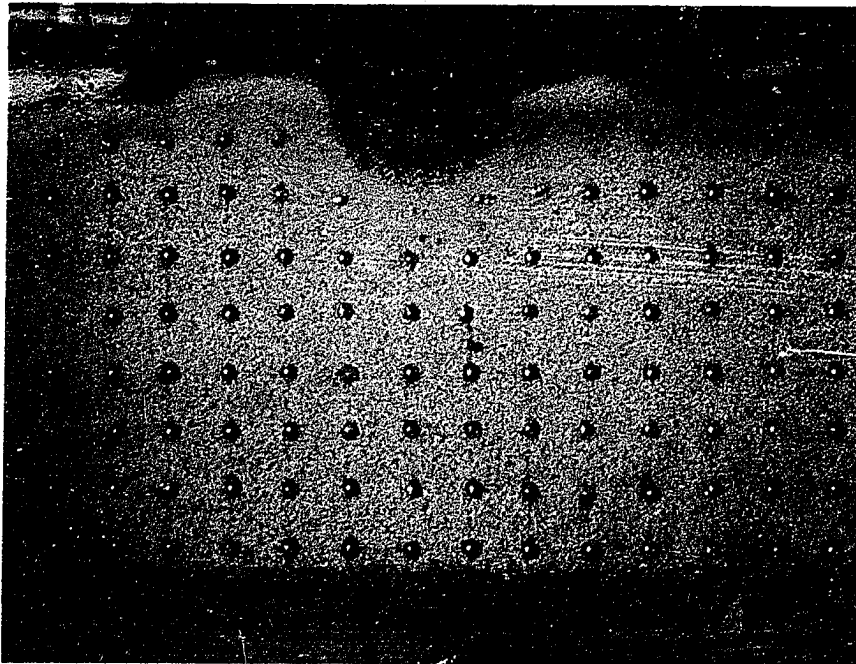


Figure 21 (b). Sliding in sand is in a rotary motion

takes place in a rotary motion. Approximate failure planes and elastic-plastic boundaries are sketched in Figure 20 (a) and (b). It will be observed that as the load on the sphere increased, the length of the cone below the sphere also increased. As in clay, there is a zone of compression between elastic-plastic boundary and the shear surface.

4. Discussion

All the experimental evidence obtained in this investigation supports the conclusion that the deformation mechanism which operates during penetration of a soil mass by a spherical penetrometer approximates the following two stages:

1. Compression of soil
2. Rupture of soil by plastic flow.

Prior to application of load on the soil surface the soil mass is in elastic equilibrium. When the load is applied on a sphere, there is a uniform radial displacement and compression of soil which brings about a change in volume by densification. In permeable soil the decrease in volume is rapid and results in downward deflection of the surface of the specimen around the indenter. Densification in turn causes a decreased porosity and an increased resistance to penetration. We may note that in the theoretical treatments it is assumed that the material is incompressible and there is no volume change throughout the process of deformation.

The mechanism of deformation may be regarded as essentially compression of a set of concentric hemispherical shells, except in a region very close to the sphere. It is probable that in these regions, large deformations occur in a restricted zone to form a cap of dead soil. Outside this

cap, the irregularities of strain are rapidly smoothed out and an approximate uniform radial strain is produced.

The onset of plastic flow is preceded by irregular settlement under increasing load. In some cases the curved rupture surface is eccentric. In most cases, because the sphere is centrally loaded, a two sided rupture takes place beneath the sphere. As shown in Figures 18 and 20 for clay and sand, the two rupture wings are perfectly symmetrical. However in some cases one-sided rupture may take place probably due to nonhomogeneous soil or loading conditions. In such a case sliding occurs in the region of least resistance as seen in Figure 16 c. In all the three soils tested, an inverted cone of soil formed at this stage, the base of the cone being against the sphere. Initially the cone is short, but as the sphere penetrates deeper into soil the height increases. The rupture surfaces and the flow lines are curved, rising up to a free surface of the soil.

At higher moisture contents the load vs. penetration curve falls below the initial straight line, and a mound of soil appears around the sphere. It appears reasonable to assume that at this stage the shear strength of soil is completely exhausted; the strains are large compared to stresses imposed, and the deformation zone is in a state of plastic flow. The point at which slope of curve changes is the ultimate bearing capacity of soil.

The theoretical treatment also assumes that deformation is entirely within a boundary described by a rupture surface. It appears, from this investigation, that this boundary does not enclose the full plastic region, since there is a further zone in which the material is stressed but remains stable because it is prevented from deforming. Here the compression and

plastic parts of the strain may be of comparable magnitude. None of the boundaries determined in the soil models correspond exactly to those of the theoretical models.

Another aspect of the deformation process is the appearance of the surface in which penetration is made. With very dry silt specimens radial cracks extend outward from the edge of depression. The most plausible explanation is that at low moisture contents the silt behaves as a non-plastic material, and these cracks are tension cracks which increase in length as the load on sphere increases.

In soils close to the optimum moisture there is a tendency for the surface around the sphere to be depressed. This depression extends to a distance well removed from indentation; therefore when the sphere first begins to sink, a large mass of soil must be subjected to compression.

In specimens at moisture contents above the optimum and in the dry sand, a mound of displaced soil appeared around the sphere. This is observed to occur in a second stage of deformation when the material above the slip surface is displaced and pushed up, in a manner suggested by the theoretical treatments.

The radial limits of the cracks, surface sinking, and surface bulging around the sphere coincide exactly with the elastic-plastic (or no strain) boundary of the sectionalized models. We must be mindful that the displacements observed in the sectionalized model have only a small component in the plane of surface, because the actual displacement is three-dimensional. The ratio $\frac{D}{d}$ ranges between 2.5 to 3.5 and the ratio between curved areas of elastic-plastic surface and sphere in contact with soil ranges between 5.6 to 7.5.

Elastic deformation in soil specimens ranges between 8 to 16 percent of the total settlement of sphere. The magnitude of elastic deformation shows no definite trend with moisture content; however it was higher in the silt than in the clay. Elastic recovery occurred after release of the indenting load.

V. PROCEDURE

The experimental investigation outlined in this report was conducted in three phases:

1. Preliminary investigation.
2. Laboratory investigation.
3. Design of field apparatus and field investigation.

A. Preliminary Investigation

The purpose of preliminary investigation was to determine suitable sizes of the specimen and the sphere, a method and duration of loading, and the best technique for measurement of penetration or contact area.

1. Loading device

The basic loading requirement was a constant static load on the sphere. A North Dakota cone penetrometer was available; the tip was therefore cut and ground concave inward to form a seat for the sphere. Figure 22 shows the North Dakota cone penetrometer, modified for use as a spherical penetrometer.

2. Specimen size

Large specimens 3 ft square by 9 in. deep were considered, the main advantage being a large number of tests on the same block, indicating degree of reliability. However, it was found that uniform density throughout the specimen could not be achieved with available equipment. Also, it was not possible to run GBR tests as specified by ASTM (45).

GBR molds were selected for laboratory tests because it was possible

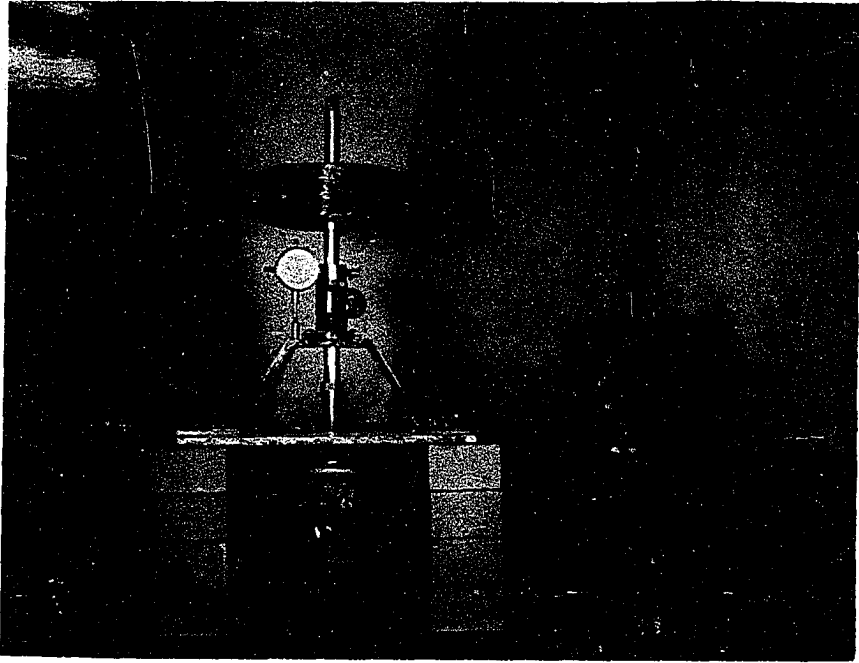


Figure 22. Spherical penetrometer used in laboratory investigations

to run three sphere penetration tests on one side and CBR test on the other side of the specimen. An average sphere bearing value could be obtained from the three tests to correlate with the CBR value on the same specimen.

In tests where correlation between the spherical penetrometer value and the CBR was not required, it was more convenient to use the smaller Proctor-size specimen molds (1/30 cft).

3. Measurement of indentation

In this phase three possibilities were explored, namely measurements of the diameter of indentation, the diameter of contact area, or the depth of penetration of the sphere. Any one of these three measurements is sufficient to determine the contact area or the cross-section area for a sphere of known diameter.

The diameter of indentation was measured with a micrometer. After the loading test, the sphere was unloaded and removed from the surface of specimen, and three readings were taken. It was found that after unloading there was some elastic rebound, as values of the curved and the cross sectional areas by this method were somewhat larger than the actual values. This method was therefore abandoned.

To measure the curved contact area sheets of thin, white recording paper and carbon paper were placed on the surface of the soil specimen. The sphere was placed on the carbon paper and loaded, and the diameter of the circular trace was measured after the test. This method, again, was found to be unreliable because the impression was not sharp and well defined and could not be measured with confidence.

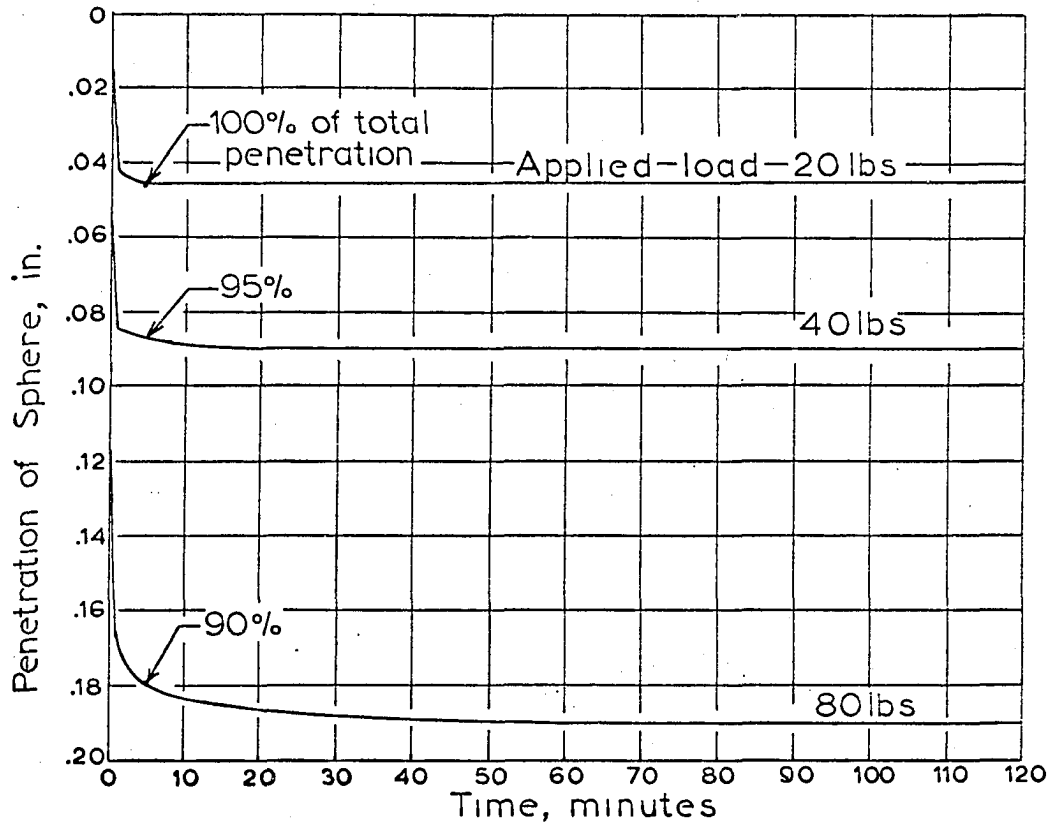
For measurement of penetration an Ames dial (least scale division = .001 in) was attached to the loading device as shown in Figure 22. The load shaft was carefully lowered until it touched the sphere on the specimen, and then locked in position and the dial zeroed. The first load was then placed on the shaft and it was gently unlocked so that the weight transferred to sphere without impact. After a while when penetration of sphere into soil specimen had ceased, a dial reading was taken. Uniform increments of load were then added and the penetration for each increment was recorded.

4. Period of loading

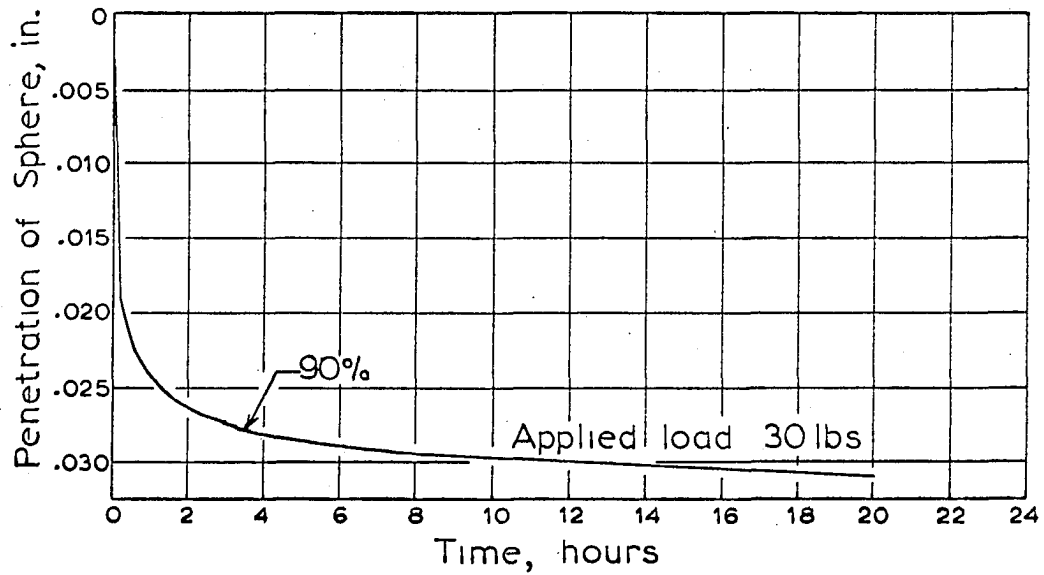
To determine a suitable duration of loading, loess and clay specimens were molded at various moisture contents and tested with spheres of 0.5 in., 0.562 in. and 0.75 in. in diameter. Loads were varied from 20 to 80 lbs and measurements of penetration of sphere were taken at 5, 10, 15, 20, 25 and 30 seconds, 1, 2, 3, 4, 5, 10, 15, 20 and 30 minutes, and 1, 2, and 24 hours. Figures 23 (a) and 23 (b) are typical penetration vs. time curves. It will be seen that with load of 20 lbs all penetration on loess samples ceased after five minutes, and with 40 lb load all penetration ceased in ten minutes. At higher loads, penetration continued up to an hour.

Penetration in clay samples continued much longer, especially in samples with moisture contents much higher than optimum. Under ordinary loads and optimum moisture content, 98 percent of all penetration was completed within 20 minutes. Figure 23 (b) shows data from a clay sample molded at 6 percent above optimum moisture content and standard Proctor

Figure 23. Penetration versus time curve
(a) for silt
(b) for clay



(a)



(b)

density; where penetration continued for 22 hours, 95 percent occurring in the first seven hours. It is seen that lighter loads require a shorter duration of loading than heavier loads, and highly cohesive soils require a longer duration of load application than less cohesive soils to reach a state of equilibrium.

The duration or rate of loading in all standard laboratory and field tests is based on the purpose for which the test values are intended to be used. That is, ideally the rate of loading should approximate anticipated conditions under a structure. In road or airfield pavements the rate of loading is very rapid, and resistance of soil will include viscous resistance. The ideal rate of loading to determine the true strength of soil in its present state however, is that a test should be fast enough that no appreciable consolidation should take place during the test but long enough so that additional resistance due to viscosity is eliminated. These two aims cannot be completely reconciled as such the rate of loading in each test simulates the actual loading conditions.

Some of the standard tests and their rates or durations are given below:

Controlled strain:

Unconfined compressive strength	0.05 to 0.1 inch per minute
Quick shear test	Between 3 to 5 minutes
C.B.R.	.05 inch per minute

Controlled stress:

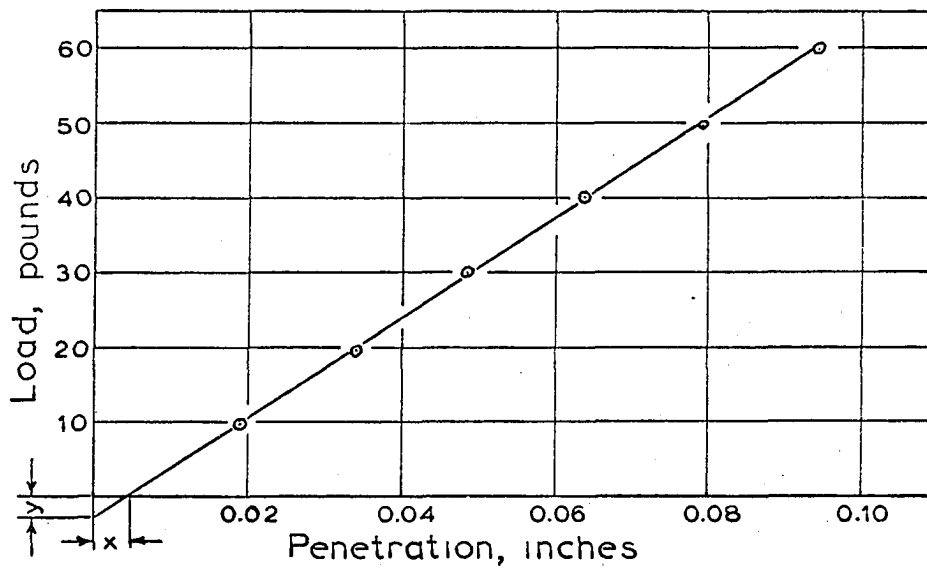
North Dakota cone test	1 minute
Plate bearing test	Until settlement is less than 0.001 inch per minute

Since the spherical bearing test is a static test and is planned to be used both for foundation and pavement designs, loading was continued until the rate of penetration was less than 0.001 inch per minute. It will be seen in Figure 23 that this will include 90-95 percent of all penetration.

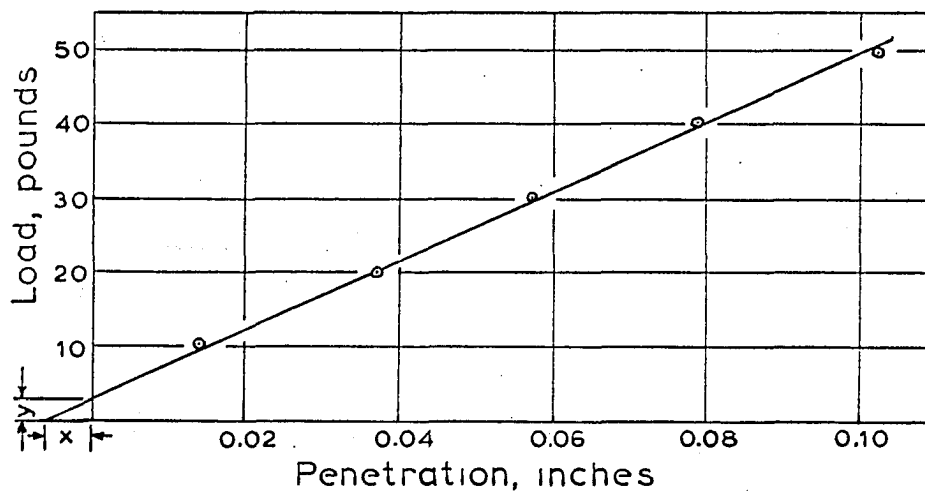
5. Establishing zero point

Plotting load against penetration results in two types of curves, as shown in Figure 24, a and b. Prior to loading, the shaft of the penetrometer was visually brought into contact with the sphere; often it was not really in contact, giving a first penetration reading in excess of the true penetration (Figure 24 a). On the other hand if the shaft depressed the sphere the first penetration reading was less than the true penetration (Figure 24 b). In order to obtain true values of penetration the following steps were used:

1. The shaft, which weighed 3 lb, was lowered to rest on the sphere and was kept there a few minutes until it had reached equilibrium. It was locked in that position and the dial reading was recorded as a zero reading.
2. The first load increment was 7 lb, which plus the weight of shaft came to 10 lb, and subsequent load increments were in steps of 10 lb. The dial reading was recorded for each load increment when penetration had reached a state of equilibrium.
3. A zero point correction was obtained graphically (Figure 24 b) and sometimes amounted to as much as .005 in. In this figure 'y' is the true load on sphere with the dial reading at zero. This correction was



(a)



(b)

Figure 24. Procedure for establishing zero point correction for load versus penetration curves

y = the true load on the sphere when dial is set at zero
 x = correction for deflection. This correction must be added algebraically to the observed deflections

added algebraically to the observed penetration readings.

6. Load-area relation

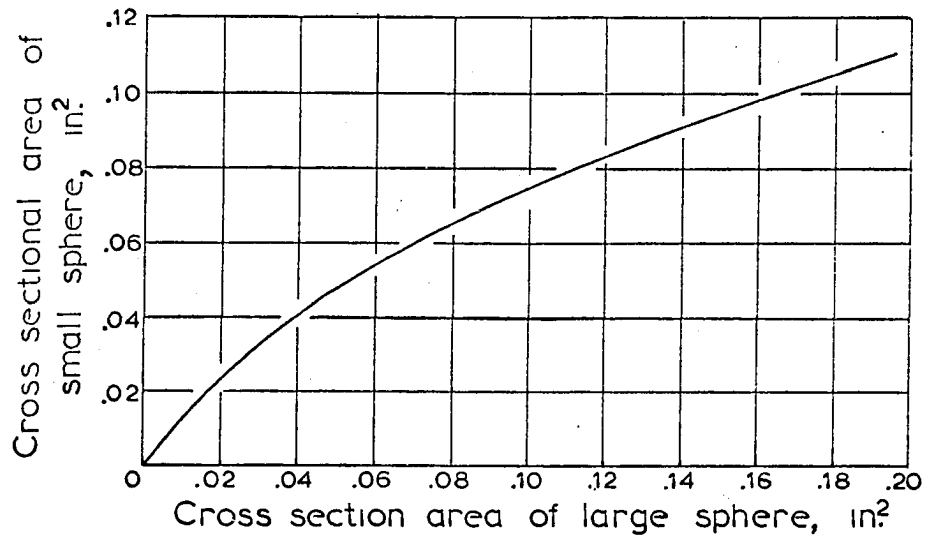
During initial investigations different sizes of spheres were tested on each specimen, and data obtained were plotted in various combinations. It was observed that:

- a. Under the same load cross-section areas for different sizes of spheres tested on the same specimen were different (Figure 25a).
- b. Under the same load curved contact areas of different sizes of spheres were approximately the same for the same soil specimen (Figure 25b).
- c. Load vs. cross-section areas of different sizes of spheres resulted in separate curves (Figure 26a).
- d. Load vs. curved contact areas of sphere for different sizes of spheres on the same specimen plotted in a straight line (Figure 26b).

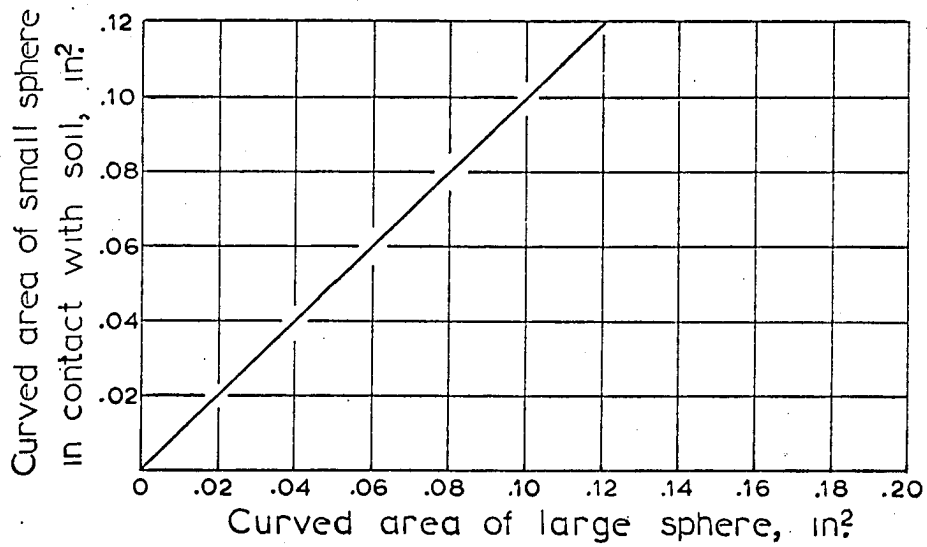
Based on these observations, the load vs. curved area relationship was considered a significant property of soil and was termed the spherical bearing value, which may be defined as the slope of the line when load in pounds is plotted against curved contact area in square inches, as shown in Figure 26b. The units are the same as stress, i.e., psi.

7. Surface variation in specimens

The area of contact of the sphere compared to area of specimen was very small. Although compaction is fairly uniform in a laboratory specimen, variations exist from point to point on the surface of the specimen. When two or three spherical bearing tests were performed on the same specimen, the bearing values obtained were somewhat different. This difference was sometimes as high as 25% with spheres of 0.5 in. diameter. The varia-

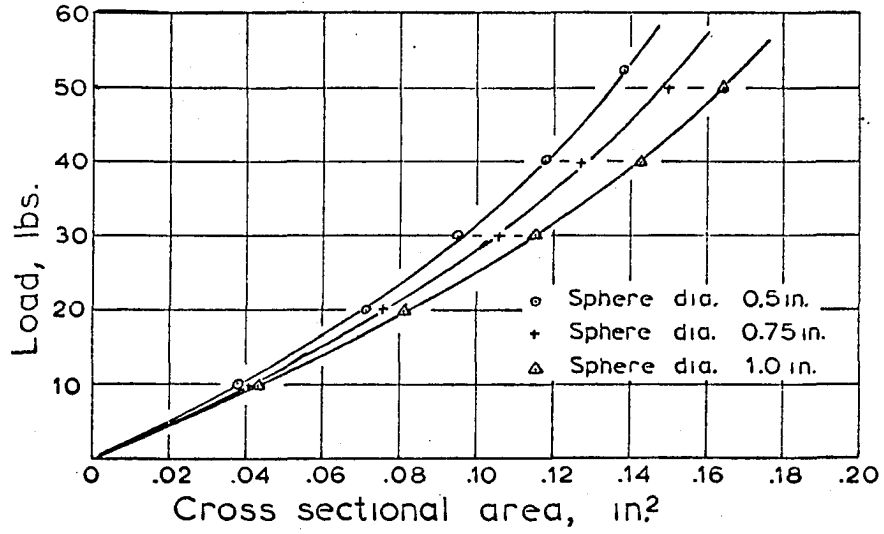


(a) Cross sectional areas

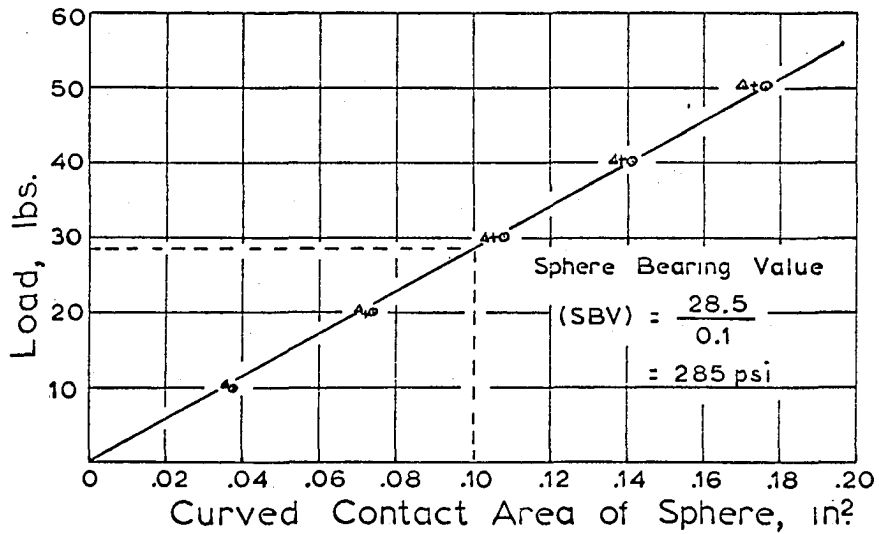


(b) Curved areas

Figure 25. Relationship between areas of different sizes of spheres testing the same specimen



(a) Load versus cross sectional area



(b) Load versus curved area

Figure 26. Relationship between load and areas of different sizes of spheres

tions diminished considerably with larger spheres, indicating that the reason was local variations of the specimen surface. In heterogeneous soils in the field such variations probably will be much larger. However, the size of sphere could not be increased beyond 1.0 inch in diameter on laboratory specimens and allow three tests for the same specimen.

8. Limit of penetration

During investigations of the deformed zone it was observed that the load vs penetration curve was initially a straight line and then it either curved up or down depending on the moisture content of the specimen. The upward trend was believed to be caused by compaction of soil, whereas a downward trend was attributed to plastic flow.

Tests with various sizes of spheres on specimens molded at different moisture contents indicated that when the sphere has penetrated between 15 and 20 percent of its diameter the straight line relation often tends to curve. The object of the test is to determine the bearing value of the soil in its present state; the limit of penetration was therefore set at 15 percent of the diameter of sphere.

B. Laboratory Investigations

1. Description of soils

Laboratory investigations were aimed at testing the spherical penetrometer in three types of soils, i.e., highly cohesive, non cohesive and a soil with both cohesion and friction properties.

The cohesive soil is an alluvial clay from the Missouri River floodplain. The sample was obtained from B horizon of a clay plug in Harrison

County, Iowa, and in its natural state is a very sticky clay. X-ray diffraction showed a strong calcium montmorillonite peak.

The intermediate soil is a Wisconsin age loess, or wind-deposited silt. This soil was chosen because of the large amount of information previously obtained. For laboratory purpose this soil has been catalogued as 20-2, and represents the friable, calcareous loess in western Iowa. It was sampled from the thick loess bordering the Missouri River and contains montmorillonite.

The non-cohesive soil was a commercially available natural silica sand from Ottawa, Ill.

Sample locations, soil series and physical properties of the soil materials are shown in Tables 1 and 2.

2. Mixing

A required amount of air-dried soil passing a No. 10 sieve and a desired percentage of water were mechanically mixed with a Hobart C-100 kitchen mixer for two minutes. This was followed by scraping down of sides of the mixing bowl, and hand mixing to insure even pulverization and distribution of moisture. Finally there followed another two minutes of mechanical mixing by the Hobart mixer, after which the mixture was kept covered with a damp cloth until the specimen was molded.

When five or more CBR specimens were desired at the same moisture content, soil and water were first mixed in a 2.5 cu ft concrete mixer for five minutes. This was followed by scraping the sides of the concrete mixer and hand mixing. This mixture was then transferred into a bin, and small

Table 1. Location of soil samples

Soil	Sample no.	County	Section	Tier north	Range	Soil series ^a	Sampling depth	Horizon
Loess	20-2	Harrison	S-15 ^b	78	43-W	Hamburg	69-70 ft.	C
Clay	-----	Harrison	NW 1/4	78	44-W	Lamour	1-2 ft.	B

^aHarrison County Soil Survey Report (42).

^bSample was obtained from a vertical cut behind the third ward school in Missouri Valley.

Table 2. Properties of soils tested in the laboratory

Soil type	Clay	Loess 20-2	Sand
<u>Physical properties</u>			
Liquid limit, %	88.8	30.8	----
Plastic limit, %	30.1	24.6	----
Plasticity index, %	58.7	6.2	N P
Specific Gravity	2.74	2.71	----
<u>Textural composition</u>			
Gravel (2 mm)	----	----	
Sand (2 - .074 mm)	0.5	0.4	100
Silt (.074 - .005 mm)	9.0	79.8	----
Clay (< .005 mm)	90.5	19.8	----
Colloidal clay (< .001 mm)	35.0	14.5	----
Field dry density, pcf	93.2	83.3	----
Field moisture content, %	33.0	17.0	----
Textural classification (B.P.R. system)	Clay	Silty-loam	Sand
AASHO-ASTM Classification	A-7-6(20)	A-4(8)	A-1-a

batches were taken out for thorough mixing by the Hobart mixer. The Hobart mixed soil was again transferred to concrete mixer and mixed for another five minutes. This ensured that the entire specimen was at the same moisture content. At all stages of mixing the soil-water mixture was kept covered with a damp cloth.

3. Molding

The bulk of the specimens were molded in CBR and Proctor molds. However, a large number of cylindrical specimens 2.8 in. in diameter by 5.6 in. high were also molded for unconfined compressive strength and triaxial shear tests. For direct-shear tests three specimens were obtained by trimming of one such cylindrical specimen.

The CBR molds were 6 in. in diameter and 7 in. high, and had a 2 in. spacer at the bottom. Thus the effective height was only 5 in., and the volume was 141.44 cu in. In order to obtain a large variety of densities, the specimens were molded at various compactive efforts, or energies per unit volume of compacted soil. In the laboratory, the compactive effort can be varied by changing the weight of the compacting hammer, the number of blows per layer of soil, or the number of layers of soil in the mold. The CBR-size specimens were made with the following compactive efforts.

Table 3. Compactive efforts on CBR specimens

Nomenclature	Layers	Blows per layer	Weight hammer, lbs.	Drop in inches
Standard AASHO	3	56	5.5	12
Iowa I	5	25	10	18
Iowa II	5	35	10	18
Iowa III	5	45	10	18
Modified AASHO	5	55	10	18

The Proctor mold was 4.0 in. in diameter and 4.59 in. high, giving a volume of 1/30 cu ft. The specimens were molded using 25 blows of 5.5 pound hammer dropped from a height of 12 inches on each of three equal layers of material. A few Proctor specimens were also molded by static compaction, and by a motor-driven Rainhart compactor, Model 662. All specimens were weighed after trimming, and representative moisture samples were taken from the bulk sample to determine a moisture content for each mixture. The dry density of each specimen was calculated from weight of the wet specimen and the moisture content.

The cylindrical specimens were molded by means of a drop-hammer molding apparatus developed by Felt and Abrams (3). This apparatus molds specimens 2.8 inches in diameter and 5.6 inches high. The desired quantity of soil-water mixture is put in the mold and compacted by a 10 lb drop hammer with a face diameter of 2.8 in. For standard AASHO density the mixture is compacted by dropping this hammer through a distance of 18 inches on each side of the specimen; various densities were obtained by varying the compactive effort.

After compaction, the specimens were ejected by a hydraulic jack. For sticky clay specimens the mold was well oiled inside to decrease resistance to extrusion. Specimens were weighed to the nearest 0.1 gm and their height measured to the nearest 0.001 in. A tolerance of ± 0.1 in. in height was maintained in the specimens molded. Specimens for moisture content determination were taken from each batch.

4. Storage

Normally specimens were tested soon after molding, but on occasions when there was a time gap between molding and testing, specimens were

wrapped in Saran Wrap and stored in a room with 100 percent humidity and 70°F temperature. Sometimes the specimens were stored for three days.

5. Spherical penetration test

The testing procedure described here evolved from preliminary investigations described earlier in this report. On a soil specimen in a CBR mold, three tests were run on one face with indentation points as shown in Figure 27. It was explained earlier that penetrations beyond 15 to 20 percent of the diameter of sphere give incorrect bearing values because of consolidation of soil in low moisture specimens or plastic flow in very high moisture specimens.

In Proctor molds only one spherical penetration test can be run on one side of specimen. Because it is advisable to run at least three tests on any laboratory specimen, Proctor molds were not desirable for this test.

During preliminary investigations three sizes of spheres, namely 0.5, 0.562, and 0.75 in. diameter, were tested. The size of the sphere had no effect on bearing value except that the smaller size spheres gave more scatter than the larger size spheres. It is, therefore recommended that a 0.75 to 1.0 inch diameter sphere be used for laboratory testing. Effects of local variations in density on the surface of the specimen will be further minimized when the average of several tests is used for design purposes.

Load increments during test were established to give at least five points before penetration of the sphere exceeded 15 percent of its diameter. Five points on the graph were considered necessary to be sure of the trend and to accurately evaluate the zero. The step-by-step procedure followed in this test is given below:

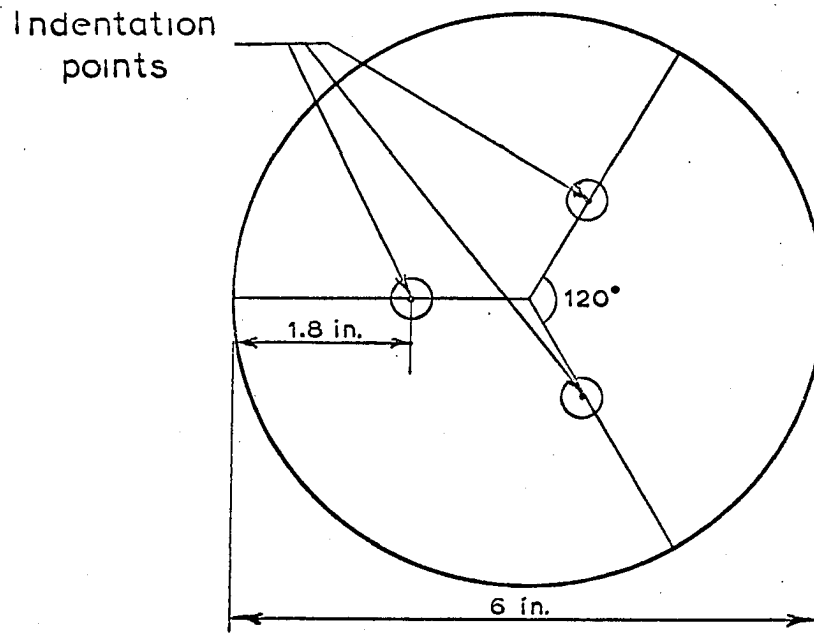


Figure 27. Recommended location of points of indentation on the surface of a specimen in a CBR mold. This choice is based on the extent of deformation zone found during model investigation

1. Mark three points on the top face of a CBR specimen after making sure that the surface is perfectly smooth. Keep the spacer inside the mold to support the bottom surface during penetrometer tests.
2. Position the marked spot on the specimen vertically below the penetrometer shaft.
3. Lubricate the sphere and place it on the marked spot without applied pressure.
4. Lower the shaft gently and rest it centrally on the sphere for one minute. Weight of shaft is 3 pounds. Place a damp cloth to enclose the exposed soil surface without the cloth touching the soil surface.
5. Lock the shaft in position and zero the Ames dial. The least scale division of the dial should be 0.001 inch.
6. Add the first load increment of 7 pounds to the shaft, and gently unlock. Total load on the sphere is now 10 pounds.
7. Let the sphere penetrate until settlement is less than 0.001 inch per minute for three consecutive minutes. Record this settlement to the nearest 0.0005 in.
8. Place each subsequent load increment without locking the shaft, but making sure that there is no impact. Record the penetration for each load increment.
9. Remove the load and the sphere and proceed in the same manner with the other two marked spots.

GBR tests were run on the opposite faces of these specimens. If the GBR tests could not be run immediately after the spherical penetrometer test, the exposed surfaces were again covered in Saran Wrap and stored in

the humidity room.

In order to cut down time required for testing, a "one-shot" method was tried. In this test only one load and its corresponding penetration gives the bearing value and cuts down the period of testing to one fourth of the standard test. The main problem here is the initial zero reading. For this purpose an ohm-meter was connected between shaft and sphere on the specimen to indicate the initial contact. A load expected to cause penetration of 10 to 15 percent of diameter of sphere was added to the shaft, and the shaft was very gently unlocked to transfer the load to sphere. Penetration was recorded when settlement was less than 0.001 inch per minute. This method was of great advantage, especially in clay when ultimate penetration of sphere is required, and values obtained did not vary more than 15 percent from the values obtained by standard method. This method may be considered more accurate because the time is less for consolidation which occurs in the standard method.

6. CBR test

Unsoaked and soaked CBR tests were run in accordance with the procedure of U.S. Army Corps of Engineers (45). CBR tests were run on opposite end of the specimen after the spherical penetration tests had been performed.

7. Unconfined compressive strength-test

The unconfined compressive strength of specimens (2.8 inch diameter and 5.6 inch high) was determined in a triaxial test machine. The only reason for not using a standard unconfined compression testing machine was

that it was not accessible at all times. Load was applied to each specimen with a rate of deformation of 0.05 inch per minute until complete failure was reached.

8. Direct shear test

Quick shear tests were run in accordance with a laboratory manual (33). The samples were trimmed from cylindrical specimens molded for unconfined compressive strength tests. The rate of shear strain application was 0.05 inch per minute.

9. Triaxial compression test

Some unconsolidated, undrained triaxial tests were also performed on some specimens. Vertical strain was applied at the rate of 0.05 inch per minute.

10. Laboratory tests on sand specimens

In a spherical penetration test on sand it was impossible to obtain the initial zero reading, even by the zero-correction-method explained earlier, because the sphere disappeared into the specimen with only the weight of shaft.

Terzaghi and Peck (43) give the following approximate method for computing the bearing capacity of footings, based on a modified Prandtl analysis:

$$q_{dr} = C \cdot N_c + \gamma \frac{b}{2} N_\gamma + \gamma D_f N_q$$

For footings on the surface of cohesionless soils the first and the third terms on the right hand side of the above equation drop out, and the bearing capacity per unit area will reflect only the weight of the soil wedge which is denoted by the middle term in the above equation. The bearing capacity of footings on the surface of highly cohesive soils is primarily function of the first term of the above equation and is practically independent of the width of the footing whereas on sands the bearing capacity increases as the width increases. Sand foundations have been known

to behave altogether differently than cohesive soil foundations.

In the Sphere Bearing test the contact area initially is very small and it increases as the load increases and as such the soil pressure will not be constant but will increase with the increase in area.

It was desired to confirm this phenomenon by the Sphere Bearing test. Since the sphere sinks in sand at very low applied loads the test could be modified in the following two ways. First, in order to mobilize larger resistance to penetration a surcharge may be used. Second, the weight of the shaft and the sphere be counter balanced so that more precise readings could be taken without the aid of the surcharge. This, however, was not attempted in the present investigation but it is suggested that the method be tried in future work on sand.

Because of the geometry of indentation with a sphere, the surcharge must be flexible to conform to the increasing contact diameter as the sphere penetrates the soil surface. This requirement can be satisfied if the surcharge is either mercury or air under pressure. Both methods were tried:

a. Mercury surcharge Ottawa sand specimens vibratory compacted dry in CBR molds were used in this testing.

1. A 3 inch layer of mercury was poured on the surface of the specimen, and a sphere penetration test was performed by the standard method. After the test when the mercury was removed it was found that mercury had penetrated and mixed with sand, probably changing the soil properties.
2. To prevent penetration of mercury into the sand, a sheet of Saran Wrap was laid on the specimen before pouring on mercury, and a penetration test was run. When Saran Wrap was removed it was found that this sheet under surcharge of mercury had acted as a flexible footing and mobilized the resistance of entire specimen surface, giving very high bearing values.

3. A third unsuccessful attempt with mercury was made by placing sphere under Saran Wrap. When 3 inch depth of mercury was poured on the specimen the sphere penetrated under the load of surcharge and depth of penetration could not be measured.

b. Compressed-air surcharge Tests were performed on a triaxial apparatus in a Plexiglass cell with an internal diameter of 7 inches. A Proctor mold was modified by drilling a hole in its bottom plate. A flexible hose from the hole at the bottom of Proctor mold was connected to drainage plug and opened to atmosphere, to insure that any leakage of high pressure air into the specimen bled out and the soil in the mold was at atmospheric pressure. The surface of the specimen was covered with a layer of talcum powder or graphite to insure smooth sliding of Saran Wrap without disturbing the soil surface. The surface was then sealed with a sheet of Saran Wrap, and air pressure applied.

Tests were conducted with sphere welded to the bottom of the triaxial loading piston. Specimens were tested under cell pressures ranging from 5 to 20 psi.

When specimens were removed after testing, it was found that although Saran Wrap was initially laid loose on the specimen and talcum powder had been used to aid sliding on the top of the specimen, the plastic still dragged the entire surface as the sphere penetrated, mobilizing unwanted frictional resistance. Unless some better technique is developed, the present method therefore can only be used for cohesive soils. Some tests were performed with wet sand specimens and are included in analysis and discussion.

C. Field Investigations

1. Description of soils

The clay soil tested is a Webster silty clay, and is the subgrade of a county gravel road north of Ames (Table 5). The soil is dark in color and highly plastic.

The glacial till tested was a compacted subgrade of interstate Highway 35 under construction. The subgrade material had been hauled from a borrow pit 200 yards away. The soil is brownish gray in color and contains gravel and pebbles with a maximum diameter of 2 inches.

The sandy soil tested is in a rest area located on highway 69 on the bank of the Skunk River. The soil is very erratic in properties and has random distribution of gravel and pebbles.

Testing sites, soil series and physical properties of the soil materials are shown in Tables 4 and 5. Soil identification tests were performed on disturbed samples obtained from test sites. In addition, laboratory direct shear, triaxial shear and unconfined compressive strength tests were performed on 2.8 inch diameter Shelby tube samples. All glacial till and sandy loam specimens were damaged during some stage of preparation or testing due to the large sized aggregate present. In situ shear test values for the soils were obtained by the bore hole shear device (14).

2. Field spherical penetrometer

Field equipment used is shown in Figure 28. Two sizes of penetrometers were machined, the larger with a curvature diameter of 12 inches and the smaller with one of 6 inches. Tests were performed at each site with both sizes of penetrometers. The loading device consisted of a loaded truck equipped with a hydraulic jack of 10,000 lb capacity. The jack was equipped with gauge graduated in increments of 200 lb. A ball swivel was placed between the top of the jack and the jacking point on the truck.

Penetration of the sphere was measured to the nearest 0.0005 in. by means of an Ames dial graduated in increments of 0.001, and set as shown

Table 4. Location of field tests

Soil	County	Section	North	Range	Soil series ^a	Depth	Horizon
Silty clay	Story	SE $\frac{1}{4}$ SW $\frac{1}{4}$,Sec.27	84N	24W	Webster	6 to 14 inches	B
Glacial till	Story	SE $\frac{1}{4}$ SW $\frac{1}{4}$ Sec. 6	84N	23W	Clarion	Highway subgrade	C
Sandy loam	Story	NE $\frac{1}{4}$ SE $\frac{1}{4}$ Sec.22	84N	24W	Wabash	Subgrade	B

^aStory County soil survey report (44).

Table 5. Properties of soils - Field tests

Soil type	Silty clay	Glacial till	Sandy loam
<u>Physical properties</u>			
Liquid limit	61.4	24.0	
Plastic limit	26.1	15.0	N.P.
Plasticity index	35.3	9.0	
In-place density, pcf	126.9	138.0	83.7
Dry density, pcf	99.5	125.8	78.8
Field moisture content, %	27.3	10.2	6.23
<u>Textural composition</u>			
Gravel (>2 mm)	-	4.2	8.6
Sand (2-0.074 mm)	24.0	42.9	66.4
Silt (0.074-0.005 mm)	24.8	28.7	14.9
Clay (<0.005 mm)	51.2	24.2	20.1
Colloidal clay (<0.001 mm)	44.1	17.5	9.3
AASHO-ASTM classification	A-7-6(20)	A-4(3.5)	A-2-4(0)

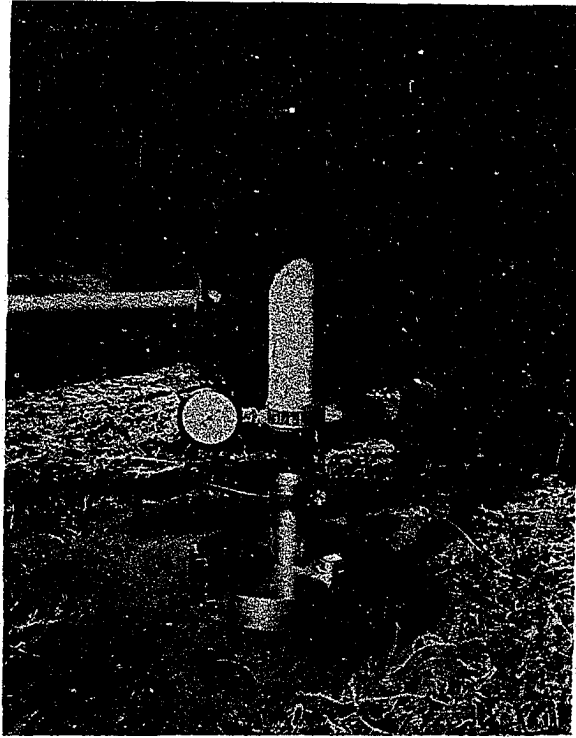


Figure 28 (a). Field spherical penetrometer with 12-in. curvature diameter

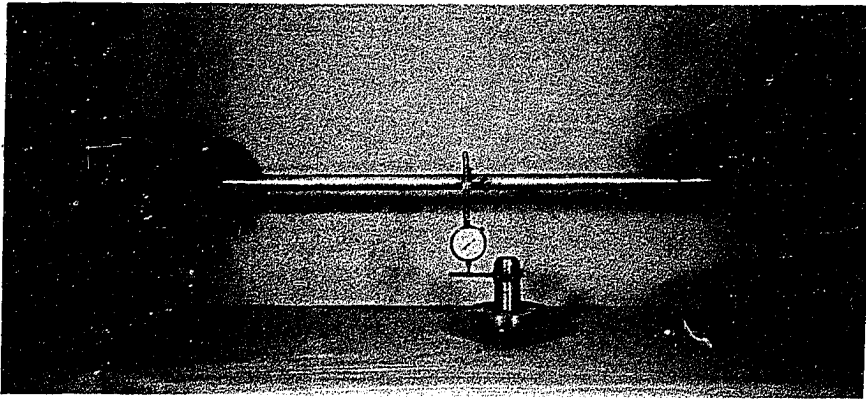


Figure 28 (b). Arrangement of equipment for field test. The light alloy pipe is supporting the Ames dial and is 10 ft long

in Figure 28 (b). The Ames dial is supported from adjustable steel arm attached to a light alloy beam consisting of a 10 ft length of 1.5 inch diameter pipe, resting at its extremities on broad-based stands. During a test, the long axis of the deflection beam was at right angles to the longitudinal axis of the loaded truck.

3. Spherical penetrometer test procedure

Field testing was done during summer, 1966. After some preliminary testing the following procedure was standardized:

1. The top six inches or more of desiccated soil was removed from an area 3 feet by 3 feet, so that the test will be completely unconfined. The area was then levelled and smoothed with a hand-trowel. On county roads the entire thickness of gravel was removed to expose the subgrade.
2. The sphere was set vertically below the jacking point with a plumb-bob.
3. The equipment was set up as shown in Figure 28. The Ames dial was zeroed.
4. First load increment was transferred to the sphere by the hydraulic jack. Pressure in the hydraulic jack was kept constant.
5. Penetration was recorded when settlement was less than 0.001 inch per minute for three consecutive minutes.
6. The minimum number of uniform load increments was five for each test.
7. Before taking a dial reading the deflection bar was gently tapped to make sure the dial was not stuck.

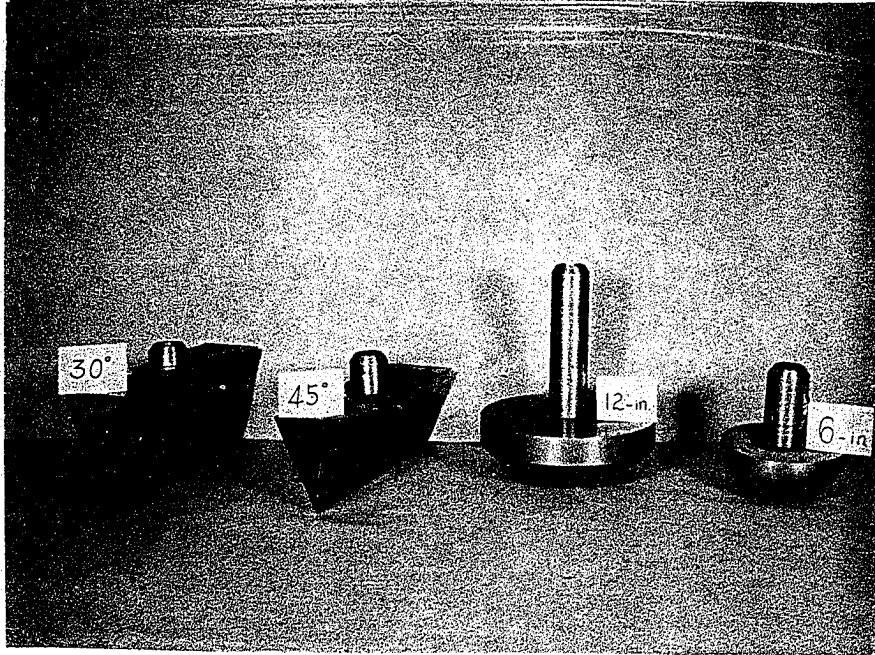


Figure 29. Penetrometers used in field investigation. The steel wedges are 12 in. long

8. Throughout the test the exposed surface was protected from sun by covering with a damp cloth.

Recording and plotting of load test data was done in the same manner as explained in laboratory procedure.

"One-shot" load tests were also performed in the field, and the values obtained were only slightly different from those obtained by the standard method.

4. Plate bearing test

Plate bearing tests were performed in accordance with ASTM specification D 1196-57 but a 12-inch diameter plate was substituted for the 30-inch plate. Load was applied in equal increments until the plate sheared through the soil surface or the limit of the load was reached.

The modulus of subgrade reaction, k , was obtained at 0.05 inch deflection.

5. Steel wedge test

Two steel wedges of internal angles of 45° and 30° as shown in Figure 29 were used in the same manner as the spherical penetrometer. The observations in field are recorded as load-settlement points. The object of this test was to determine ultimate bearing capacity of foundations by a procedure outlined by Meyerhof (25) and correlate it with spherical penetrometer values. However, no reliable values could be obtained in glacial till or gravelly soils due to the presence of gravel and pebbles in soil.

6. Layout of test site

Figure 30 illustrates the general arrangement followed in the field

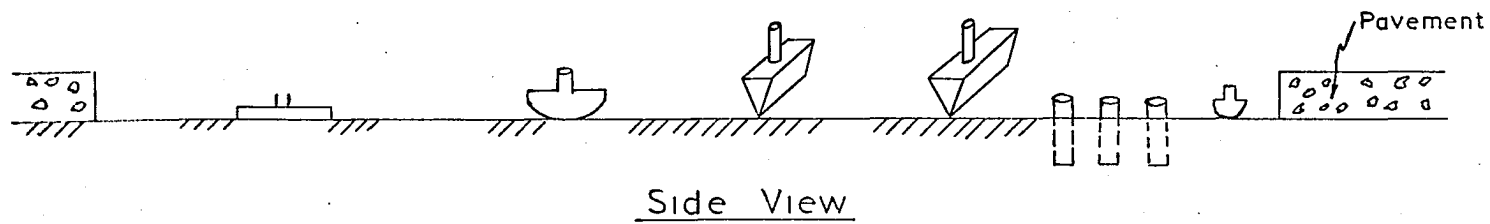
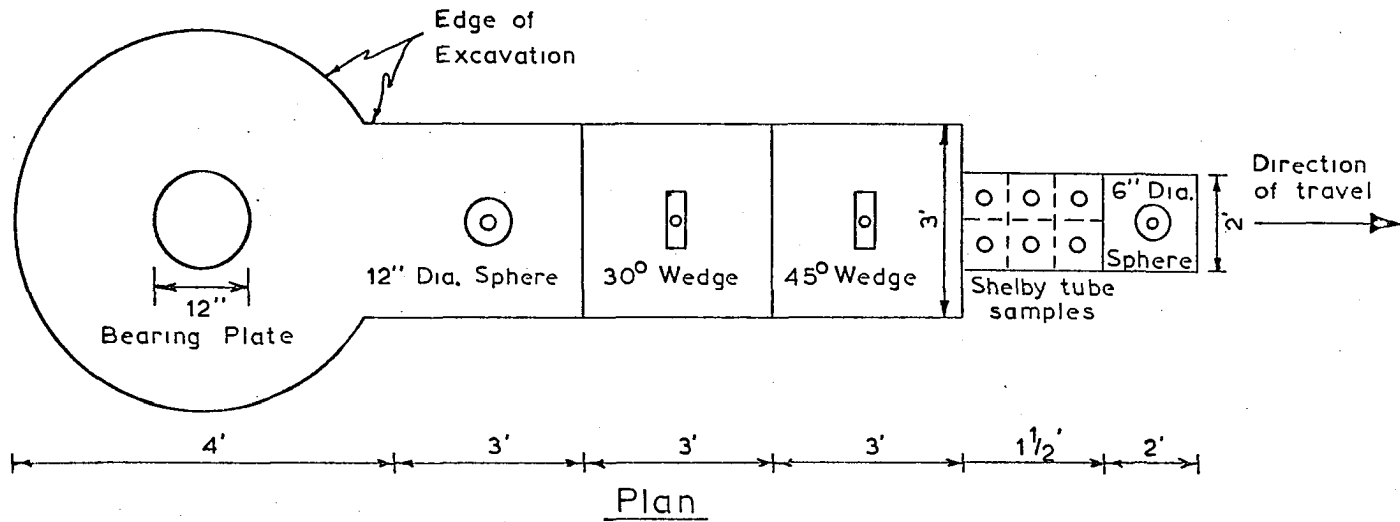


Figure 30. Typical site layout for testing and sampling in field

tests. Aggregate or desiccated soil was excavated to a depth of 6 to 9 inches. All testing and sampling was done in this pit. Often more than two spherical penetration tests were conducted and in that case the pit was extended in the direction of travel of truck. With a party of two each field test was completed in eight to ten hours. Laboratory testing on disturbed and undisturbed specimens was done either the same night or the day following field testing.

VI. PRESENTATION AND DISCUSSION OF RESULTS

A. Presentation of Data

During the initial phases of laboratory investigation most tests were performed on a silty soil-loess, and some were performed on clay and wetted sand. During this phase the investigations were mainly concerned with determining if there was a correlation between SBV (Sphere Bearing Value) and the CBR (California Bearing Ratio). All of the CBR tests during this phase were performed on unsoaked specimens. Results of these tests are given in Table 6. These tests are numbered 1 through 99 and 110 through 124, a total of 114 tests. Ten tests, 90 through 99, were performed for statistical analysis of CBR values, and no SBV data for these specimens are included in Table 6.

In the next phase of investigations tests were performed on a different batch of loessal soil to confirm if the correlation obtained between SBV and CBR in the previous phase would hold. Unconfined compressive strength tests, triaxial shear tests, soaked CBR, and soaked SBV tests were also performed in this phase. There are 31 tests in this phase and their results are given in Tables 7 and 8.

Tests on clay included unsoaked and soaked CBR, unsoaked and soaked SBV, unconfined compressive strength, and direct shear tests. Bearing data could not be obtained from the soaked tests because the montmorillonitic clay soil swelled up excessively after four days of soaking. A number of "one-shot" SBV tests were performed in clay utilizing only one load increment to reduce the testing time. Tests 178 through 180 are twenty-four-hour tests to determine the rate of penetration and maximum penetration of

the sphere. Results of tests on clay are given in Table 9.

Tests were also performed on Ottawa Sand. The unsuccessful tests on dry sand were mentioned earlier; no results were obtained from these tests. Data from wetted sand have been included in Table 10.

To summarize, laboratory Sphere Bearing tests were performed on 180 specimens molded from silt, sand or clay. Values obtained from these tests were correlated with CBR, unconfined compressive, direct shear and triaxial shear tests.

The field tests were performed on glacial till, gravelly-sandy loam and silty clay. Undisturbed Shelby tube samples from the field test sites were brought to the laboratory to determine their strength characteristics. Great difficulty was experienced in testing heterogeneous soils containing large sized gravel, which often occurred in the shear plane. Resulting bearing values were erratic and were discarded. In order to determine the shear strength parameters of these soils the bore-hole-shear device was used at all test sites. Results of these and other field tests are given in Table 11.

A statistical treatment of the data is given in a later section entitled Statistical Analysis.

Data presented in Tables 6 through 11 do not include details such as rate of penetration, load increments, duration of the tests, and observations on shape and extent of the deformation zone. All this information was recorded for each test at the time it was performed and is available at the Soil Engineering Research Laboratory, Engineering Research Institute, Iowa State University, Ames, Iowa.

Table 6. CBR and SBV data of laboratory tests performed on loessal silt

Specimen no.	Compactive effort	Moisture content %	Dry density pcf	Unsoaked CBR %	Sphere bearing value, psi			Average
					1	2	3	
(1 - 9 Preliminary Investigations)								
10	Std. AASHO	12.36	94.6	20	264	-	-	264
11	Mod. AASHO	"	110.8	93	645	-	-	645
12	Iowa I	"	102.8	43	236	-	-	236
13	Iowa II	"	105.4	62	550	-	-	550
14	Iowa III	"	110.4	82	584	-	-	584
15	Std. AASHO	13.75	97.6	21	330	-	-	330
16	Mod. AASHO	"	110.9	94	500	-	-	500
17	Iowa I	"	102.4	36	340	-	-	340
18	Iowa II	"	108.3	56	412	-	-	412
19	Iowa III	13.40	108.5	58	386	-	-	386
20	Std. AASHO	15.78	103.4	26	346	280	-	314
21	Mod. AASHO	16.20	112.8	26	199	-	-	199
22	Iowa I	"	108.5	37	309	254	-	280
23	Iowa II	16.11	110.2	37	232	-	-	232
24	Iowa III	15.84	112.6	40	232	-	-	232
25	Std. AASHO	17.94	108.7	14	121	-	-	121
26	Mod. AASHO	18.56	108.2	5	71	77	88	80
27	Iowa I	18.04	108.8	10	123	161	135	139
28	Iowa II	18.36	108.2	6	77.2	77.2	-	77.2
29	Iowa III	18.32	108.3	5	81.5	-	-	81.5
30	Std. AASHO	20.93	103.0	3	44	60	-	52
31	Mod. AASHO	20.97	102.3	2	39.6	39.6	-	39.6
32	Iowa I	"	101.7	2.6	44	57.4	79.4	59.5
33	Iowa II	"	103.5	2.3	35.3	-	-	35.3
34	Iowa III	21.0	102.7	2.7	44	-	-	44
35	Mod. AASHO	"	104.6	2.4	41.3	41.3	41.3	41.3
36	Std. AASHO	13.43	94.6	20	238	298	247	260
37	Mod. AASHO	13.45	111.3	90	700	730	645	692
38	Iowa I	13.59	103.0	35	265	381	282	309
39	Iowa II	13.35	106.8	58	370	463	500	468
40	Iowa III	13.46	107.0	62	474	506	603	516
41	Std. AASHO	14.49	-	32	370	407	338	372
42	Mod. AASHO	14.08	115.3	88	584	705	606	639
43	Iowa I	14.04	105.2	42	309	-	-	309
44	Iowa II	"	107.8	45	-	-	-	-
45	Iowa III	14.15	108.2	56	400	-	-	400
46	Std. AASHO	16.87	104.5	25	265	310	254	276
47	Mod. AASHO	16.90	111.03	15	155	-	-	155
48	Iowa I	16.73	107.7	27	187	-	-	187
49	Iowa II	"	110.6	22	154	-	-	154
50	Iowa III	16.60	111.2	16	207	-	-	207
51	Std. AASHO	17.80	106.9	18	265	254	243	254
52	Std. AASHO	17.80	105.0	20	243	232	260	252
					257	266	-	

Table 6. (Continued)

Specimen no.	Compactive effort	Moisture content %	Dry density pcf	Unsoaked CBR %	Sphere bearing value, psi			
					1	2	3	Average
53	Std.AASHO	17.80	105.8	19	232	258	257	203
					266	-	-	
54	Mod.AASHO	17.65	109.4	8	123	132	121	136
					161	143	-	
55	"	"	108.7	7	121	117	137	133
					137	150	-	
56	Iowa I	"	108.0	21	205	158	227	198
					203			
57	Iowa II	"	109.5	12	115	154	198	157
58	Iowa III	"	110.6	10	155	139	165	
					150	155	-	155
59	"	"	110.4	11	133	170	133	
					155	150		150
60	Std.AASHO	21.50	101.3	2	44.1	55	55	
61	"	"	102.2	2	44.1	44.1	39.8	46.4
					39.8	39.8	-	
62	Mod.AASHO	21.59	102.5	2	34	35	35	35
63	Iowa I	21.37	100.3	1	35.3	35.3	30.9	
64	Iowa II	21.09	102.6	1.7	33.0	26.4	50.6	37.4
					39.8	-	-	
65	Iowa III	21.60	103.0	1.5	33.0	37.5	51	40
					40	-	-	
66	Std.AASHO	17.56	103.5	23	294	287	326	287
					243	-	-	
67	Mod.AASHO	16.50	113.0	23	276	298	260	260
68	Iowa I	16.42	107.8	37	330	320	320	
69	Iowa II	16.64	109.7	31	276	291	260	276
70	Iowa III	16.59	113.0	23	276	254	223	
					236	-	-	
71	Std.AASHO	-	-		352	364	-	358
72	Mod.AASHO	-	-	72	574	556	-	
73	Iowa I	-	-	39	397	397	320	371
74	Iowa II	-	-	59	463	485	440	
					440	485	-	
75	Iowa II	-	-	50	485	485	487	455
					420	-	-	
76	Iowa III	-	-	68	506	551	551	536
77	Std.AASHO	15.46	103.9	20	208	230	208	
78	Mod.AASHO	"	117.4	25.6	265	286	280	315
79	Iowa I	"	113.5	36.6	330	330	320	
80	Iowa II	"	116.2	32.3	298	330	330	320
81	Iowa III	"	113.3	28	286	265	286	
82	Mod.AASHO	14.93	115.4	40	370	370	352	365
83	Iowa II	10.95	106.0	37	430	463	408	
84	Iowa III	"	109.1	51	398	364	430	370

Table 6. (Continued)

Specimen no.	Compactive effort	Moisture content %	Dry density pcf	Unsoaked CBR %	Sphere bearing value, psi			
					1	2	3	Average
85	Mod.AASHO	10.95	112.4	53	320	430	650	466
86	Iowa II	12.61	108.5	33	353	375	331	353
87	Iowa III	"	111.4	43	308	364	397	356
88	Mod.AASHO	"	117.3	74	298	430	463	397
89	Mod.AASHO	15.1	118.7	33	-	-	-	-
90	Std.AASHO	15.31	100.8	14	-	-	-	-
91	"	"	97.7	12	-	-	-	-
92	"	"	100.4	15	-	-	-	-
93	"	"	100.8	12	-	-	-	-
94	"	"	102.7	14	-	-	-	-
95	"	"	100.1	13	-	-	-	-
96	"	"	102.3	15	-	-	-	-
97	"	"	101.8	15	-	-	-	-
98	"	"	104.0	14	-	-	-	-
99	"	"	101.4	15	-	-	-	-
110	Iowa II	10.21	101.6	56	661	467	496	542
111	Iowa III	10.12	105.4	63	650	716	838	735
112	Mod.AASHO	10.15	107.9	76	815	870	-	832
113	Std.AASHO	14.34	102.0	27	335	386	356	360
114	Mod.AASHO	14.27	111.5	80	530	540	684	585
115	Iowa I	14.26	104.2	37	423	310	396	377
116	Iowa II	14.23	110.5	58	390	485	480	475
117	Iowa III	14.15	111.3	67	435	506	518	487
118	Iowa III	12.85	109.4	68	530	640	530	566
119	Mod.AASHO	13.04	111.1	78	716	838	620	725
120	Std.AASHO	11.27	97.3	25.7	331	353	419	378
121	Iowa I	10.87	99.6	37	490	478	452	471
122	Iowa II	10.86	102.6	60	540	606	430	525
123	Iowa III	10.75	105.3	84	540	816	672	675
124	Mod.AASHO	10.70	108.8	99	771	993	803	855

Table 7. SBV, triaxial quick test and unconfined compressive strength data of laboratory tests performed on loessal silt

Specimen no.	Compactive effort	Moisture content %	Dry density pcf	Sphere bearing value, psi				Triaxial test		Unconfined compressive strength, psi
				1	2	3	Average	C.psi	ϕ	
125	Std.AASHO	17.8	110	122	128	-	125			
126	"	13.3	101	190	190	-	190	15.3	21.5	40.8
127	"	14.0	100	161	162	-	163	17.5	19	42.3
128	"	"	"	163	165	-				
129	"	16.0	106	180	181	-	182	17.5	18.5	47.0
130	"	"	"	185	182	-				
131	"	18.5	111	75	-	-	95	17.5	22.5	52.8
132	"	"	"	108	101	-				
133	"	20.0	105	107	104	-	105			
134	"	11.4	99	181	181	-	179	9	25.5	33.2
135	"	"	"	181	171	-				
136	"	16.8	107	145	163	-	166	-	-	38.5
137	"	"	"	182	176	-				
138	"	17.0	107	168	173	-	177	16.5	15	47
139	"	"	"	177	190	-				
140	"	16.7	105	174	176	-	176	11.5	21.5	35
141	"	"	"	176	176	-				
142	"	14.6	102	182	203	-	182	13.4	20.5	32
143	"	"	"	168	175	-				
144	"	13.1	98	163	127	-	194	10	25	39
145	"	"	"	247	238	-				

Table 8. Unsoaked and soaked SBV and CBR and unconfined compressive strength data of laboratory tests performed on loessal silt

Specimen no.	Compactive effort	Moisture content %	Dry density pcf	Average SBV, psi	Unsoaked CBR %	Soaked SBV psi	Soaked CBR %	Unconfined compressive strength psi
146	Std.AASHO	11.9	--	196	17.4	14	2	-
147	with	"	99	320	29.5	18	2	-
148	Rainhart	12.8	97	194	18.0	45	2.3	30
149	compactor	13.6	99	304	24	40	5.4	31.4
150	"	14.5	103	242	26.8	64	2.2	46.7
151	"	15.6	104	298	28.8	45	10	43.3
152	"	16.5	107	260	27.0	57	21.2	41.7
153	"	17.2	105	196	21.8	66	19.5	31.5
154	"	18.2	105	128	8	38	2.5	27.3
155	"	19.6	104	55	5	41	2.6	26.0

Table 9. Unsoaked and soaked^a CBR, SBV and cohesion data of laboratory tests performed on clay

Specimen no.	Compactive effort	Moisture content %	Dry density pcf	Unsoaked CBR %	Unsoaked SBV psi	UCS psi
156	Std.AASHO	26.2	80	17.5	205	53.1
157	"	"	"	-	-	-
158	"	28.0	82	15.0	162	41.1
159	"	"	84	11.5	163	42.5
160	"	"	"	"	"	"
161	"	31.0	88	-	150	48.1
162	"	32.0	84	8.5	114	30.3
163	"	31.85	83	-	113	31.4
164	"	34.50	82	7	90	23.8

^aSBV and CBR data on soaked specimens could not be obtained due to excessive swelling of clay.

Table 9. (Continued)

Specimen no.	Compactive effort	Moisture content %	Dry density pcf	Unsoaked CBR %	Unsoaked SBV psi	UCS psi
165	Std.AASHO	34.50	84	7	100	29.6
166	"	36.0	80	6.2	65	19.2
167	"	"	84	-	79	24.7
168	"	38	78	5.4	57	15.2
169	"	"	82	-	69	18.4
170	"	40.5	73	3.8	42	11.2
171	"	"	80	-	48	13.1
178	Static	26	98	-	308	43.55 ^b
179	compac-	24.8	93.6	-	346	47.80 ^b
180	tion	39.5	80.8	-	50	6.55 ^b

^bCohesion from direct shear test.

Table 10. CBR and SBV data of laboratory tests performed on wet and dry Ottawa sand specimens

Specimen no.	Compactive effort	Moisture content %	Dry density, pcf	Unsoaked CBR	Sphere bearing value, psi			
					1	2	3	Average
100	-	-	-	15				
101	Std.AASHO	7.35	119.8	55	197	140	147	161
102	Mod.AASHO	"	128.4	131	198	231	220	216
103	Std.AASHO	6.11	116.7	37	198	187	187	192
104	Mod.AASHO	"	129.7	176	408	452	-	430
105	Std.AASHO	7.71	120.3	52	198	143	176	172
106	Mod.AASHO	8.64	129.4	44	143	117	165	141
107	Std.AASHO	7.00	118.1	39	187	198	-	192
108	Mod.AASHO	"	128.5	124	269	331	287	295
109	Std.AASHO	7.89	122.3	37	82	82	-	82

Table 11. Field data: SBV, plate bearing tests, wedge tests and bore hole shear tests

Test no.	Soil classification	In place density pcf	Sphere bearing value, psi			Plate bearing test		Wedge		Bore hole shear test	
			Diameter			$k=\sigma/.05$	Theoretical failure stress, ^a psi	45° W/Ax psi	30° W/Ax psi	C. psi	Ø
			12-in.	6 in.	0.75 in.	pci					
Rest area - Hwy. 69											
1	Sandy loam	98.5	55	-	-	170	48	40	-	0.5	38
2	"	"	86	-	-	260	49	-	-	1.0	38
3	"	"	90	94	87	250	51	24	27	"	"
4	"	"	85	70	82	220	61	40	30	"	"
5	Gr. Sandy loam	"	115	118	-	420	52	-	43	-	-
6	"	"	108	118	-	300	40	22	40	-	-
7	"	"	190	157	-	-	-	-	-	-	- ^b
			200	185							
Hwy. 35 - Under construction											
8	Glacial till	130	118	-	-	400	51	60	-	2.1	32
9	"	"	150	150	-	450	-	-	-	"	"
			150	140							
			140								
10	"	"	150	175	103	360	51	80	70	"	"
				175							
11	"	"	120	120	-	440	59	52	37	"	"
12	"	"	175	175	181	560	37	-	72	3.5	32
				200							
13	"	"	203	300	-	600	67	84	70	"	"
				335							
14	"	"	200	250	-	550	75	132	69	"	"
				300							
15	"	"	175	175	-	450	42	57	49	"	"
			175	205							

^a Shown in Figure 36 on page 120.

^b Direct shear test values from Shelby tube samples: $C = 4$ psi, $\phi = 38$.

Table 11. (Continued)

Test no.	Soil classification	In place density pcf	Sphere bearing value, psi			Plate bearing test		Wedge		Bore hole shear test	
			12-in. Diameter	6 in.	0.75 in.	$k=\sigma/.05$ pci	Theoretical failure stress, psi	45° W/Ax psi	30° W/Ax psi	C. psi	ϕ
16	Glacial till	130	170 170	175	"	"	"	"	"	3.5	32 ^c
<u>County road - North of Ames</u>											
17	Silty clay	85	70	72	"	300	57	37	"	9.2	2
18	"	"	68	"	"	360	71	"	"	"	"
19	"	"	75	96	"	"	"	"	"	"	"
20	"	"	70	60	"	"	"	"	"	"	"
			60	60	"	"	"	"	"	"	" ^d

^cUCS = 46.6 psi.

^dUCS = 25.7 psi.

B. Statistical Analysis

1. General

The aim of this analysis was to compare variabilities of various tests performed during the course of investigation, to establish the best prediction lines, and to determine limits of confidence bands for various tests performed.

Variance is a measure of the spread of observed values about the true value. Thus, for good prediction, low values of σ are desired. Analysis for variance was possible only in the CBR and SBV tests. A similar analysis for the unconfined compression test, plate bearing and other tests was not feasible due to the unequal number of readings on different locations.

Various methods are available for predicting one variable from the other where a linear relationship exists between the two variables with both subject to error. However, the analysis here is based on the ordinary least-squares method. This method leads to a biased estimator, since the assumptions underlying a valid application of least-squares include, among others, that the independent variable be free of error. Despite this, the least squares line can be used for prediction purposes. Since coefficient of variance of the SBV was found to be about half that of the CBR, the SBV was assumed to be free of error in establishing the prediction line and the confidence bands.

2. Comparison of variability of SBV and CBR

A set of ten CBR specimens (Table 12, 90 - 99) were molded from loessal silt at 15.3 percent moisture content and standard AASHO compactive effort. Unsoaked CBR tests were performed under identical conditions to

Table 12. CBR values

i	1	2	3	4	5	6	7	8	9	10
Specimen no.	90	91	92	93	94	95	96	97	98	99
CBR value Y_i (%)	14	12	15	12	14	13	15	15	14	15

determine variability. Table 12 gives the values obtained.

$$\begin{aligned}\sigma_{\text{CBR}}^2 &= \frac{1}{9} \left[\sum Y_i^2 - \frac{(\sum Y_i)^2}{10} \right] \\ &= \frac{1}{9} \left[1945 - \frac{19321}{10} \right] \\ &= 1.4333\end{aligned}$$

$$\sigma_{\text{CBR}} = 1.973$$

$$\bar{Y}, \text{ mean value} = 13.9\%$$

$$\text{C.V.}, \text{ coefficient of variance} = \frac{\sigma_{\text{CBR}}}{\bar{Y}} = \frac{1.973}{13.9} = 0.1419 .$$

Similarly four sets of specimens were molded in CBR molds at moisture contents and compactive efforts shown in Table 13. Six SBV tests were performed on each unsoaked specimen -- three tests on each side. On some specimens all six tests could not be performed because the specimen surfaces were uneven and disturbed; as such the number of tests in each set are not equal.

Table 13. Details of SBV tests

Set no.:	1	2	3	4
Specimen no.:	51,52,53	54,55	58,89	60,61
Compactive effort:	Std.AASHO	Mod.AASHO	Iowa 3	Sts.AASHO
Moisture content, %:	17.6	17.8	17.6	21.5

i	SBV, psi	SBV, psi	SBV, psi	SBV, psi
1	123	265	155	44.1
2	132	254	139	55.0
3	121	243	165	55.0
4	161	243	150	44.1
5	143	232	155	44.1
6	121	260	133	39.8
7	117	257	170	39.8
8	137	266	133	39.8
9	137	232	150	-----
10	150	258	155	-----
11	----	257	----	-----
12	----	266	----	-----
$\bar{\sigma}_{SBV}$	204	151	155.2	40.4

$$G, \text{ Grand total, } \sum_{i=1}^{40} (SBV_i) = 6242$$

$$G^2 = 38,962,564$$

$$CT, \text{ correction term} = \frac{G^2}{40} = 974,064$$

$$TSS, \text{ total sum of squares} = \sum_{i=1}^{40} (SBV)^2 - CT = 220,664$$

$$\text{SBV sum of squares} = \sum_1^4 \frac{(\sum \text{SBV})^2}{i} - \text{GT} = 215,504$$

$$\text{Error sum of squares} = (\text{TSS} - \text{SBV SS}) = 5160$$

$$\sigma_{\text{SBV}}^2 = \frac{\text{Error sum of squares}}{i - 4} = 143.33$$

$$\sigma_{\text{SBV}} = 11.973$$

$$\bar{X}, \text{ mean value} = \frac{G}{40} = \frac{6242}{40} = 156.05$$

$$\text{C.V., coefficient of variance} = \frac{\sigma_{\text{SBV}}}{\bar{X}} = \frac{11.973}{156.05} = 0.0767$$

Coefficient of variance can also be expressed as scatter, which in this analysis is 14.2 percent for CBR and 7.67 percent for SBV. In the subsequent prediction analysis we will, therefore, assume that the SBV is free of error.

3. Estimation of CBR from SBV

As indicated in the test procedure, three SBV tests were run on one side of specimen in CBR mold and a CBR test on the other side. It was observed that the SBV and the corresponding CBR value of a specimen for a given moisture content, compactive effort and soil seem to be related. This relationship can be visualized when the observational points (X_i, Y_i) , $i = 1, 2, 3, \dots, n$, are plotted where Y_i is the SBV observation for the i^{th} specimen and X_i is the CBR value of the same specimen (n being the total number of specimens observed).

From the observation points (X_i, Y_i) on the graph it seems that the relationship is best for moisture contents between 12% to 19% with loess at all compactive efforts. This indicates that in very dry or very wet

specimens the relationship is not as clear cut as shown in Figure 35.

In order to estimate the relationship between SBV and CBR values of specimens for moisture contents between 12 to 19% inclusive, we fit a linear regression line. For this purpose the model we assume is:

$$Y_i = b_0 + b_1 X_i + e_i$$

where $e_i \sim N(0, \sigma^2)$.

The following table shows the SBV and CBR values for 68 observations for moisture contents 12 to 19%, inclusive.

Table 14. CBR and SBV for moisture contents between 12% and 19% of loessial soil specimens

Specimen no.	CBR, % X_i	SBV, psi Y_i
10	20	264
11	93	645
13	62	550
14	82	584
17	36	340
18	56	412
19	58	386
20	26	314
21	26	199
22	37	280
23	37	232
24	40	232
25	14	121
26	5	80
27	10	139
28	6	77
29	5	82
36	20	260
37	90	692
38	35	309
39	58	468

Table 14. (Continued)

Specimen no.	CBR, % X_i	SBV, psi Y_i
40	62	516
41A	32	372
42	88	639
43	42	309
45	56	400
46	25	276
47	15	155
48	27	187
49	22	154
50	16	207
51	18	254
52	20	252
53	19	203
54	8	136
55	7	133
56	21	198
57	12	157
58	10	155
59	11	150
66	23	287
67	23	260
68	37	324
69	31	276
70	23	247
72	72	565
73	39	371
74	59	462
75	50	455
76	68	536
77	20	215
78	26	315
79	37	327
80	32	320
81	28	280
82	40	365
83	37	433
84	51	370
85	53	466
86	33	353
87	43	356
110	56	542
114	80	585

Table 14. (Continued)

Specimen no.	CBR, % X_i	SBV, psi Y_i
115	37	377
116	58	475
117	67	487
118	68	566
119	78	725

$$n = 68$$

$$\Sigma X = 2,596.00 \quad \Sigma Y = 22,859.00$$

$$\bar{X} = 38.176 \quad \bar{Y} = 336.161 \quad \Sigma XY = 1,108,001.00$$

$$\Sigma X^2 = 134,672.00 \quad \Sigma Y^2 = 9,288,363.00$$

$$\frac{(\Sigma X)^2}{n} = 99,106.11 \quad \frac{(\Sigma Y)^2}{n} = 7,684,321.70 \quad \frac{(\Sigma X)(\Sigma Y)}{n} = 872,675.94$$

$$\Sigma x^2 = 35,565.89 \quad \Sigma y^2 = 1,604,041.3 \quad \Sigma xy = 235,325.06$$

In this analysis it is assumed that a true straight-line relationship exists. This line can be represented by the equation

$$\hat{Y} = b_0 + b_1 X$$

where \hat{Y} is the true SBV for a given specimen, X is the true CBR value of the same specimen, b_1 is the slope of the line and b_0 is the Y intercept of the line.

and

$$t_{0.05(n-2)} = 1.997 \text{ (28, p. 528).}$$

$$Y \begin{matrix} \text{---}^u \\ \text{---}^L \end{matrix} = 83.59 + 6.616X \pm 1.997 \times 26.72 \left(1 + \frac{X^2}{134672}\right)$$

Note: The subsequent analysis for determination of prediction and confidence lines will not be shown. The procedure followed is exactly the same.

4. Estimation of plate bearing from the SBV

Tests in the field to determine the modulus of subgrade reaction (k) at 0.05 in. deflection, and the SBV is obtained at the same place, were similarly treated by the technique of linear regression. Plate tests were performed with a 12-inch diameter circular plate. A total of 16 observations are available from field tests, Table 16.

Table 16. Modulus of subgrade reaction and corresponding sphere bearing values from field tests^a

Field test no.	Soil	SBV, psi X_i	k, psi Y_i
1	Sandy loam	55	170
2	"	86	260
3	"	90	250
4	"	79	220
5	Gravelly sandy loam	117	420
6	"	110	300
8	Glacial till	118	400
9	"	150	450
10	"	143	360
11	"	120	440
12	"	177	560
13	"	203	600
14	"	200	550
15	"	175	450
17	Silty clay	72	300
18	"	68	360

^aData from Table 11.

b. Silt Eighteen observations on silt are listed in Table 20.

Table 20. SBV and corresponding UCS values of silt^a

Specimen no.	SBV, psi X_i	UCS, psi Y_i
126	190	40.8
127	163	42.3
129	182	47.0
131	95	52.8
134	179	33.2
136	166	38.5
138	177	47
140	176	35
142	182	32
144	194	39
148	194	30
149	304	31.4
150	242	46.7
151	298	43.3
152	260	41.7
153	196	31.5
154	128	27.3
155	55	26

^aValues from Tables 7 and 8.

Table 21. Analysis of variance

Source of variation	Degree of freedom	Sum of squares	Mean sum of squares
Regression	1	24,106	24,106
Residual	17	3,006.43	54.83
Total	18	27,112.43	--

Equation of prediction line

$$Y = 0.18553 X$$

Equation of 95 percent confidence lines

$$Y \begin{matrix} \text{---}^u \\ \text{---} \\ \text{---}^L \end{matrix} = 0.18553 X \pm 2.110 \times 7.406 \left(1 + \frac{X^2}{700,325}\right)$$

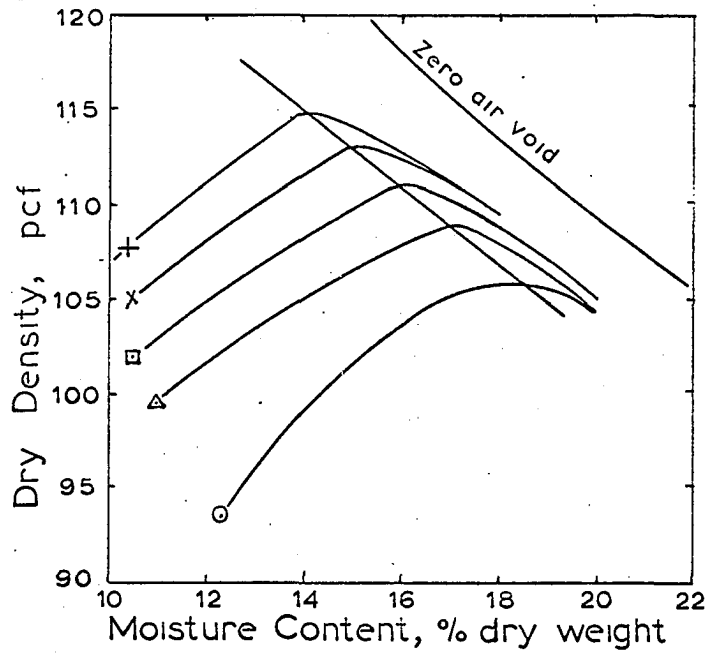
C. Discussion of Results

1. Sphere Bearing Value versus California Bearing Ratio

One of the objectives of the investigation was to establish, if possible, a relationship between Sphere Bearing Value and the CBR. If a relationship could be established then it would be possible to predict the CBR value by means of the more rapid Sphere Bearing tests, either in the laboratory or in the field.

In the laboratory, the moisture content was varied from 10 percent to 21 percent and specimens were molded at five different compactive efforts. Figure 31 shows effect of moisture content and compactive effort on the dry density of silt. In Figures 32, 33 and 34 we see the effect of moisture content, compactive effort and dry density on both the CBR and SBV. It may be seen that the CBR and SBV both decrease as the moisture content increases, and both increase as the density increases with moisture content constant. The shape of the curves is almost identical for the two tests.

Statistical analysis of data in Table 6 gives a coefficient of variance of 0.142 (14.2%) for the CBR tests and 0.0767 (7.67%) for the Sphere Bearing tests, or almost half. This indicates that an individual Sphere Bearing test is far more reliable and reproducible than a CBR test.



LEGEND
(Also for Figures 32-34)

Symbol	Name	Layers	Blows per layer	Weight of hammer lb.	Drop, in.
+ ———	Mod. AASHO	5	55	10	18
X ———	Iowa III	5	45	10	18
▣ ———	Iowa II	5	35	10	18
△ ———	Iowa I	5	25	10	18
⊙ ———	Std. AASHO	3	56	5.5	12

Figure 31. Effect of moisture content and compactive effort on the dry density of silty soil (loess 20-2)

Figure 32. Effect of density and moisture content on the CBR and the SBV of silty soil

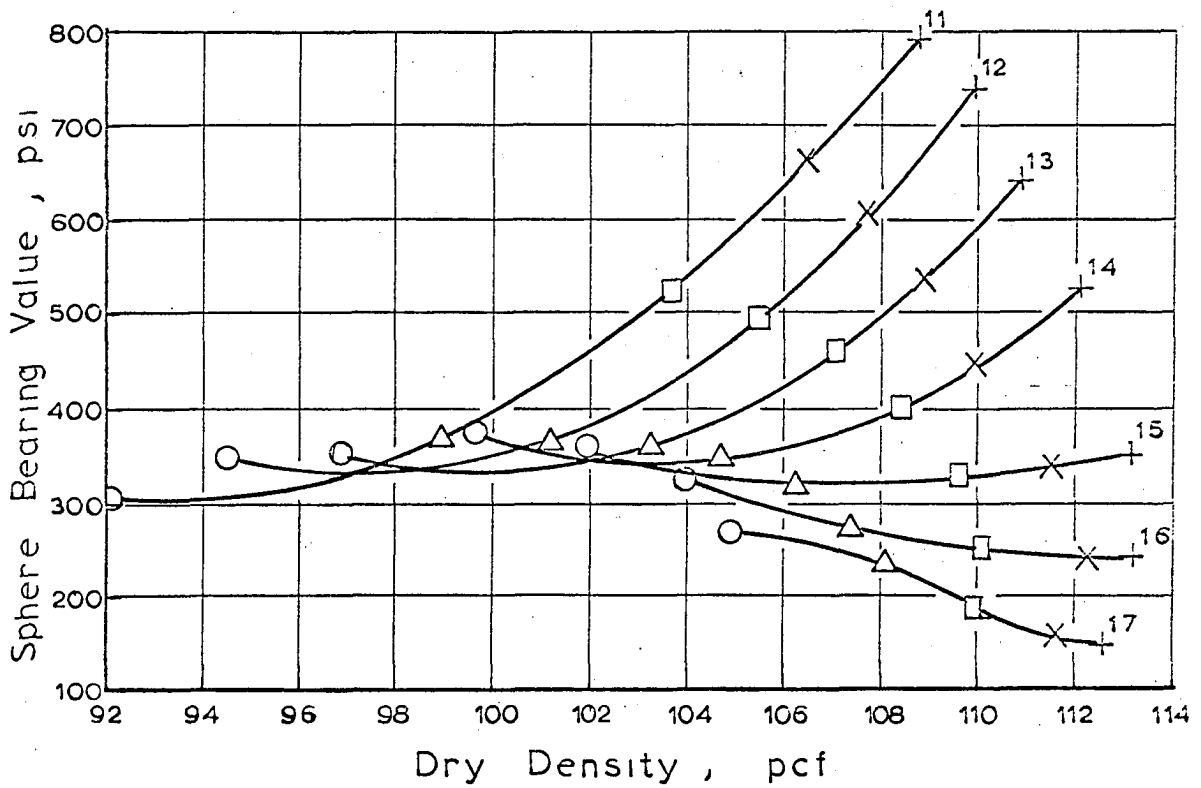
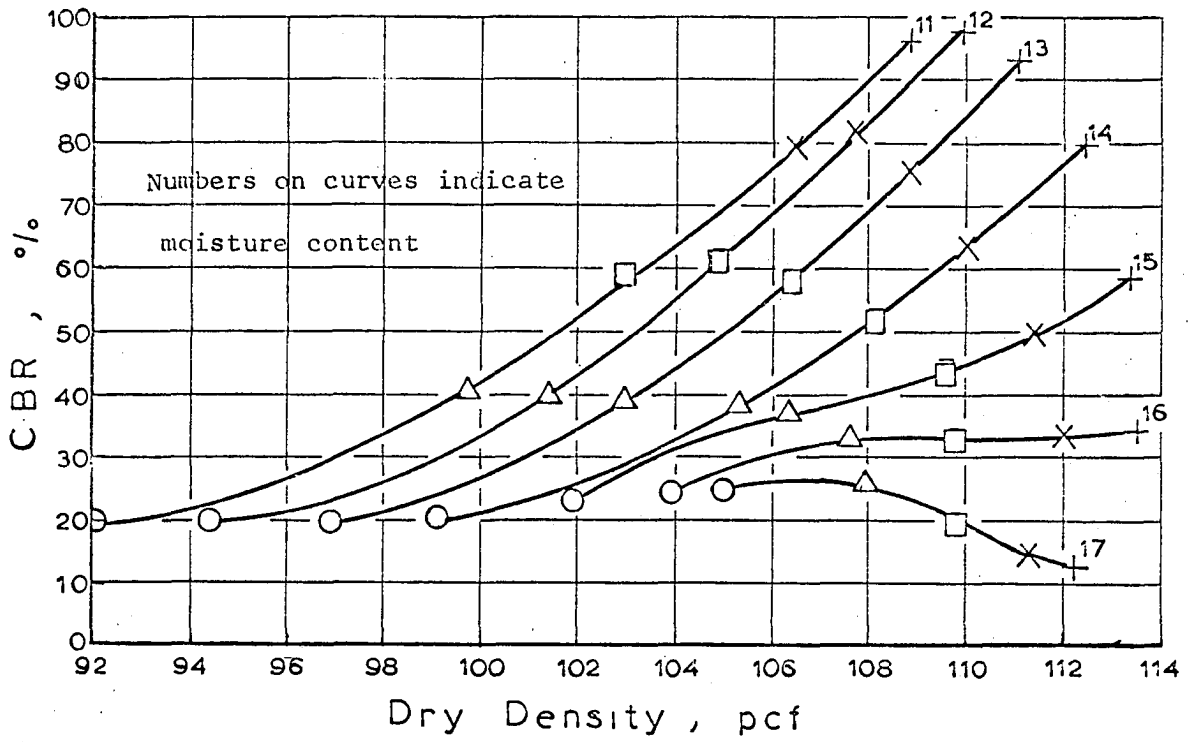


Figure 33. Effect of moisture content and compactive effort on the GBR and the SBV of silty soil

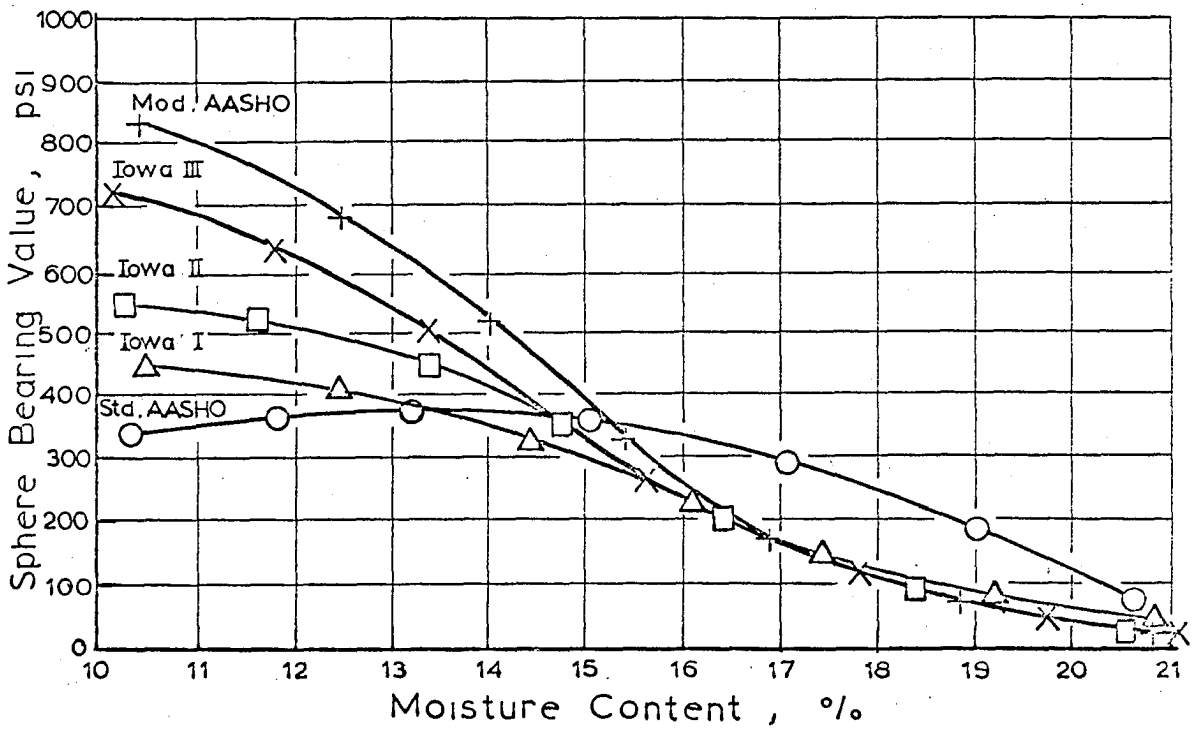
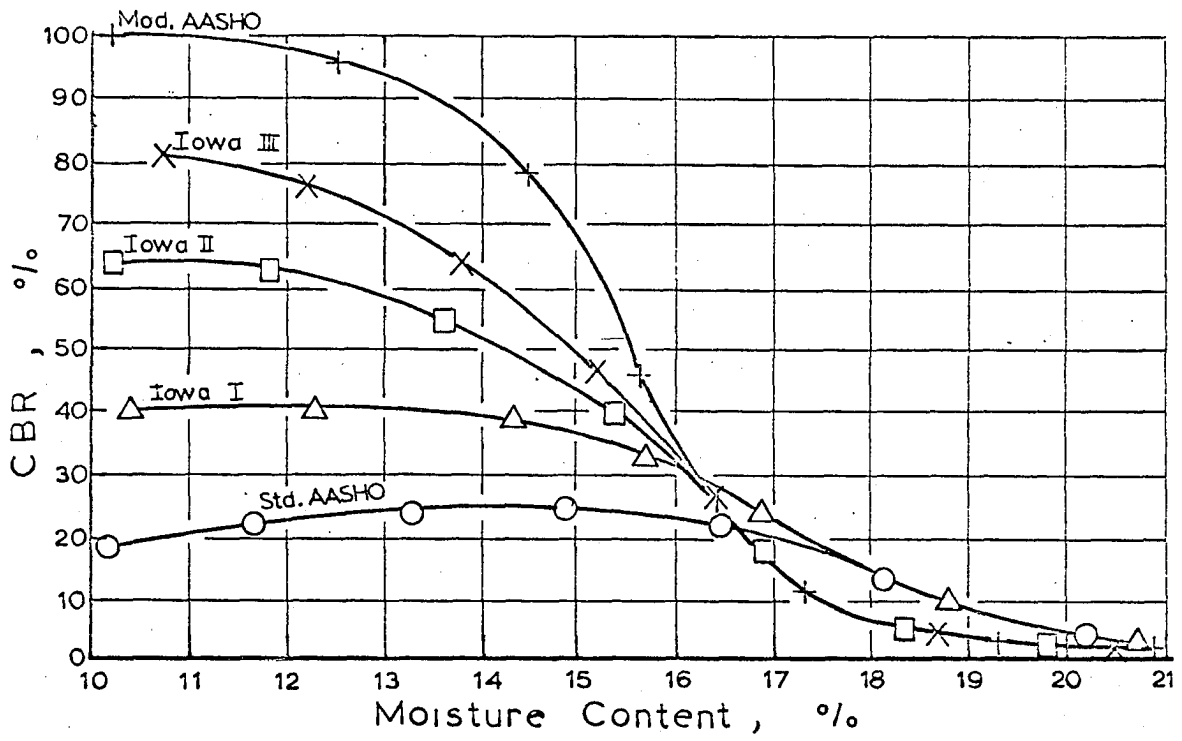
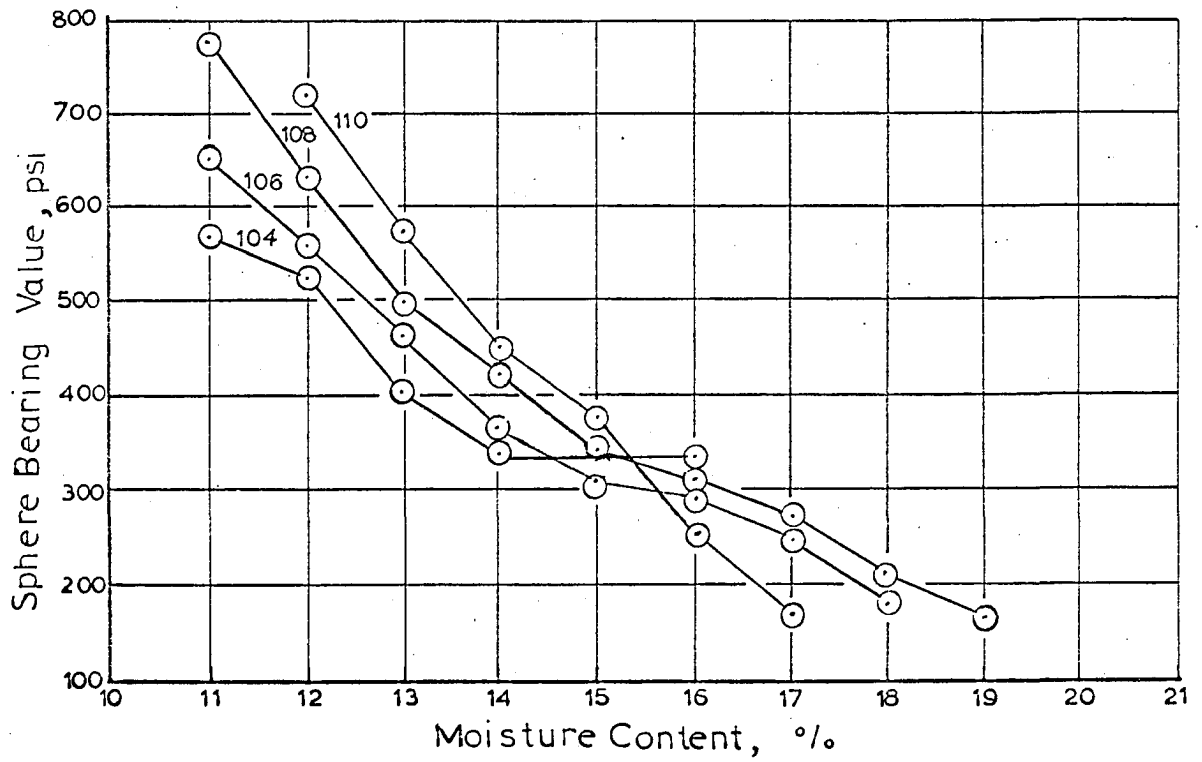
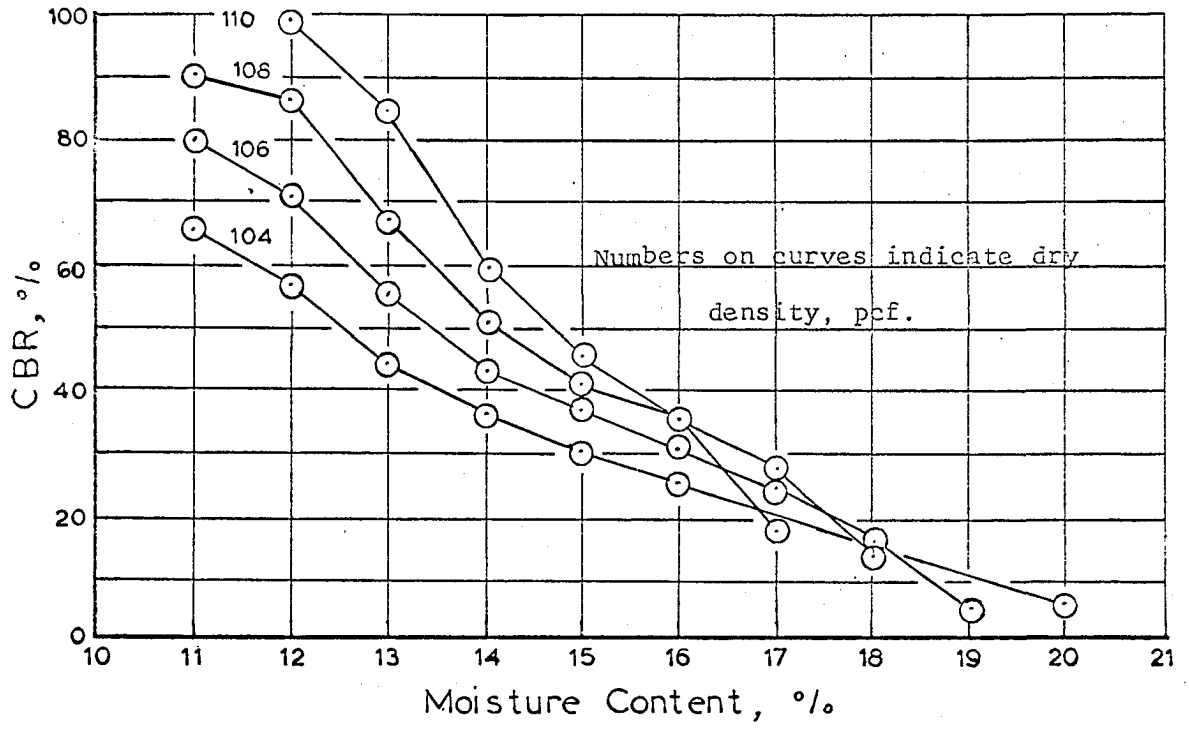


Figure 34. Effect of moisture content and density on the CBR and the SBV of silty soil



Consistency of the Sphere Bearing test was also observed in the field tests as seen in Table 11. For example, the test series 2, 3 and 4 were performed on different days and yet their values are within 5 percent of each other, which is not true of any other tests in these or any other series in Table 11.

The regression line and 95 percent-confidence band in Figure 35 are based on data in Table 6. Specimens that were either very dry ($< 11\%$ moisture content) or very wet ($> 20\%$ moisture content) were not included in the statistical analysis. However, all the CBR and SBV test results in Table 6 are included in Figure 35.

Specimens that were considerably below the optimum moisture content (X's in Figure 35) have a much higher SBV compared to the CBR. At such low moisture contents the void ratio is high, and when load is applied to the sphere the soil under it densifies and offers increased resistance to penetration, whereas in the CBR test the soil under the punch is sheared rapidly and has much less time for densification. On the other hand at very high moisture contents the CBR value is observed to be much higher than the corresponding Sphere Bearing Value, and secondly all the CBR values fall in a very narrow range between 1 and 5 percent CBR. It is felt that at very high moisture contents both the tests measure viscosity rather than strength properties of the soil, and since the CBR test has a much higher shearing rate it produces more viscous resistance.

Highway and airport subgrades are invariably compacted at or about optimum moisture content for standard or modified AASHO density. It is seen in Figure 31 that for loess this moisture content is between 14

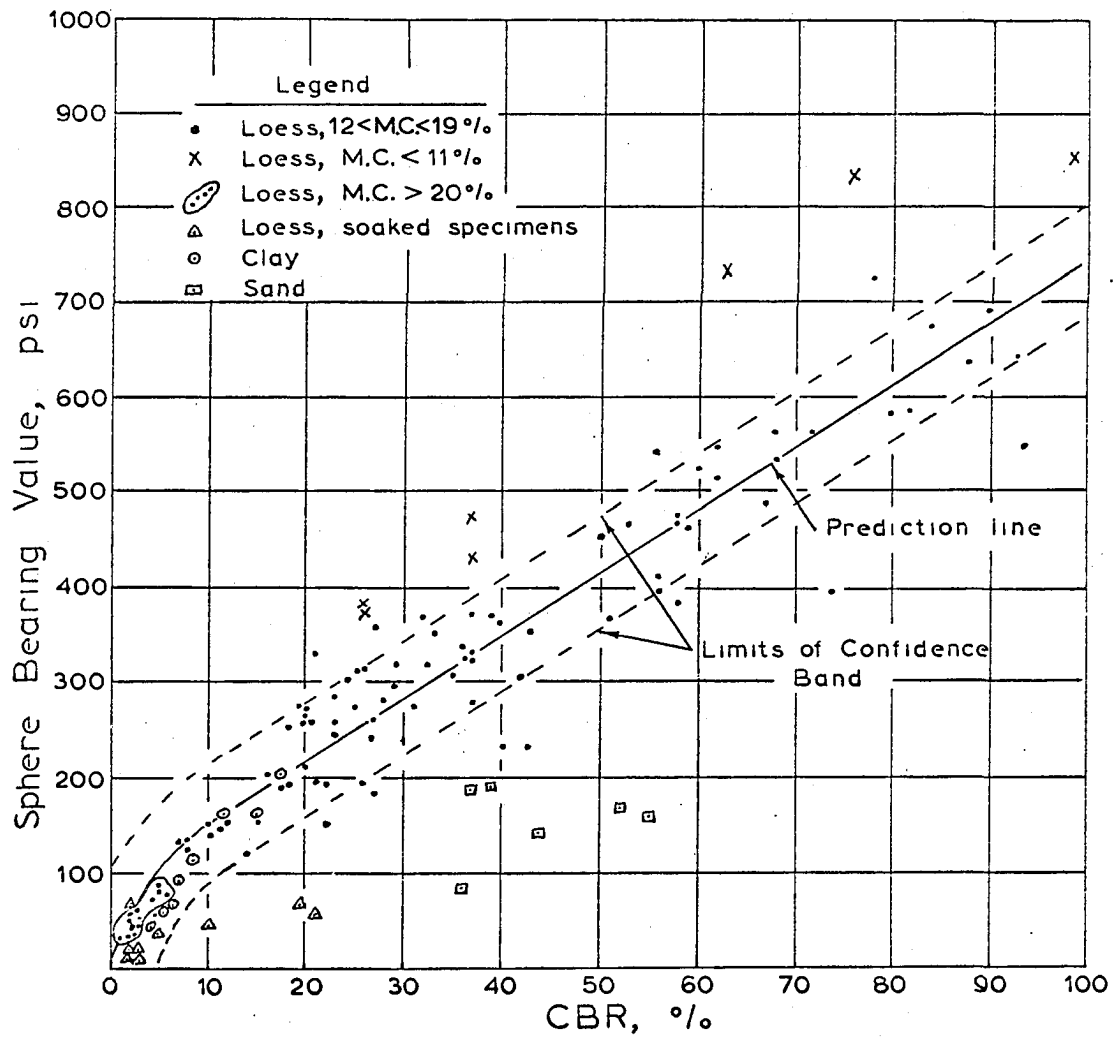


Figure 35. Relationship between the Sphere Bearing Value and the CBR

percent and 18 percent, whereas the 95 percent confidence band in Figure 35 enclosed the entire range of moisture contents above 11 percent. The correlation obtained between the CBR and the SBV is therefore satisfactory.

Test data given in Tables 7, 8, 9 and 10 were plotted in Figure 35 to test whether the correlation obtained for loess applies to the other soils. The clay follows the correlation, but the sand does not. (Tests on sand were discussed earlier under the sections on Preliminary Investigation and Procedure.) All the CBR tests were performed with a 10 lb surcharge on the specimen, whereas all the Sphere Bearing tests were performed without any surcharge. Since cohesionless sand does not develop any resistance to deformation unless it is confined, the sand CBR test values shown in Figure 35 are much higher than the corresponding Sphere Bearing Values. The Sphere Bearing Values of these tests are merely an indication of apparent cohesion of wetted sand.

No relationship could be found between the Sphere Bearing test data and the corresponding CBR ratings of the soaked specimens. The data, however, are also plotted in Figure 35. It was noted that after a specimen had been soaked for four days its surfaces became very soft and did not offer much resistance to penetration of the sphere. Furthermore, for a one-inch diameter sphere the limit of penetration (15 percent of the diameter of the sphere) is 0.15 inch; in a soaked specimen the top half-inch of soil is very soft, and the sphere often penetrated under its own load.

To sum up, a correlation exists between the SBV and the CBR which may be expressed by the following prediction equation:

$$Y = 83.8 + 6.616 X$$

where Y is the Sphere Bearing Value in psi and X is the unsoaked GBR index value. The relation is found to be correct for all soils except cohesionless sand.

2. Sphere Bearing test versus plate bearing test

When load is applied to a circular plate placed on a soil, the soil deforms and the plate settles. If the load is increased the settlement increases. For small loads the settlement is small and approximately proportional to the applied load, as shown in Figure 36, but as the load increases, a point is reached beyond which the settlement increases much more rapidly. The initial straight-line part of the stress-deflection curve is attributed to pseudo-elastic distortion and compression of the soil, whereas the steep part is caused by shear failure, analogous to the breaking of a beam under load (23, p. 538). Between is a transition region of local cracking or partial failure. The intersection of two tangents, one drawn to the elastic branch of the curve and a second drawn to the steep branch, defines the theoretical point of soil failure, or the maximum load that the soil can carry.

Rigid pavement designs for highways and airports are based on modulus of subgrade reaction "k" which is obtained from the straight-line part of the stress-deflection curve of plate bearing tests. Foundations are often designed on theoretical failure-point criteria of plate bearing tests.

Plate bearing tests are expensive and time consuming, so one objective of the study was to develop a correlation between the Sphere Bearing Value,

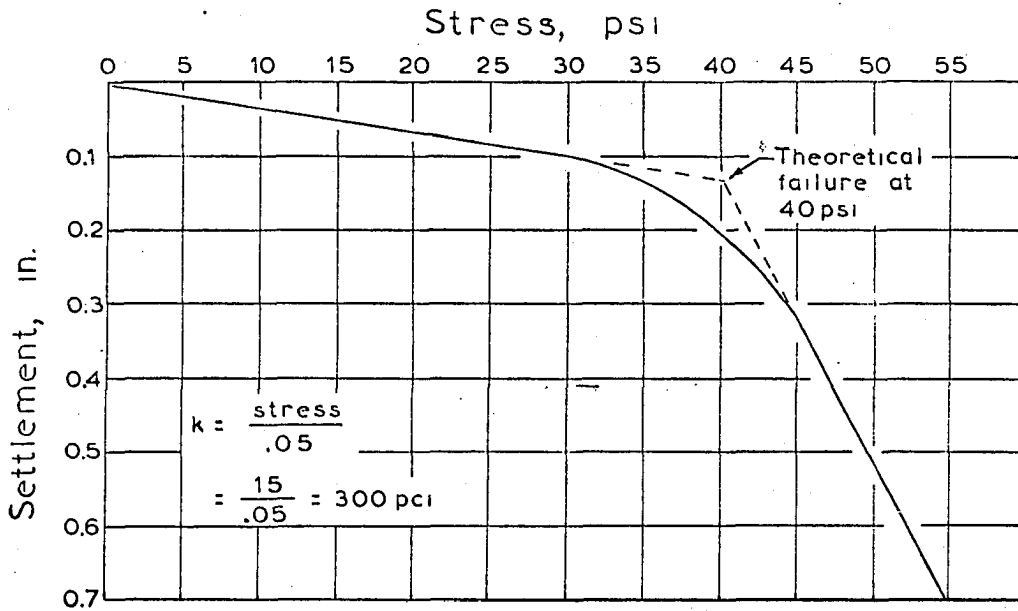


Figure 36. Stress-settlement curve of the plate bearing test

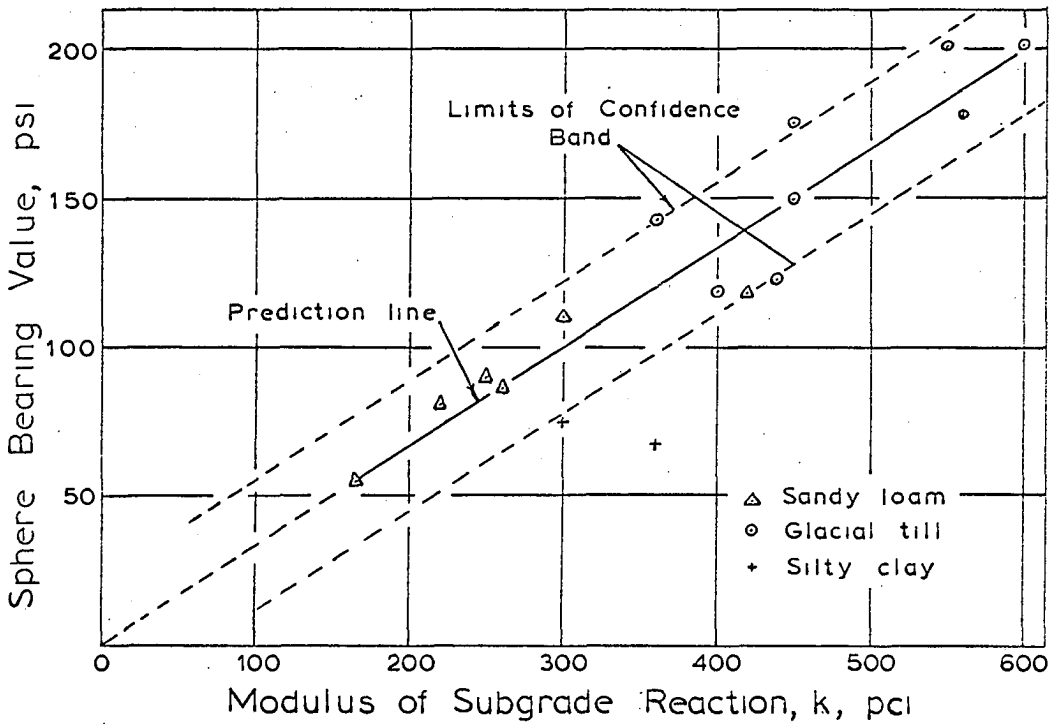


Figure 37. Relationship between SBV and k

the modulus of subgrade reaction (k) and the theoretical failure stress.

The numerical values of the Sphere Bearing test and the 12 inch circular plate tests performed in the field are given in Table 11. It may be seen that no correlation exists between the SBV and the theoretical failure stress. However, an excellent linear relationship was found by statistical analysis of Sphere Bearing Value vs. the modulus of subgrade reaction. The equation of the prediction line is:

$$k = 3.01 X$$

where k is the modulus of subgrade reaction of soil in pci with a 12 inch diameter plate, and X is the Sphere Bearing Value in psi. The 95 percent confidence band and the prediction line are shown in Figure 37. In Table 11 may be seen that the k values are far less reproducible than SBV, and tests repeated on the same soil give widely different values. The width of the band is due more to the variability of plate bearing test than the Sphere Bearing test.

In order to determine the effect of differences in predicted k on the thickness of pavement, a few examples are worked out in Table 22. The pavement thickness was designed using the PCA design curves (31, p. 19), using a wheel load of 10,000 lb and flexural stress in the concrete of 400 psi. The upper and lower k values were picked up from the two limits of the confidence band for three Sphere Bearing Values of 50, 100 and 150 psi.

Table 22. Effect of k on thickness of rigid pavements

SBV psi	k, pci		pavement thickness, in.		Difference in.
	Upper limit	Lower limit	Upper limit	Lower limit	
50	215	85	6.39	6.00	0.39
100	360	235	5.60	5.90	0.30
150	520	385	5.35	5.60	0.25

It may be seen in Table 22 that even for wide range in k value, the pavement thickness based on predicted k varies by less than 0.4 inch. Thus small errors in the selection of k will not seriously affect pavement design.

The correlation between the SBV and k is based on limited field data but it can be extended with further testing to include higher values of k. It should then be possible to predict values of k with the relatively inexpensive Sphere Bearing test.

3. Sphere Bearing test versus steel wedge test

The steel wedge test is not standard but was devised to fit Meyerhof's (25) empirical method for ultimate bearing capacity of wedge-shaped foundations.

The main problem encountered in this test was that the presence of gravel and even small pebbles under the edge caused the wedge to penetrate unevenly. The results obtained, given in Table 11 and in Figure 38 are widely scattered and quite unreliable. Although a prediction line and confidence band were drawn, no correlation could be established between the SBV and Meyerhof's values.

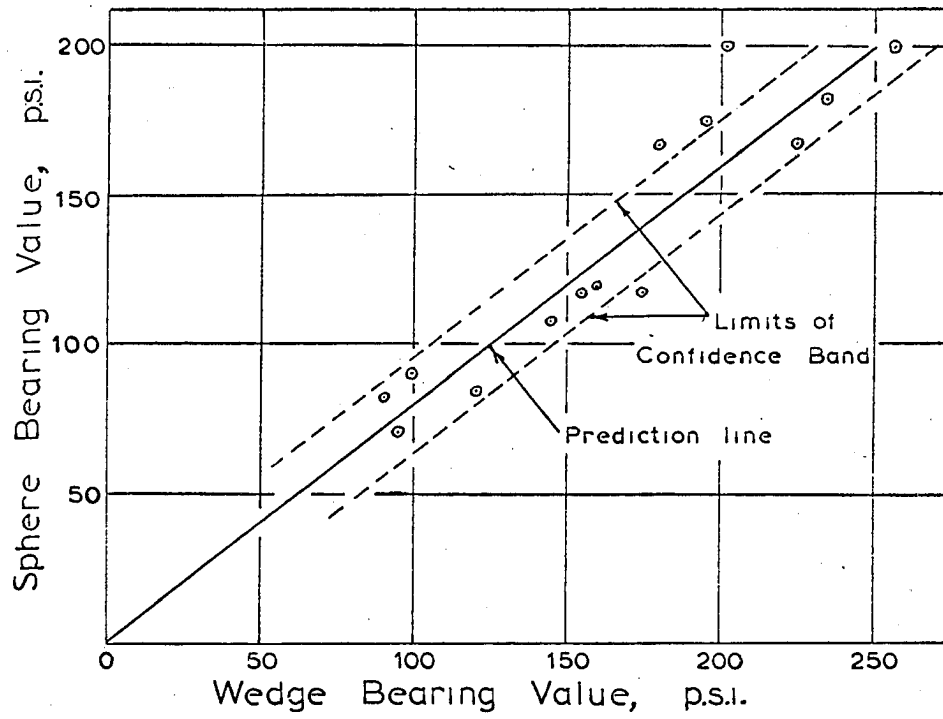


Figure 38. Relationship between SBV and wedge bearing value ($\frac{W}{A_x}$)

4. Sphere Bearing test versus unconfined compressive strength

In cohesive soils a simple and direct determination of ultimate bearing capacity is often based on the unconfined compressive strength. The ultimate bearing capacity of footings at the surface of cohesive soils has been worked out by Prandtl, Fellenius and Terzaghi independently with reasonably good agreement between their solutions. Taylor (41) has simplified their solutions in terms of unconfined compressive strength as

$$q_u = 3.5 p_c$$

where q_u is the ultimate bearing capacity of circular or square footings and p_c is the unconfined compressive strength of the soil. Taylor approximates unconfined compressive strength as twice the cohesion of soil.

In an earlier section it was discussed that the mean pressure over the surface of a spherical indenter over the region of contact with metal has a value of about $3Y$, where Y is the constant yield stress of the metal. Yield stress of metals may be considered analogous to the unconfined compressive strength of soils. It was also observed that the shape and extent of deformation zone in soils under a spherical penetrometer was remarkably similar to that described by Ishlinsky in deformation of metals. The ratio of curved area formed by the elastic-plastic boundary and curved area of sphere in contact with the soil ranged between 5.6 to 6.7 in clay and 6.7 to 7.4 in silt.

Figure 39 shows the SBV plotted against the UCS strength of clay. The regression line has the equation

$$Y = 3.66 X$$

where Y is the Sphere Bearing Value and X is the unconfined compressive

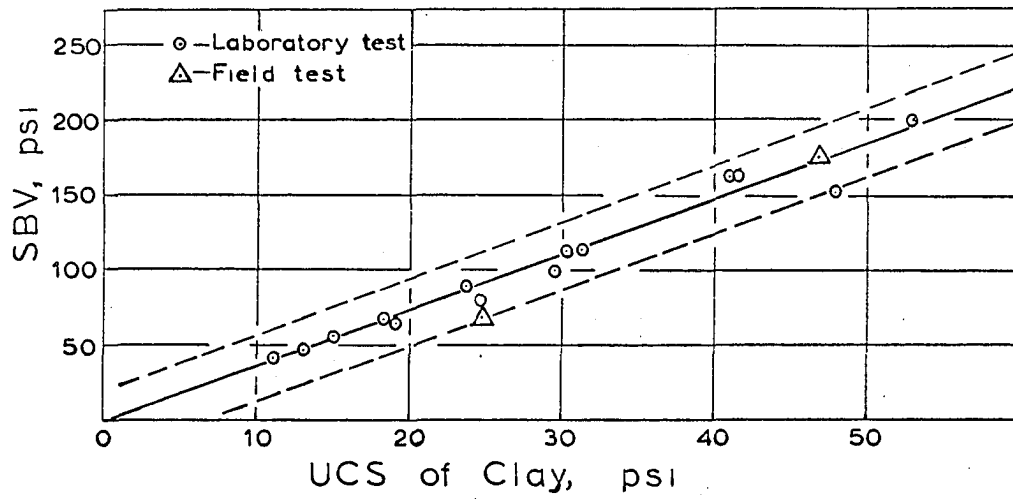


Figure 39. Relationship between SBV and UCS of clay

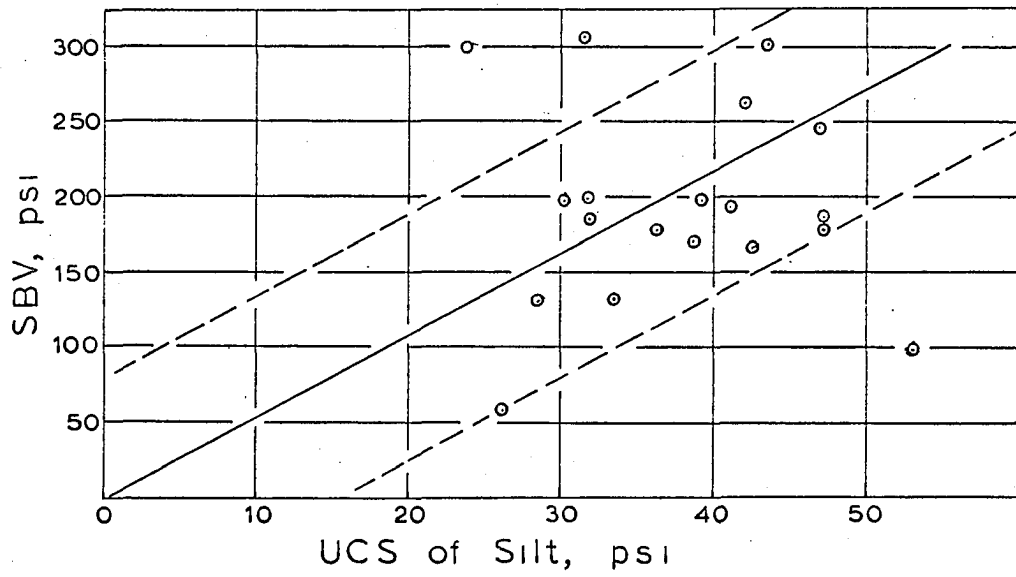


Figure 40. Relationship between SBV and UCS of silt

strength. The 95 percent confidence band is narrow and all the points fall within this band. Two values of field tests on glacial till plotted in this figure also fall within the confidence band.

Data on silt are plotted in Figure 40; the points are widely scattered, and the confidence band is much wider than for the clay. Also, the slope of the prediction line is steeper than in the clay and has the equation

$$Y = 5.38 X.$$

We will first discuss the erratic behavior of silt. In his study of shear strength properties of Western Iowa Loess, Akiyama (1) performed triaxial tests on undisturbed samples and found that small variations in field moisture content considerably altered both the cohesion and the angle of internal friction in an unpredictable manner. Triaxial-quick-tests were performed in the present investigation on compacted specimens similar to those for the Sphere Bearing tests; results are given in Table 7 and Figure 41. It may be seen that values of c and ϕ are just as erratic as the unconfined compressive strength, and with small variations in moisture content the values change in an unpredictable manner.

The steeper slope of prediction line in silt means that the soil offers greater resistance to penetration of a sphere than expected from the unconfined compressive strength. This phenomenon is assumed to be caused by two factors. First, the Sphere Bearing Test induces drainage in the permeable soil mass under the sphere, whereas the unconfined compressive strength test is rapid and no drainage is permitted. Drainage of silt samples was also observed in model sphere bearing investigations, where the specimen surface was observed to deflect downwards around the

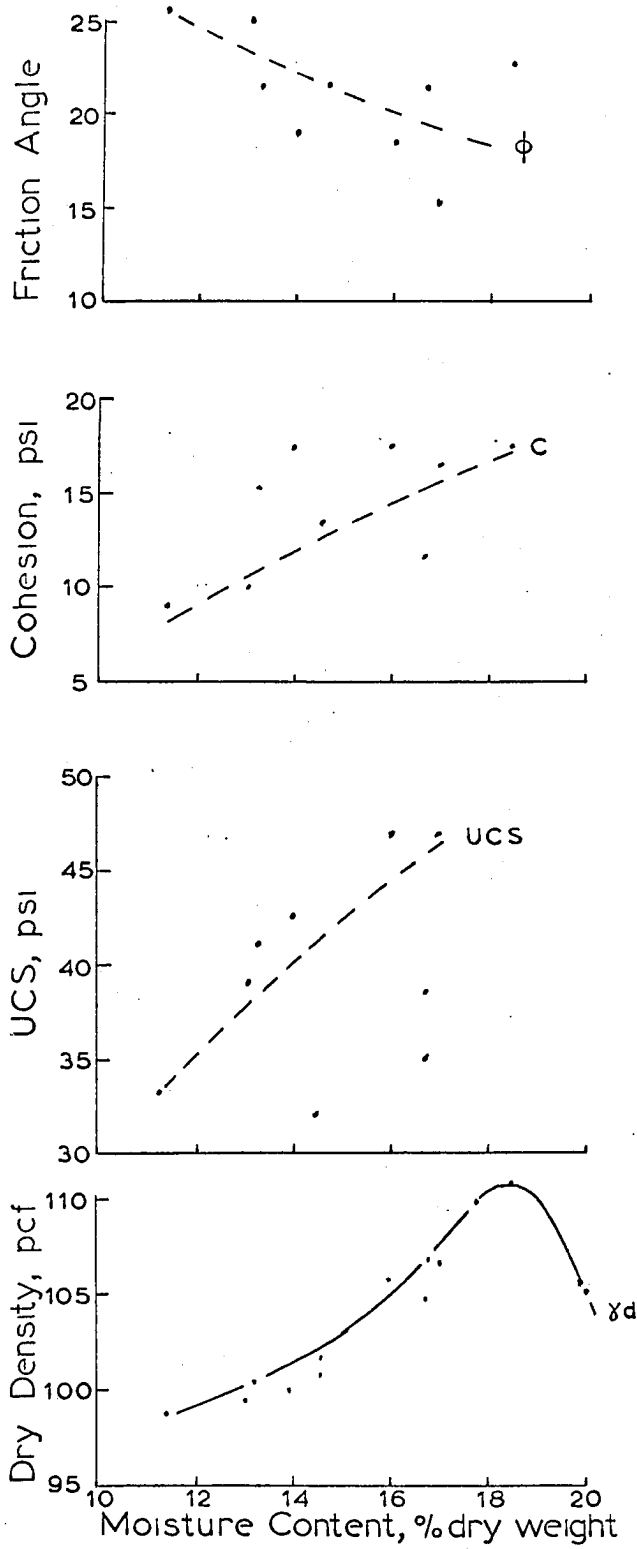


Figure 41. Effect of moisture content on Western Iowa loess

sphere under load. Drainage increases the resistance of specimen to deformation; hence the higher Sphere Bearing Values. Second, the greater confinement in sphere-deformed zone compared to the unconfined compressive test mobilizes more internal friction. We may recall that in the model tests the ratio of the curved areas in silt was higher than in clay, which may also contribute to the higher Sphere Bearing Values.

It is therefore, reasonable to assume that the Sphere Bearing test is more a measure of the ultimate resistance of soil to deformation, or in other words, is a measure of the ultimate bearing capacity of soil.

5. Sphere Bearing Value and ultimate bearing capacity of soil

The bearing capacity of a soil is the maximum load per unit of area which the soil can support without rupture, and is often termed as ultimate bearing capacity. The methods that have been formulated for the determination of the ultimate bearing capacity of soils are based on the concept that was first developed by Prandtl for the punching of metals and later modified by Terzaghi and others for use in soils whose strength can be expressed by

$$S = G + N \tan \phi$$

where S is the shearing strength, G the cohesion, N the normal stress and ϕ the frictional angle. The general approach of all these investigators is similar and the expression can be simplified to

$$q_D = C \cdot N_c + \gamma \frac{b}{2} N_\gamma + q' N_q$$

where γ is the effective soil unit weight, q' is the surcharge, and b is the width of foundation. The quantities N_c , N_γ and N_q are dimensionless bearing capacity factors that depend on ϕ and shape of the failure zone

assumed by the different investigators. The factors N_c , N_γ and N_q respectively relate to soil cohesion, unit weight and surcharge. Values of these factors from the analyses of Terzaghi and Meyerhof are given by Leonard (23, p. 542). The shape of the failure zone in these analyses is more or less similar to that assumed by Prandtl.

Terzaghi (43, p. 172) from model studies and empirical data modified the above equation for circular foundations as follows:

$$q_D = 1.3 C N_c + 0.6 \gamma r N_\gamma + \gamma D_f N_q$$

where r is the radius of circular foundation and D_f is the height of soil above the base of the footing.

Field values of cohesion and friction angle were obtained by the bore hole shear device near sites of the Sphere Bearing tests. Data are given in Table 11.

The ultimate bearing capacity of soils tested was computed according to the above equation for a one-square-inch circular footing. The last term on the right was dropped because surcharge was essentially zero. Calculated bearing values are given in Table 23 along with the SBV obtained at the test sites in three different soils. Three sets of laboratory data have also been included in this table.

In Figure 42 the calculated bearing capacity is plotted against the Sphere Bearing Value. A regression line may be sketched in at 45 degrees, and all the points lie about this line except one for a gravelly-sandy loam. The c and ϕ values for this site were obtained from Shelby tube samples by direct shear tests in the laboratory; however (Tables 11 and 23) the value of C of 4 psi appears high for a gravelly-sandy loam. It

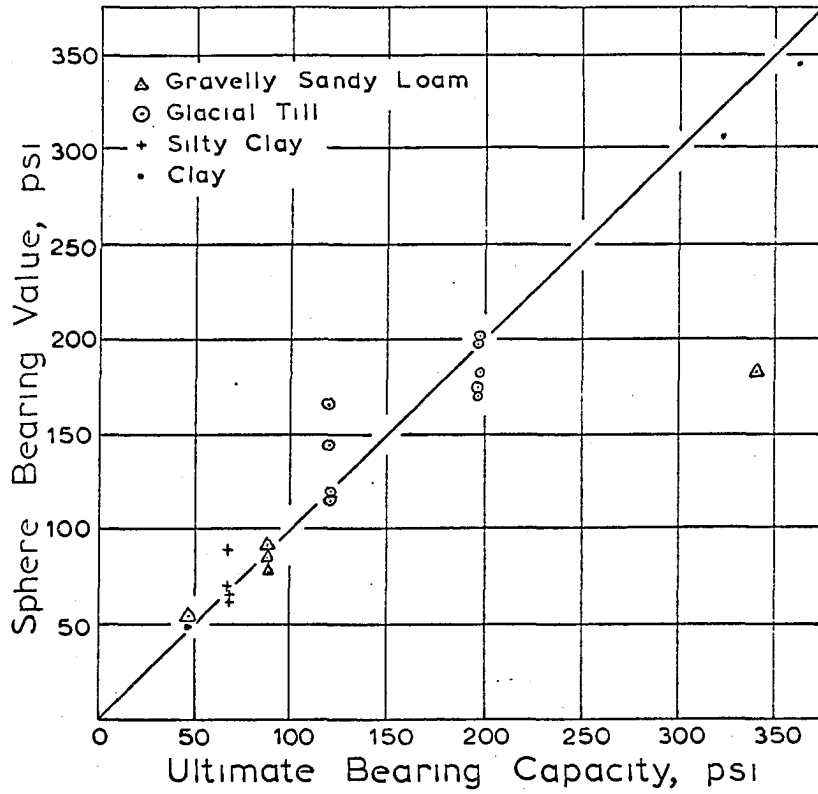


Figure 42. Relationship between the SBV and the ultimate bearing capacity of soil as determined by Terzaghi's equation for circular footings.

is felt that during testing in the laboratory the samples may have drained and consolidated, resulting in a higher cohesion than its actual value in the field.

In the case of laboratory tests performed on the clay with a friction angle zero, the ultimate bearing capacity equation reduces to

$$q_D = 1.3 C (5.7) = 7.41 C$$

which may be approximated to 3.7 times the unconfined compressive strength.

This corresponds to the slope of the regression line in Figure 39 where SBV was found to be 3.66 times unconfined compressive strength.

On the basis of available data it is felt that the bearing value obtained in the Sphere Bearing test gives a reliable ultimate bearing capacity of soils, with the exception of clean sands.

Table 23. The ultimate bearing capacity of soil by Terzaghi's equation for circular footings

Test no.	Soil Classification	C psi	ϕ	γ pcf	$q_{D_{psi}}$	SBV psi
Fd 1	Sandy loam	0.5	38	98.5	46.5	55
Fd 2	" "	1.0	38	98.5	88.0	86
Fd 3	" "	"	"	"	"	92
Fd 4	" "	"	"	"	"	80
Fd 7 ^a	" "	4.0	38	"	340.0	183
Fd 8	Glacial till	2.1	32	130	120.0	118
Fd 9	" "	"	"	"	"	146
Fd 10	" "	"	"	"	"	167
Fd 11	" "	"	"	"	"	120
Fd 12	" "	3.5	32	"	197.0	183
Fd 13	" "	"	"	"	"	203
Fd 14	" "	"	"	"	"	200
Fd 15	" "	"	"	"	"	175
Fd 16	" "	"	"	"	"	172

^aC and ϕ values were obtained from Shelby tube samples in lab by direct shear.

Table 23. (Continued)

Test no.	Soil Classification	C psi	ϕ	Y_{pcf}	qD_{psi}	SBV psi
Fd 17	Silty clay	9.2	2	85	69.4	71
Fd 18	" "	"	"	"	"	68
Fd 19	" "	"	"	"	"	89
Fd 20	" "	"	"	"	"	65
Lab 178 ^b	Clay	43.55	-	123	322	308
Lab 179 ^b	"	47.8	-	116	362	346
Lab 180 ^b	"	6.55	-	113	48.5	50
	"					

^bvalues of C were obtained from remolded specimens by direct shear; the remaining C and ϕ values were obtained by bore hole shear device.

D. Pavement Design Method from the Sphere Bearing Value

No pavement design method has yet been devised that has a sound theoretical basis throughout. The most reliable methods at the moment are empirical methods based on experience of local conditions. According to Wooltorton (49)

An ideal method would take account of the true strength and deformation characteristics of the material in each layer, at all times during the life of the road. It would also take account of the true distribution of stress throughout the road and subgrade, together with factors for the anticipated traffic intensity and distribution of wheel loads across the road width. No design method can yet do this reliably.

The most common cause of structural failure of pavement arises from increased deformation of the subgrade with each application of load, with consequent failure of the layers above. The strength of the pavement at the time it is constructed will not necessarily remain the same throughout its life. It may be higher at times and will almost certainly be lower at other times. Changes in the strength of the subgrade are due to many causes and a satisfactory theoretical method to account for all the

variables is not available. Methods in part based on theory require that the road engineer be familiar with climatic and traffic conditions and local soil properties to be able to make valid quantitative assumptions.

Boussinesq's elastic theory is employed in this semi-rational pavement design method by assuming that the soil mass and the pavement above it are semi-infinite, elastic, homogeneous and isotropic media, and the wheel load is uniformly distributed over a flexible circular area equivalent to the contact area of a wheel (Figure 43). The equation (50, p. 22) for vertical stress is given by

$$\sigma_Z = p \left[1 - \frac{Z^3}{(a^2 + Z^2)^{3/2}} \right] \quad (1)$$

which can be written as

$$Z = \left[\frac{a^2}{\left(\frac{p}{p - \sigma_Z} \right)^{2/3} - 1} \right]^{1/2} \quad (2)$$

where Z = depth, distance of the point on the subgrade from the surface,
 a = radius of applied circle of loading,
 p = applied pressure or intensity of loading at the surface, and
 σ_Z = vertical stress due to applied load.

Since vehicle loads are transmitted to the surface of the pavement through tires, the contact pressure between the tire and the pavement is assumed to be equal to the tire inflation pressure. Assuming that the contact area is circular we can express the radius "a" in terms of wheel load P and inflation pressure p

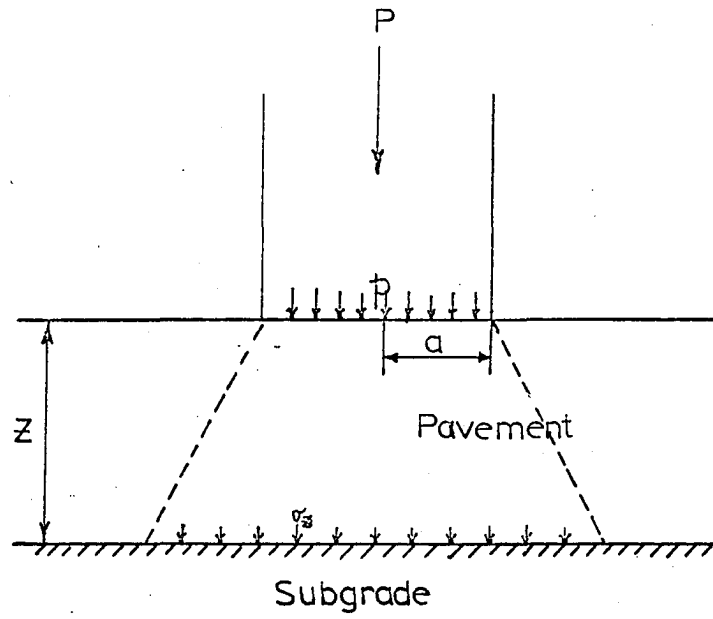


Figure 43. Stress acting on subgrade due to wheel load

$$a = \left[\frac{P}{p\pi} \right]^{\frac{1}{2}} \quad (3)$$

If we assume that a subgrade has an ultimate bearing capacity equal to its Sphere Bearing Value, and the intensity of transmitted pressure should not exceed the SBV, then we can determine the minimum thickness Z of the pavement at which the vertical stress on the subgrade will equal σ_z . Equation (2) can then be written

$$Z = \left[\frac{\frac{P}{p\pi}}{\left(\frac{P}{p-SBV} \right)^{\frac{2}{3}} - 1} \right]^{\frac{1}{2}} \quad (4)$$

If we now consider an aggregate in the subbase of a pavement to be a sphere resting on the surface of the subgrade, and subjected to a load intensity equal to the SBV of the subgrade, then the subgrade will be at the point of incipient rupture. As long as the load intensity on the aggregate is below the SBV of the subgrade the pavement will not fail. However, if the load intensity is increased, the load application is repeated, or the subgrade is weakened due to ingress of water, then the aggregate will sink into the subgrade and cause the overlying pavement to fail. In order to avoid the failure of pavement the pavement designer should know the degree of saturation that the subgrade will be subjected to during the life of the pavement, the maximum wheel loads and the intensity of traffic, to allow an appropriate safety factor in design.

In Figure 44 pavement design curves are presented which have been obtained by solution of the equation (4) for wheel loads from 4,000 lb

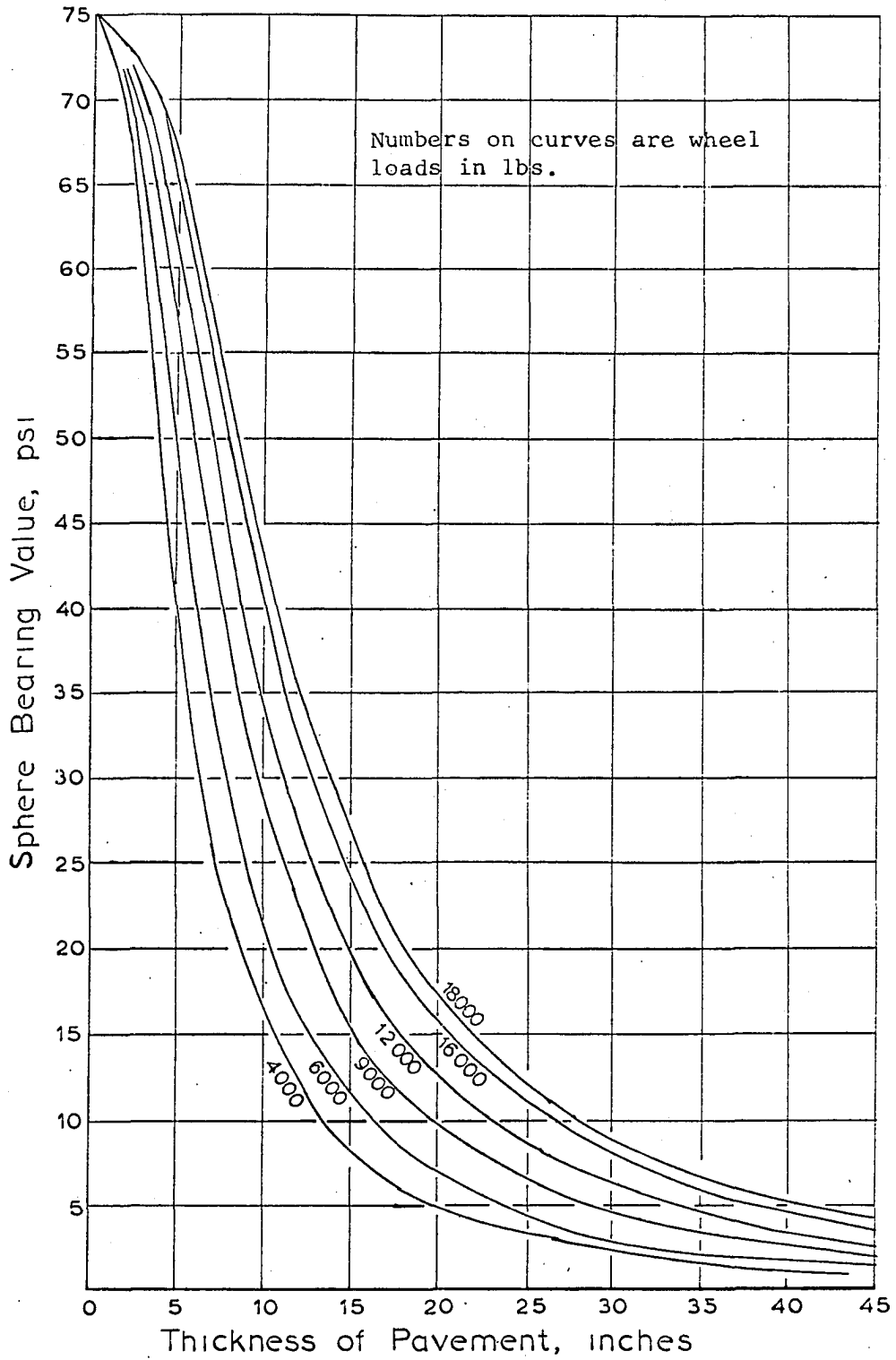


Figure 44. Pavement design curves for use with SBV, developed from Boussinesq's elastic theory

to 18,000 lb. The inflation pressure for all wheel loads is assumed to be 75 psi, whereas the CBR design curves for highway pavements assume a uniform tire pressure of 60 psi for all wheel loads (30). The safety factor in the design curves in Figure 44 is one, and an appropriate safety factor must be based on experience with the factors discussed earlier.

Use of the curves is demonstrated by the following example: Wheel load 18,000 lb, subgrade SBV 300 psi, and safety factor 6. We enter Figure 44 with SBV of 50 psi ($\frac{300}{6}$) and obtain a pavement thickness of 8.5 inches.

To determine the correlation between pavement thickness from the CBR method and from the one suggested in this report, a wheel load 18,000 lb and safety factor 5.5 for the Sphere Bearing test was assumed. Pavement thicknesses were obtained by both the CBR and the SBV method for all the test data in this investigation. These values are shown in Figure 45, and a remarkable similarity may be observed. The CBR design curves are justified for regions where climatic conditions are severe and the subgrade is saturated, but in other regions the CBR method may be overly conservative. Here a lower SBV safety factor should result in an adequate and economical pavement.

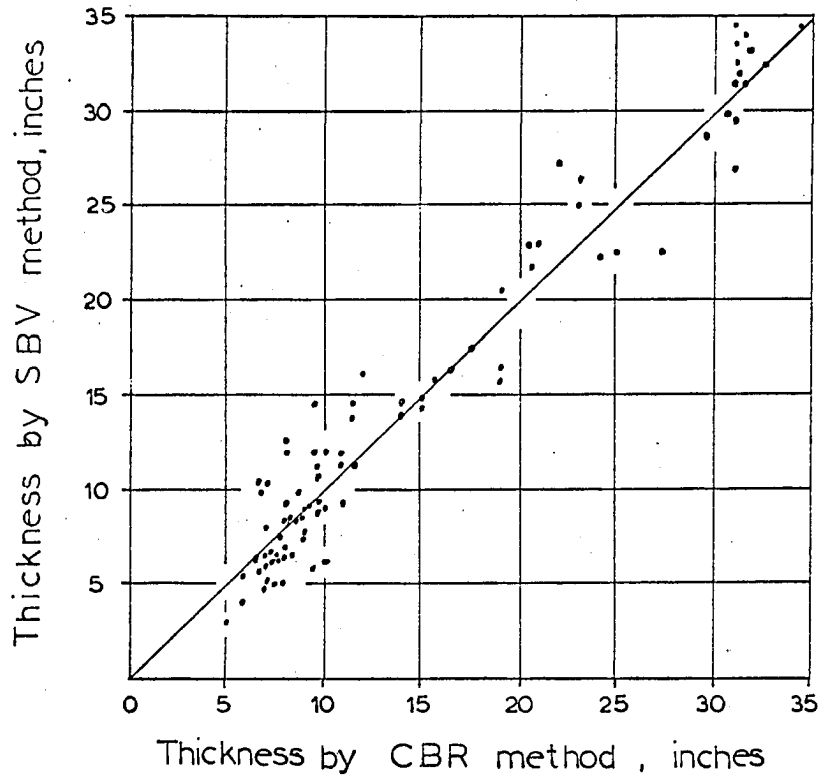


Figure 45. Relationship of pavement thickness for wheel load 18,000 lb by SBV and CBR design curves

VII. SUMMARY AND CONCLUSIONS

This investigation was aimed at exploring a rapid method to determine the strength properties of subgrades for use in pavement design. On reviewing indentation tests for hardness of metals it was found that the Brinell Hardness Number was not constant if either the diameter of the sphere or the applied load was changed. In order to determine the distortion factor due to size of sphere and applied load, use was made of the theory of similitude and dimensional analysis. The analysis indicated that the diameter of the sphere or the load applied to it should not influence the "hardness number" of cohesive soils.

Development of classical bearing capacity theories was traced to the theories of plastic deformation of metals by Prandtl, Hencky and Ishlinsky. It was shown that Terzaghi, Meyerhof and others modified the theories on deformation of metals based on their study on deformation zones in soil mass. However, since no such study had been made for spherical penetrometers in soils, a model investigation of the deformed zone was conducted. It was observed that the deformation mechanism which operates during penetration of a soil mass by a spherical penetrometer approximates two stages: compression of soil, and rupture by plastic flow. Compression in the soil mass occurs as a set of concentric hemispherical shells; the rupture surface was found to be circular. The boundary of this surface did not enclose the full plastic region, since there was a further zone in which the material was stressed but remained stable.

The most significant observation was that the ratio of the curved areas of the elastic-plastic boundary in soil and that of the sphere in contact with soil ranged between 5.6 to 7.5 for soils ranging from sand to clay, which corroborated observations in cohesive soils where the mean pressure on the surface of the sphere was found to be approximately 7 times the cohesion of the sample.

The Sphere Bearing Value obtained, regardless of the size of the sphere, is the same. One reason for this consistency may be absence of perimeter shear in Sphere Bearing test, which was observed in model investigation. This is unlike any other bearing test; for example, in a plate bearing test the values obtained vary with the size of the plate due to strong influence of perimeter shear and perimeter-area ratio. The SBV may, therefore, be considered a fundamental property of soil.

Great difficulty was encountered in testing samples of clean dry sand with the sphere penetration device, since the initial zero reading could not be established nor could the depth of penetration be accurately measured. Clean dry sand offers very little resistance to the penetration of a sphere and its SBV is negligible which is not surprising since trafficability of clean dry sand under similar conditions is also zero. However, under the confining pressure of a pavement the bearing capacity of sand is much higher. A modified Sphere Bearing device where confining pressure can be applied to cohesionless soils is likely to give an accurate indication of its bearing capacity.

The 0.75 inch diameter sphere which was satisfactory for fine grained

soils tested in the laboratory gave erratic bearing values when used on heterogeneous soils in the field. For field use a 6 inch to 12 inch diameter sphere gives consistent and accurate bearing values.

Testing time was reduced by loading the sphere only once instead of a series of load increments. This procedure is recommended for all future tests.

The following conclusions are based on the experimental results:

1. The sphere bearing test has far better reproducibility than other tests that were performed during this investigation. For example, the GBR test had twice as much scatter as the Sphere Bearing test.

2. A straight-line relation exists between the unsoaked GBR and the SBV for specimens that are neither saturated nor excessively dry (Figure 46). No correlation was found between the soaked GBR and the SBV.

3. A straight line relation was found to exist between the SBV and the modulus of subgrade reaction (k) obtained in plate bearing tests. Since k values in the field were limited to 600 pci the curve in Figure 46 has been extended by dashed lines.

4. A straight line relation with a narrow 95 percent confidence band was found between the SBV and the unconfined compressive strength (UCS) in clayey soils. In loessel soils the slope of the line was steeper and the scatter was much greater than in the clayey soils.

5. The ultimate bearing capacity of soil was determined by Terzaghi's formula for circular footings for values of C and ϕ obtained by the bore hole shear device in the field. The ultimate bearing capacity obtained by Terzaghi's equation for shallow footings was found

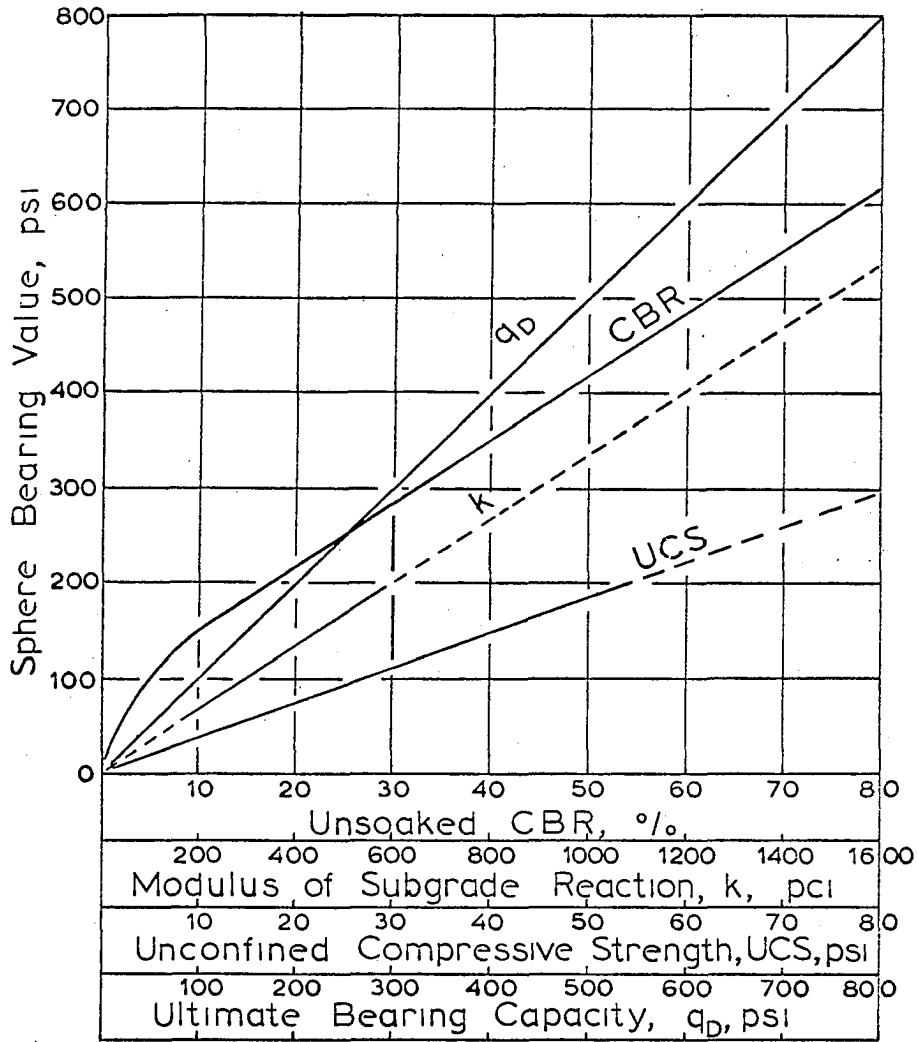


Figure 46. Sphere Bearing Value versus CBR, Modulus of subgrade reaction, unconfined compressive strength of clay and ultimate bearing capacity of soil

to be very close to the Sphere Bearing Value of the soil (Figure 46).

6. Pavement thicknesses from Sphere Bearing Values with a safety factor of 5.5 and modified Boussinesq elastic theory were approximately the same as those obtained by the CBR method. According to Yoder (50, p. 421)

... a study was made of pavement thickness requirements for given loading and subgrade conditions. For this particular problem several state highway engineers were asked to report the required thicknesses Since a considerable range in thickness was reported by the various states, a study was made to determine the reasons for this Consider the CBR of the subgrade, the minimum value reported was 2 percent and the maximum value was 10 percent. The reason for variation from one laboratory test to another can be explained by testing techniques. Another possible reason for differences is determination of the failure criteria which is largely a matter of judgment; complete agreement between engineers would be a coincidence."

The Sphere Bearing test is a simple test which can be performed in the laboratory and in the field and will give the same values. No arbitrary conditions of drainage, confining pressure or the strain rates are necessary for determining the bearing capacity of soils, nor is there any need for large load trailers in the field to determine an arbitrary plate bearing k value from a curve where both stress and deformation can be chosen at will. Determination of bearing capacity by conventional methods necessitates bringing undisturbed samples from the field to determine the C and ϕ values, which vary with the type of test and are seldom consistent. The bearing capacity obtained will depend on the method used, whereas the actual bearing capacity of soil can be determined by applying a single load to the sphere; when its penetration reaches a state of equilibrium, the average pressure on the surface of the sphere

gives a value which is reasonably accurate for design purposes. The value so obtained can be used, with appropriate safety factor, for design of pavements and shallow footings, evaluation of subgrade under a pavement to restrict heavy wheel loads during spring thaw, or compaction control during construction.

VIII. SUGGESTIONS FOR FURTHER RESEARCH

The following areas for further investigation are suggested:

1. A testing program be initiated to determine method of soaking laboratory specimens so that the degree of saturation is the same as that in the field during maximum saturation of the subgrade. An appropriate safety factor may then be determined for use with the SBV obtained from soaked specimens to design pavement thickness by pavement design curves suggested in this report.
2. A technique be developed for investigation of cohesionless soils with the Sphere Bearing test.
3. A method be explored to use the Sphere Bearing test as a measure of trafficability.

IX. LITERATURE CITED

1. Akiyama, F. N. Shear strength properties of Western Iowa loess. Unpublished M.S. thesis. Ames, Iowa, Library, Iowa State University of Science and Technology. 1963.
2. American Society for Testing Materials. Ball penetration in fresh portland cement concrete. American Society for Testing Materials Standards Part 4, Designation C 360-55 T: 707-708. 1961.
3. American Society for Testing and Materials. Making and curing soil-cement compression and flexural test specimens in the laboratory. American Society for Testing and Materials Standards Part 2, Designation D 1632-63: 476-485. 1966.
4. American Society for Testing Materials. Symposium on load tests of bearing capacity of soils. American Society for Testing and Materials Special Technical Publication 79: 31-40. 1948.
5. Barkan, D. D. Dynamics of bases and foundations. New York, New York, McGraw-Hill Book Company, Inc. 1960.
6. Bernett, E. C., Scott, R. F., Jaffe, L. D. and Frink, E. P. Bearing capacity of simulated lunar surfaces in vacuum. AIAA Journal 2, No. 1: 93-98. 1964.
7. Bowden, F. P. and Tabor, D. The friction and lubrication of solids. Part II. Oxford, England, The Clarendon Press. 1964.
8. Boyd, Keith. An analysis of wheel load limits as related to design. Highway Research Board Proceedings 22: 185-198. 1942.
9. Brownlee, K. E. Statistical theory and methodology in science and engineering. New York, New York, John Wiley and Sons, Inc. 1965.
10. Demirel, T. and Enustun, B. V. Turkish report on soils. Permanent International Association of Road Congress Reports 10, No. 2: 1-14. 1955.
11. Fox, N. S. Field model test for the prediction of foundation settlement. Unpublished Ph.D. thesis. Ames, Iowa, Library, Iowa State University of Science and Technology. 1966.
12. Goodman, L. J., Hegedus, E. and Liston, R. A. Scaling considerations in plate sinkage tests. Unpublished mimeographed paper presented at Highway Research Board annual meeting, January, 1966. Ames, Iowa, Department of Civil Engineering, Iowa State University of Science and Technology. 1966.

13. Great Britain Department of Scientific and Industrial Research. Soil Mechanics for road engineers. London, England, Her Majesty's Stationery office. 1964.
14. Handy, R. L. and Fox, N. S. A soil borehole direct-shear test device. Iowa State University of Science and Technology, Engineering Experiment Station, Soil Research Laboratory Contribution 66-8. 1966.
15. Harr, M. E. Foundations of theoretical soil mechanics. New York, New York, McGraw-Hill Book Company. 1966.
16. Hill, R., Lee, E. H. and Tupper, S. J. The theory of wedge indentation of ductile materials. Royal Society Proceedings 188A: 273-290. 1947.
17. Housel, W. S. Dynamic and static resistance of cohesive soils. American Society of Testing and Materials Special Technical Publication 254: 4-35. 1959.
18. Housel, W. S. Laboratory manual of soil testing procedures. Ann Arbor, Michigan, Civil Engineering Department, University of Michigan. 1939.
19. Ishlinsky, A. J. Analysis of spherical indentation. (Translated title) Prikl. Matem. i Mekh. SSSR. 8, No. 3: 233-253. 1944. Original available but not translated; cited in Tabor, D. The hardness of metals. Oxford, England. The Clarendon Press: 48. 1951.
20. Jaffe, L. D. and Scott, R. E. Lunar surface strength: implications of lunar 9 landing. Science 153: 407-408. 1966.
21. Kelly, J. W. A simple field test for consistency of concrete. American Society for Testing Materials Bulletin 163: 70-71. 1950.
22. Kondler, R. L. and Krizek, R. J. Correlation of load bearing tests on soils. Highway Research Board Proceedings 41: 557-590. 1962.
23. Leonard, G. A. Foundation engineering. New York, New York, McGraw-Hill Book Company, Inc. 1962.
24. Meldrum, H. R., Perfect, D. E. and Mogen, C. A. Soil survey of Story County. Iowa Agricultural Experiment Station Report 9. 1941.
25. Meyerhof, G. G. The ultimate bearing capacity of wedge shaped foundations. Fifth International Conference on Soil Mechanics and Foundation Engineering Proceedings 2: 105-109. 1961.

26. Murayama, S. and Ueshita, K. The ball-drop type test as a rapid method of measuring the CBR. Mimeographed paper. Kyoto, Japan, Department of Civil Engineering, Kyoto University. Circa 1963.
27. Murphy, G. Similitude in engineering. New York, New York, The Ronald Press Co. 1950.
28. Ostle, Bernard. Statistics in research. Ames, Iowa, The Iowa State University Press. 1963.
29. Porter, O. J. Foundation for flexible pavements. Highway Research Board Proceedings 22: 84-106. 1942.
30. Porter, O. J. The preparation of subgrades. Highway Research Board Proceedings 18: 324-331. 1938.
31. Portland Cement Association. Concrete pavement design. Chicago, Illinois, author. 1951.
32. Proctor, R. R. Fundamental principles of soil compaction. Engineering News Record III, No. 10: 286-289. September 7, 1933.
33. Raymond, F. Davidson. Laboratory manual in soil mechanics. 2nd ed. New York, New York, Pitman Publishing Corporation. 1959.
34. Schimming, Bruce B. Study of dynamic and static failure envelopes. American Society of Civil Engineers Proceedings 92: 82-112. 1966.
35. Sokolovsky, V. V. Statics of soil media. London, England, Butterworths Scientific Publications. 1960.
36. Spangler, M. G. Soil engineering. 2nd ed. Scranton, Pa., International Textbook Co. 1960.
37. Stevenson, W. H., Brown, P. E., Benton, T. H., Forman, L. W. and Meldrum, H. R. Soil survey of Iowa. Iowa Agricultural Experiment Station Report 55: 1-71. 1929.
38. Stranton, J. H. Military airfields. Construction and design problems. American Society of Civil Engineers Proceedings 70, No. 1: 28-54. 1944.
39. Swanberg, J. H. and Hansen, G. G. Development of a procedure for the design of flexible bases. Highway Research Board Proceedings 26: 45-57. 1946.
40. Tabor, D. The hardness of metals. Oxford, England, The Clarendon Press. 1951.

41. Taylor, D. W. Fundamentals of soil mechanics. New York, New York, John Wiley and Sons, Inc. 1948.
42. Terzaghi, K. Theoretical soil mechanics. New York, New York, John Wiley and Sons, Inc. 1948.
43. Terzaghi, K. and Peck, R. B. Soil mechanics in engineering practice. New York, New York, John Wiley and Sons, Inc. 1949.
44. Tsyrovitch, N. A. Bases and foundations on frozen soil. Highway Research Board Special Report 58: 32-35. 1960.
45. U.S. Army. Corps of Engineers. Suggested method of test for California Bearing Ratios of soils. In American Society for Testing and Materials. Committee D-18 on Soils for Engineering Purposes. Procedures for testing soils. pp. 386-397. Philadelphia, Pa., author. 1950.
46. U.S. Army. Corps of Engineers. Trafficability of soils, development of testing instruments. Waterways Experiment Station, (Vicksburg, Miss.) Technical Memorandum 3-240. 3rd supplement. 1948.
47. U.S. War Department. Office of the Chief of Engineers. Engineer manual. part 12. Airfield pavement design. Washington, D.C., author. 1947.
48. Westergaard, H. M. Theory of concrete pavement design. Highway Research Board Proceedings 2: 107-112. 1928.
49. Wooltorton, F. L. D. The scientific basis of road design. London, England, Edward Arnold, Ltd. 1954.
50. Yoder, E. J. Principles of pavement design. New York, New York, John Wiley and Sons, Inc. 1965.

X. ACKNOWLEDGEMENT

The subject matter of this investigation was obtained as a part of the research being done under Project 597-S at Engineering Research Institute of the Iowa State University. Project 597-S is sponsored by the Iowa Highway Research Board and is financed by the Iowa State Highway Commission.

The author expresses his sincere appreciation to Dr. Turgut Demirel, Project Director and Associate Professor of Civil Engineering for his untiring interest, counsel and guidance in this investigation, and to Dr. Richard L. Handy, Professor of Civil Engineering for his valuable guidance during the investigation and preparation of this manuscript.

The helpful advice and assistance given by Professor J. M. Hoover and Dr. R. A. Lohnes are gratefully acknowledged.

Special thanks are due Mr. Charles N. Easton for his valuable and unselfish assistance during all phases of the investigation.